



## **Terms and Conditions of Use of Digitised Theses from Trinity College Library Dublin**

### **Copyright statement**

All material supplied by Trinity College Library is protected by copyright (under the Copyright and Related Rights Act, 2000 as amended) and other relevant Intellectual Property Rights. By accessing and using a Digitised Thesis from Trinity College Library you acknowledge that all Intellectual Property Rights in any Works supplied are the sole and exclusive property of the copyright and/or other IPR holder. Specific copyright holders may not be explicitly identified. Use of materials from other sources within a thesis should not be construed as a claim over them.

A non-exclusive, non-transferable licence is hereby granted to those using or reproducing, in whole or in part, the material for valid purposes, providing the copyright owners are acknowledged using the normal conventions. Where specific permission to use material is required, this is identified and such permission must be sought from the copyright holder or agency cited.

### **Liability statement**

By using a Digitised Thesis, I accept that Trinity College Dublin bears no legal responsibility for the accuracy, legality or comprehensiveness of materials contained within the thesis, and that Trinity College Dublin accepts no liability for indirect, consequential, or incidental, damages or losses arising from use of the thesis for whatever reason. Information located in a thesis may be subject to specific use constraints, details of which may not be explicitly described. It is the responsibility of potential and actual users to be aware of such constraints and to abide by them. By making use of material from a digitised thesis, you accept these copyright and disclaimer provisions. Where it is brought to the attention of Trinity College Library that there may be a breach of copyright or other restraint, it is the policy to withdraw or take down access to a thesis while the issue is being resolved.

### **Access Agreement**

By using a Digitised Thesis from Trinity College Library you are bound by the following Terms & Conditions. Please read them carefully.

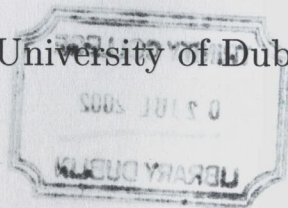
I have read and I understand the following statement: All material supplied via a Digitised Thesis from Trinity College Library is protected by copyright and other intellectual property rights, and duplication or sale of all or part of any of a thesis is not permitted, except that material may be duplicated by you for your research use or for educational purposes in electronic or print form providing the copyright owners are acknowledged using the normal conventions. You must obtain permission for any other use. Electronic or print copies may not be offered, whether for sale or otherwise to anyone. This copy has been supplied on the understanding that it is copyright material and that no quotation from the thesis may be published without proper acknowledgement.

# A Dynamic Study of Cavity Polaritons

*This thesis is dedicated to my family  
for their constant love and support*  
L. A. Dunbar

A thesis submitted for the degree of Doctor of Philosophy at the

University of Dublin



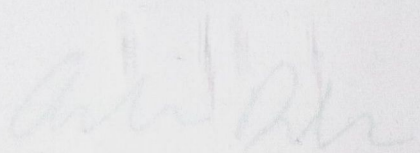
under the supervision of  
Prof. John Hegarty  
Department of Physics  
Trinity College Dublin

---

February 2002

*This thesis is dedicated to my family  
for their enduring love and support.*

This thesis has not been submitted as an exercise by any other person or persons.  
The work described is entirely my own, except for the acknowledgements and the collaborative work noted in the text.  
I hereby grant permission that Trinity College Library may lend or copy this thesis.



L. Andrew Dumbor

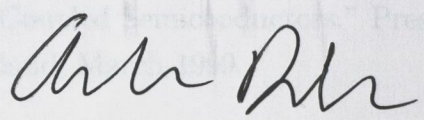
# Publications

L. A. Dunbar, A. L. Bradley, J. P. Doran, R. P. Stanley, R. Houdré, U. Oesterle and M. Degens. "Acoustic Phonon Scattering in a Strongly Coupled Microcavity." Presented at *Confined Photon Systems: Fundamentals and Applications*, Cargèse, Corsica, August 1998.

A. L. Bradley, L. A. Dunbar, J. P. Doran, J. Hensley, R. Houdré, U. Oesterle and M. Degens. "Supercritical Raman Scattering in a Microcavity." Presented at *Confined Photon Systems: Fundamentals and Applications*, Cargèse, Corsica, August 1998.

## Declaration

This thesis has not been submitted as an exercise for a degree at any other University. The work described is entirely my own, except for the assistance mentioned in the acknowledgements and the collaborative work noted in the list of publications. I agree that Trinity College Library may lend or copy this thesis on request.



L. Andrea Dunbar

H. Follmar, M. G. Bunch, L. P. Barry, A. L. Bradley, J. P. Doran, J. S. Ross and G. Hill. "Two-Photon Induced Photoluminescence in Bulk AlGaAs: A Theoretical Investigation." *Journal of Applied Physics*, Vol. 92, No. 12, pp. 7331-7334, December 2002.

H. Follmar, L. P. Barry, A. L. Bradley, J. P. Doran, J. S. Ross and G. Hill. "Two-Photon Induced Photoluminescence in Bulk AlGaAs: A Theoretical Investigation." *Journal of Applied Physics*, Vol. 92, No. 12, pp. 7331-7334, December 2002.

# Publications

L. A. Dunbar, A. L. Bradley, J. P. Doran, R. P. Stanley, R. Houdré, U. Oesterle and M. Ilegems. "Acoustic Phonon Scattering in a Strongly Coupled Microcavity." Presented at *Confined Photon Systems: Fundamentals and Applications*, Cargèse, Corsica, August 1998.

A. L. Bradley, L. A. Dunbar, J. P. Doran, J. Hegarty, R. P. Stanley, R. Houdré, U. Oesterle and M. Ilegems. "Suppression of Acoustic Phonon Scattering in Semiconductor Microcavities." Presented at *Cleo Europe'98*, Glasgow, Scotland, September 1998.

A. L. Bradley, L. A. Dunbar, J. Hegarty, R. P. Stanley, U. Oesterle, R. Houdré, M. Ilegems and J. P. Doran. "Dephasing of Strongly Coupled Exciton-Photon Systems." In *Excon'98*, Proceedings of the third international conference on Excitonic Processes in Condensed Matter, Eds. R. T. Williams and W. M. Yen, **98-25**, pp. 10-19, 1998.

L. A. Dunbar, A. L. Bradley, J. P. Doran, J. Hegarty, R. P. Stanley, R. Houdré, U. Oesterle and M. Ilegems. "Investigation of Acoustic Phonon Scattering in Strongly Coupled Semiconductors." Presented at *Institute of Physics*, Newcastle, Northern Ireland, March 1999.

H. Folliot, M. Lynch, L. P. Barry, A. L. Bradley, L. A. Dunbar, J. Hegarty and J. F. Donegan. "Two Photon Induced Photoconductivity Enhancement in Semiconductor Microcavities: A Theoretical Investigation." Submitted to: *J. Opt. Soc. Am. B*

H. Folliot, M. Lynch, L. P. Barry, A. L. Bradley, J. Hegarty, J. F. Donegan, L. A. Dunbar, J. S. Roberts and G. Hill. "Two Photon Absorption Photocurrent enhancement in Bulk AlGaAs Semiconductor Microcavities." To be published: *Appl. Phys. Lett.*, March 2002.

L. A. Dunbar, M. Lynch, A. L. Bradley, J. F. Donegan, J. Hegarty, R. P. Stanley, U. Oesterle, R. Houdré and M. Ilegems. "Collisional Broadening of Semiconductor Microcavity Polaritons." To be published: *Phys. Stat. Sol. (b)*, March 2002.

L. A. Dunbar, R. P. Stanley, M. Lynch, J. Hegarty, U. Oesterle, R. Houdré and M. Ilegems. "Excitation Induced Coherence in Semiconductor Microcavities." Submitted: *Phys. Rev. B*, November 2001.

# Summary

Strong coupling between an atom and a cavity field is a well established phenomenon in the field of cavity quantum electrodynamics. However it was not until 1992 that improvements in growth technology resulted in the advent of strong coupling in semiconductor microcavities. The strong coupling in these novel systems is between a quantum well exciton and the confined photon field. Due to the similarities with three dimensional polaritons these states were called cavity polaritons.

Due to their fast recombination rates cavity polaritons were anticipated in the early 1990s as a solution to the challenge of ultra-fast switching, which is needed in modern telecommunications. The recombination rate of the cavity polariton, being the average of the photon and exciton recombination rates, results in very fast recombination times. However, it was found that due to the peculiarities of the dispersion curve, these fast recombination rates were not realisable for non-resonantly (electronically) injected polaritons.

The unusual dispersion curve that results from the admixture of an exciton photon system and its effect on scattering processes is one of the main topics of this thesis. The effect of the lower cavity polariton dispersion curve on the acoustic phonon broadening and polariton-polariton broadening is investigated using four wave mixing. A suppression of both of these scattering processes is detected on the lower polariton branch. Both suppressions, although from different mechanisms, are a result of the nature of the lower polariton dispersion curve. The suppression is shown to increase towards negative detunings, where the polariton is more photon-like.

In the last three years stimulated emission of the cavity polariton has opened up new prospects for the strong coupling regime both in the commercial world and in the more fundamental aspects of research. For example, a new 'inversionless' polariton laser has recently been suggested which could be of commercial interest, and speculation as to whether a Bose-Einstein condensate can occur due to the bosonic nature of the polariton has resulted in much controversy in the research field. We endeavour to add to this knowledge by investigating the coherence time of the polariton with increased excitation. Longer coherence times are measured with an increased occupation, this is one of the signatures of a Bose Einstein condensate.

## Acknowledgements

I would like to thank my supervisor, Prof. John Hegarty, for providing me with the opportunity to study physics after my sojourn in the city, and whose positive outlook was a great source of encouragement.

John Donegan has performed many supervisory roles over the last eight months including reading my thesis, for which I am extremely grateful. For her tutelage during the first year, my appreciation to Louise. Vincent was once coined the patron saint of postgraduates and I cannot think of a more apt title, thank you for all your help with the lasers.

Outside of Trinity I would like to thank Christiano Ciuti, Romuald Houdré, Ross Stanley and John Doran for many fruitful discussions. I would like to thank Ross and John for proof reading my thesis. In particular I would like to thank Ross Stanley for his support and encouragement.

My three contemporaries, with whom I shared the ups and downs of our time at Trinity, Alan whose constant pessimism was a source of optimism for the rest of us, JP whose laid back attitude was an inspiration to me, and Cian for his unwavering support. Thank you to the people in the lab: Hervé, Declan, Richard, Gary, Karl, Canice, Tom McCormack, Daire, Brendan, Pascal, Dave Fewer, Christophe, Tara, Fred, Fergal, Paul, Adrian Donohoe and Tom Aherne.

There are several new friends that I have made during my time at Trinity, I would like to mention, Paddy, a flat mate as well as a colleague and now a good friend and Tina from whom I have never had to 'take a step back'. There are two people with whom I shared both friendship and a love of physics, whose 'no question is stupid' attitude resulted in learning as well as laughing nights in the pub - Stevieboy and Mick. A special thanks to Mick, who has been a mentor as well as a friend and without whom this thesis would not have been realised.

Finally I would like to thank those I love, my family, particularly Bex for her support over the last few weeks and ~~Cian~~ Cian whose company (and humour) over the last three years has been a constant source of joy.



# Contents

<b>1</b>	<b>Introduction</b>	<b>1</b>
<b>2</b>	<b>Background</b>	<b>5</b>
2.1	Introduction . . . . .	5
2.2	Weak coupling . . . . .	6
2.3	Strong coupling . . . . .	11
2.3.1	Quantum model . . . . .	12
2.3.2	Linear dispersion theory . . . . .	16
2.4	Distributed Bragg reflectors . . . . .	20
2.5	Quantum well excitons . . . . .	23
2.5.1	Quantum wells summary . . . . .	27
2.6	Bulk polaritons . . . . .	30
2.7	Cavity polaritons . . . . .	33
2.7.1	Dispersion . . . . .	35
2.7.2	Bottleneck . . . . .	36
2.7.3	Inhomogeneous broadening . . . . .	38
2.8	Summary . . . . .	42
<b>3</b>	<b>Sample characterisation</b>	<b>43</b>
3.1	Introduction . . . . .	43

3.1.1	Sample growth and structure . . . . .	44
3.2	Sample properties . . . . .	46
3.3	Experimental characterisation of the samples . . . . .	50
3.3.1	Photoluminescence . . . . .	52
3.3.2	Pump-probe . . . . .	55
3.3.3	Femtosecond reflectivity . . . . .	59
3.4	Summary of results . . . . .	64
<b>4</b>	<b>Four Wave Mixing</b>	<b>66</b>
4.1	Introduction . . . . .	66
4.2	Two-level model . . . . .	69
4.3	Conclusion . . . . .	79
<b>5</b>	<b>Acoustic phonon broadening of the lower polariton</b>	<b>80</b>
5.1	Introduction . . . . .	80
5.2	Acoustic phonons . . . . .	82
5.3	Theory of exciton and polariton scattering by acoustic phonons . . . . .	85
5.4	Sample and experimental setup . . . . .	89
5.5	Experimental results . . . . .	93
5.6	Theory and analysis . . . . .	96
5.7	Conclusions . . . . .	101
<b>6</b>	<b>Polariton-polariton collisional broadening</b>	<b>103</b>
6.1	Introduction . . . . .	103
6.2	Background and theory . . . . .	104
6.3	Samples and experimental setup . . . . .	110
6.4	Experimental results . . . . .	111

6.4.1	Results on the 2QW sample . . . . .	113
6.4.2	Threshold dependence on detuning . . . . .	114
6.4.3	Threshold dependence on detuning in the 1QW sample . . . . .	116
6.4.4	Comparing the two samples . . . . .	117
6.4.5	Polariton density . . . . .	117
6.5	Comparison with literature, and conclusions . . . . .	119
<b>7</b>	<b>Excitation induced coherence</b>	<b>121</b>
7.1	Introduction . . . . .	122
7.2	Background . . . . .	123
7.2.1	Bose-Einstein condensation . . . . .	123
7.2.2	Excitons as Bose particles . . . . .	126
7.2.3	Cavity polaritons as Bose particles . . . . .	128
7.3	Sample and experimental setup . . . . .	132
7.4	Experimental results . . . . .	135
7.4.1	Results on 2QW sample . . . . .	135
7.4.2	Results on 1QW sample . . . . .	137
7.5	Experimental artifacts and saturation of the strong coupling regime . . . . .	139
7.6	Analysis of results . . . . .	145
7.7	Comparison with literature . . . . .	148
7.8	Conclusions . . . . .	149
<b>8</b>	<b>Conclusions</b>	<b>151</b>
8.0.1	Future work . . . . .	153
<b>A</b>	<b>Biexcitons</b>	<b>155</b>
<b>B</b>	<b>Other interesting results</b>	<b>157</b>

# Chapter 1

## Introduction

Technological advances have opened up new branches of physics throughout history. One famous example is the invention of the vacuum pump by Geissler in 1855, which resulted in the discovery of cathode rays. Similarly, technological advances in the growth of semiconductors has given access to a wealth of new physics.

The tailoring of the material parameters offered by growth techniques such as metalorganic chemical vapour deposition and molecular beam epitaxy [1], have resulted in the fabrication of low dimensional structures such as quantum wells. A quantum well is a narrow layer of low bandgap material sandwiched between a higher bandgap material. Quantum wells demonstrate the quantum nature of electrons which become trapped in them, resulting in the classic particle-in-a-box (or more accurately classic particle-in-a-sheet) with discrete energies. Today there are a vast number of applications of quantum wells in the optoelectronics industry [2], one of the most successful of which is the quantum well laser.

Growth techniques have also enabled optical confinement as an integral part of semiconductor devices. In a pioneering paper Purcell [3] predicted a change in the spontaneous emission lifetime by cavity confinement. This has recently led to intense research in

low dimensional optically confined systems such as planar microcavities, microdisks and photonic bandgap structures and the placing within them of low dimensional bandgap confined emitters such as quantum wells, quantum wires and quantum dots [4].

Whilst this work was being carried out in semiconductor physics, in cavity quantum electrodynamics theoretical work led to the prediction of 'strong coupling'. This strong coupling between an atomic resonance and strongly confined optical field has now been experimentally confirmed [5, 6].

In the semiconductor field, optical confinement can be broadly split into two regimes, the *weak coupling* regime and the *strong coupling* regime. The weak coupling regime is often called the perturbative regime as the optical confinement has a perturbative effect on the electronic emitter, and as such is well described by Fermi's golden rule. This weak coupling regime has so far been more commercially successful than the strong coupling regime. The strong coupling regime results in a non-perturbative modification of the states of the system. The main physical difference between the two regimes is increased optical confinement in the strong coupling regime resulting in a greater interaction between the emitter and the cavity field.

The strong coupling states due to the interaction between excitons and light, so called polaritons, were predicted as early as 1958 [7] in three dimensional semiconductors. However, three dimensional polaritons form steady states due to conservation of crystal momentum. Hence they only radiatively decay via scattering at the surface, making them extremely difficult to study experimentally [8, 9].

With confinement in one dimension by the quantum well the excitonic nature becomes two dimensional. This breaks the conservation of crystal momentum in one direction allowing the polaritons to couple with radiative modes. When quantum well excitons are placed in a planar microcavity this can result in strong coupling. Thus, strong coupling which was already well established in atomic systems was achieved in exciton quantum well - planar microcavity systems [10]. The new radiatively coupled modes of

the system, so called cavity polaritons, have resulted in a vast array of research work in this novel regime [11, 12, 13, 14]. It is these states that we study in this thesis.

Recently strong coupling has progressed and is now being studied in lower dimensional systems [15, 16] and engineered in organic systems [17].

The two dimensional strong coupling regime in semiconductor microcavities was initially predicted to give a fast radiative recombination times of a few picoseconds, as the recombination time in the strong coupling regime is the average of the exciton and the cavity lifetime. However, it has since been found that when carriers are injected, their relaxation times are very slow, hundreds of picoseconds, due a bottleneck [18] which results from the modified dispersion curve. This dispersion curve is of fundamental interest and much of this thesis involves studying the effect of the dispersion curve on various scattering processes.

More recently in 2000, two experiments [19, 20] demonstrated stimulated scattering in the polariton system. These experiments generated huge interest as they demonstrated the bosonic behaviour of the polaritons. This interest is still strong today and the bosonic behaviour of cavity polaritons is one of the topics studied here.

Although the work presented here is on III-V microcavity polaritons, there is much interest in II-VI polaritons. II-VI materials were initially plagued by growth problems but improvements have been made and, due to the larger oscillator strength of the excitons in II-VI materials, there is a stronger interaction [21, 22]. The large splitting in these materials presently makes them good candidates for stimulated emission [23, 24] and prospective room temperature polariton lasers.

This thesis is laid out as follows:

Chapter 1 is as presented above.

Chapter 2 contextualises the work with respect to previous work performed, both on quantum well excitons, and on the strong versus weak coupling of confined optical

systems. The basic physics is introduced along with two models to provide an understanding of the strong coupling regime in the semiconductor microcavity system.

Chapter 3 presents a description of the samples studied and a series of experiments used to characterise our strong coupling samples.

Chapter 4 discusses the nonlinear technique of four wave mixing which is used to study the samples in the subsequent three chapters.

Chapter 5 investigates the effect of acoustic phonon broadening on the lower polariton branch. The results from the four wave mixing are shown to be in agreement with a simple phenomenological model.

Chapter 6 reviews the theory presented on the collisional broadening in quantum wells and cavity polaritons. The theoretically predicted threshold in broadening of the lower polariton branch is experimentally investigated. The effect of detuning on the threshold and the resulting change in the dispersion curve is also explored.

Chapter 7 focuses on more recent work, the bosonic properties of polaritons. A short literature review of stimulated scattering of the lower polariton branch is given. The variation of the coherence time of the lower polariton branch with intensity and an increase in coherence with intensity (occupation) is measured. These results are shown in both samples.

Chapter 8 summarises the results of this thesis and suggests some further experiments.

## Chapter 2

# Background

In this chapter we present background information in order to place our work within its general field of research. The two regimes of *weak coupling* and *strong coupling* are revised. Two simple models of the strong coupling regime, a quantum mechanical model and a linear dispersion model are briefly reviewed in order to obtain an insight into strong coupling. The relevant physics of excitons in Quantum Wells (QW), and distributed Bragg reflectors are considered. Previous work on bare (no cavity) QWs and on three dimensional polaritons are briefly reviewed in order to compare the particular characteristics of strong coupling in our system with previous work. Two important considerations, the dispersion and the broadening of the microcavity polariton systems, are then discussed.

### 2.1 Introduction

There are two ways in which to contextualise this work. One way is to look at the previous work done on QWs and then to try and ascertain from the work done in this thesis whether, when the QW is put in a planar microcavity (and there is strong



interaction) its properties are fundamentally modified. The second way is to discuss the general work on confined optical systems and relate this to our specific case of microcavity polaritons; and importantly in such a case, ask whether the emission is a filtered emission or the result of fundamentally changed states. Essentially the two questions are the same.

In the introduction we discuss the semiconductor microcavity system in terms of the general work on confined optical and electrical systems. Apart from an extremely brief discussion on the properties of excitons in bare QWs presented here we discuss the relevant work on excitons in each chapter.

The microcavity concept does need addressing, and we will do this first. The microcavity regime that this thesis concentrates on is that of the strong interaction between the photon modes confined by the microcavity and the electronic excitation, in this case a QW exciton; the so called *strong coupling regime*. As yet, however, more research has been carried out on the more commercially successful regime where the interaction between the photon modes and the electronic excitation is weak; the so called *weak coupling regime*, which we will discuss first.

## 2.2 Weak coupling

The important difference between the strong and weak coupling regimes is that the weak coupling regime obeys Fermi's Golden Rule (FGR). FGR gives the transition rate at which particles are scattered from one state to another by a perturbation. In fact, the weak coupling regime is often known as the perturbative regime whilst the strong coupling regime is often known as the non-perturbative regime. The intermediate regime has been studied and a smooth transition from strong to weak coupling has been shown [25]. Due to the large interaction strength in our samples it can be stated that they are clearly in the strong coupling regime. The weak coupling regime is

presented here as an aid to understanding the strong coupling regime.

For an electron dipole transition the spontaneous emission rate,  $\gamma_{\text{sp}}$ , from FGR is given as [26],

$$\gamma_{\text{sp}} = \frac{1}{\tau_{\text{sp}}} = \frac{2\pi}{\hbar^2} \rho(\omega_e) \langle |\vec{d} \cdot \vec{\epsilon}(\vec{r})|^2 \rangle \quad (2.1)$$

where  $\tau_{\text{sp}}$  is the spontaneous emission lifetime,  $\vec{\epsilon}(\vec{r})$  is the vacuum electric-field at the location  $\vec{r}$  of the emitter,  $\vec{d}$  is the electric dipole moment and  $\rho(\omega_e)$  is the density of photon modes at the emitter's angular frequency  $\omega_e$ . The averaging of the squared dipolar matrix element is performed over the various photon modes seen by the emitter.

From equation (2.1) we can see that the spontaneous emission rate is modified by the mode density  $\rho(\omega_e)$  and the intensity of the vacuum field at the location of the electric dipole  $\vec{\epsilon}(\vec{r})$ . As a microcavity can change both the mode density and the intensity of the vacuum field at different positions, it can change the spontaneous emission rate. Actually it is predicted that, for perfect lossless mirrors  $\frac{\lambda}{2}$  apart, a factor of 3 enhancement can be obtained [27]. In practice using metallic mirrors an enhancement factor of 2.3 has been demonstrated [28]. For structures with dielectric mirrors the maximum change that would theoretically be seen would reduce to  $\pm 20\%$  due to reduced optical confinement as a result of so called 'leaky' modes [29]. To maximise the change in the spontaneous emission rate lower dimensional microcavities, which give increased optical confinement, are needed. With three dimensional confinement the enhancement factor of the spontaneous emission rate for a monochromatic emitter (*i.e.* one that is ideally spatially and spectrally coupled to the mode) is given by the Purcell factor [3]. Recently, microdisks have shown a Purcell factor of 190 and an increase in the spontaneous emission rate by a factor of 12 [30].

While microcavities can affect the emission rate, it is easier to obtain a change in spatial distribution of the emission. A change in spatial distribution can occur with

no change in the spontaneous emission rate; the overall density of photon modes stays the same as does the average electric field. An enhancement of the emission occurs when a specific mode, that exists at a certain angle from the dipole, interacts with an increased electric field intensity at that angle. A suppression of the emission occurs when a specific mode that exists at a certain angle from the dipole interacts with a decreased electric field intensity at that angle. Thus, although enhancement is obtained in some directions of the emission, a suppression occurs in other directions resulting in no change in the overall spontaneous emission rate. This change in the spatial emission rate can nonetheless help directionality and increase the light emitted from the structure by channelling more light into angles below the critical angle; that is, the angle at which total internal reflection first occurs. This behaviour is dependent on the refractive index of the material.

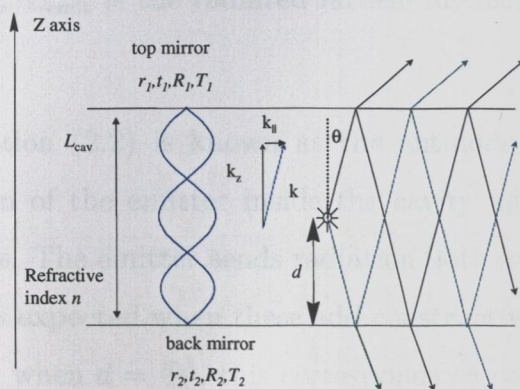


Figure 2.1: An emitter inside a microcavity, the emitter is placed a distance  $d$  from the back mirror. The emission of the emitter from the top mirror can be seen to depend on its distance from the back mirror as the two beams emitted (black) and (green) will interfere, this is taken into account by an antinode factor. The number of modes the cavity will support depends on the cavity wavelength, refractive index and the emitted wavelength. One of the unique features of a microcavity is that it will only support a small number of modes because the cavity wavelength is small. The Airy factor reproduces the intrinsic ~~enhancement~~ or inhibition of each mode by the cavity, see equation (2.2).

To look more closely at the change of the spatial distribution we examine the emitter inside a microcavity, where the source field is described by,  $E_{\text{emit}}(z) = E_0 \exp(i[\omega t -$

$k_z z$ )<sup>1</sup>. The cavity length is  $L_{\text{cav}} = \frac{m\lambda_{\text{cav}}}{2n}$ ,  $m$  is an integer and  $n$  is the refractive index of the cavity medium (see figure 2.1).  $\lambda_{\text{cav}}$  is the wavelength of the cavity for which the cavity is designed,  $\omega$  is the electric field angular oscillating frequency,  $k_z = \frac{2\pi n}{\lambda} \cos \theta$  is the wavevector in the  $z$ -direction and  $\theta$  is the angle between emission and  $z$ -axis.  $\lambda$  is the wavelength of the emitted radiation in free space. If the source was not in the cavity its emission intensity pattern would be approximated by  $|E_{\text{emit}}|^2 = E_0^2 \cos^2 \theta$ . If a dipole is positioned at a distance  $d$  from the back mirror the resultant farfield emission intensity,  $E^2$ , at an internal angle  $\theta$  is found by summing the two series of waves one emitted at  $\theta$  and the other emitted at  $\pi - \theta$  giving [31],

$$|E_{\text{res}}|^2 = |E_{\text{emit}}|^2 \times \frac{T_1}{|1 - r_1 r_2 \exp(2i\phi)|^2} \times |1 + r_2 \exp(i2\phi')|^2 \quad (2.2)$$

$\phi = k_z L_{\text{cav}}$  and  $\phi' = k_z d$ .  $E_{\text{emit}}$  is the radiated farfield intensity in the absence of any microcavity.

The third term in equation (2.2) is known as the antinode factor,  $\xi$ , and it takes into account the position of the emitter inside the cavity and the angle of emission relative to the cavity axis. The emitter sends radiation both forward and backward. A maximum contribution is expected when these add constructively. Assuming that  $\theta=0$  the maximum will occur when  $d = \frac{m\lambda}{2n}$ , this corresponds to positioning the emitter at an antinode in the cavity. By changing the position of the emitter inside the cavity ( $d$ ) it is possible to modify the antinode enhancement at different angles. However, as will be shown, the airy factor does not depend on the emitter position, and the farfield pattern is dependent on the multiply of both the airy and antinode factor. This result means that, moving the position of the emitter only changes the relative intensities at different angles.

Each beam also undergoes classical interference which gives rise to the Airy factor,

---

<sup>1</sup>The  $z$ -direction is also known as the perpendicular direction and is the growth direction of the planar microcavity.

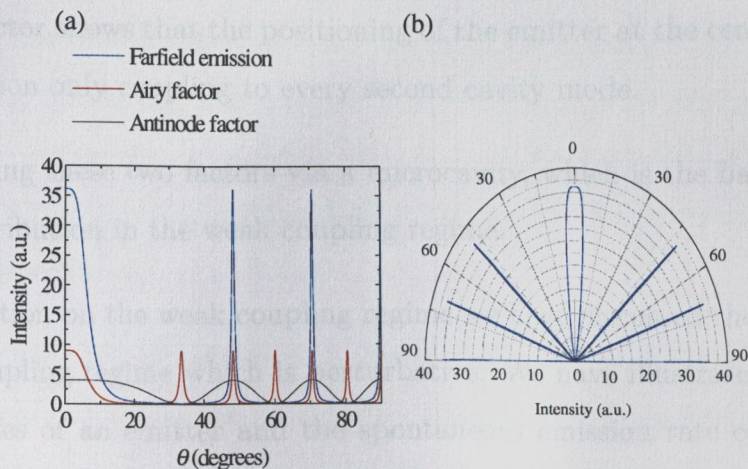


Figure 2.2: Figure showing how the Airy factor and antinode factor combine to create the farfield emission profile. (a) The emission profile of an isotropic source (monochromatic emission at wavelength  $\lambda$ ) positioned at the centre of a microcavity supporting six modes ( $m_c=6$ ) ( $L_{cav} = \frac{3\lambda}{n}$ ), for  $r_2 = +1, r_1 = +0.8$ , and  $T_1 = 0.36$ , (b) same emission profile on a polar plot.

$|1 - r_1 r_2 \exp(2i\phi)|^{-2}$ . It reproduces the intrinsic enhancement/inhibition of each mode by the cavity and dictates the number of modes that can be supported. (The difference between a large cavity and a microcavity is the reduced number of modes, in a given bandwidth, that a microcavity can support due its small width.) The Airy factor reaches a maximum when  $k_z L_{cav} = m2\pi$ ,  $m$  is an integer.  $k_z$  is effectively quantised with  $k = \sqrt{k_z^2 + k_{\parallel}^2}$ . The cavity dispersion is then,

$$E(k_{\parallel}) = \sqrt{E_0^2 + \frac{c^2 \hbar^2 k_{\parallel}^2}{n^2}} \quad (2.3)$$

For a given wavelength and cavity length, the number of modes, that is the number of cavity resonances, is  $m_c = \frac{k_z L_{cav}}{\pi}$ .

For a cavity that supports six modes (due to the Airy factor) with the emitter placed at the centre of the microcavity the emission is shown in figure 2.2; the antinode factor

is also shown. The six modes of the cavity are clearly visible in the Airy factor, while the antinode factor shows that the positioning of the emitter at the centre of the cavity results in emission only coupling to every second cavity mode.

It is by modifying these two factors via a microcavity, which is the basis of control of the spatial distribution in the weak coupling regime.

In this brief section on the weak coupling regime we have discussed the basic concepts of the weak coupling regime which is perturbative. We have illustrated how both the spatial properties of an emitter and the spontaneous emission rate can be modified. There are many more subtleties which we do not discuss here, the reader is referred to the work by Benisty *et al.* [31, 32].

## 2.3 Strong coupling

Strong coupling is beyond FGR in that perturbation theory is no longer valid. The interaction between the electronic excitation and the cavity changes the energy states of the system. Instead of a single resonance, when the two energies (the cavity energy and the electronic excitation energy) are resonant, there is a splitting and new states are formed that are a combination of the two photonic and electronic states. When the energy states are not resonant they are said to be detuned and the detuning,  $\Delta$ , is defined as,

$$\Delta = E_{cav} - E_{ex}, \quad (2.4)$$

where  $E_{cav}$  is the energy of the cavity resonance and  $E_{ex}$  is the energy of the electronic resonance.

Strong coupling is well established in atomic systems in Cavity Quantum ElectroDy-

namics (CQED) [6] and one of the models that we discuss is acquired from this field. A second model is based on linear dispersion theory. This model produces similar results to the CQED atomic model, and may be viewed as the cavity acting like a filtering system. Are we dealing with a quantum system or a classical system? Are the properties of the system a genuine admixture of the two systems or are we essentially looking at exciton emission filtered by a cavity?

The next section in this chapter is as follows. We comment on two well established models in the field to gain a greater understanding of strong coupling. The first is the simplest possible quantum mechanical model of an absorber in a cavity. The second is the classical linear dispersion model.

### 2.3.1 Quantum model

The model we examine is a well established model in CQED and is called the Jaynes-Cummings model [33]. This atomic model uses the Hamiltonian of the atom, the photon and their interaction as its starting point,

$$H = H_{atom} + H_{photon} + H_{inter}. \quad (2.5)$$

The  $H_{atom}$  is the Hamiltonian for the atomic oscillator,

$$H_{atom} = \frac{1}{2} \hbar \omega_{at} (\sigma^+ \sigma + \sigma^- \sigma^+), \quad (2.6)$$

where  $\sigma^+$  and  $\sigma^-$  represent the creation and annihilation operators.  $|a\rangle$  is the ground state,  $|b\rangle$  is the excited state with energies  $-\frac{\hbar\omega_{at}}{2}$  and  $+\frac{\hbar\omega_{at}}{2}$  respectively. The operator rules are,

$$\sigma^+|a\rangle = |b\rangle, \quad \sigma^+|b\rangle = |b\rangle, \quad \sigma^-|a\rangle = |a\rangle, \quad \sigma^-|b\rangle = |a\rangle. \quad (2.7)$$

$H_{photon}$  is the photon Hamiltonian, the single photon mode is represented by a harmonic oscillator with an infinite series of  $|n\rangle$  states with  $n$ , an integer number of photons:

$$H_{photon} = \frac{1}{2}\hbar\omega_{ph}(c^+c^- + c^-c^+), \quad (2.8)$$

The creation and annihilation operators are given by,

$$c^+|n\rangle = \sqrt{n+1}|n+1\rangle, \quad c^-|n\rangle = \sqrt{n}|n-1\rangle, \quad c^-|0\rangle = |0\rangle. \quad (2.9)$$

$H_{inter}$  is the interaction Hamiltonian, the interaction between the atom and cavity,

$$H_{inter} = \hbar g(c^- \sigma^+ + c^+ \sigma^-), \quad \text{where} \quad g = \frac{d}{2\hbar} \sqrt{\frac{\hbar\omega_{ph}}{2\epsilon_0 V_{cav}}}. \quad (2.10)$$

$V_{cav}$  is the cavity volume,  $d$  is the atomic dipole matrix element.  $\sqrt{\frac{\hbar\omega_{ph}}{2\epsilon_0 V_{cav}}}$  is  $E_{vac}$ , the root mean square of the vacuum field amplitude.

At resonance, the detuning,  $\Delta$ , is equal to zero. If there is no interaction then the quantum state with the atom in the ground state and the photon in the cavity, will be degenerate at resonance with the quantum state that has the atom in the excited state and no photon in the cavity. The interaction Hamiltonian lifts this degeneracy and the normal states of the system become a superposition of the bare eigenstates,

$$E_{\pm} = \left(n + \frac{1}{2}\right)\hbar\omega_{ph} \pm \hbar\Omega \quad \text{where} \quad \Omega = \sqrt{g^2(n+1) + \left(\frac{\Delta}{2}\right)^2}, \quad (2.11)$$

$\Omega$  is called the Rabi frequency. At resonance the eigenstates are an equal mixture of



the photon and atom states,

$$|\pm, n\rangle_{\Delta=0} = \frac{1}{\sqrt{2}}(|b, n\rangle \mp |a, n+1\rangle). \quad (2.12)$$

The square of the coefficients give the weighting of the atom and photon, at resonance this is  $\frac{1}{2}$  for each state; when the system is not at resonance the mixing coefficients become unequal. The coefficient depends on the detuning and the strength of interaction which can be characterised by the Rabi splitting.

As an example, to illustrate the relevance of this model for the system we study, if we take  $|e\rangle$  as the exciton state and  $|c\rangle$  as the cavity state, for the LPB ( $|lp\rangle$ )[34],

$$|lp\rangle = C_e|e\rangle + C_c|c\rangle \quad (2.13)$$

the coefficients are give by,

$$C_e = \sqrt{\frac{\Delta + (\Delta^2 + \Omega^2)^{\frac{1}{2}}}{2(\Delta^2 + \Omega^2)^{\frac{1}{2}}}} \quad C_c = -\frac{\Omega}{\sqrt{2(\Delta^2 + \Omega^2)^{\frac{1}{2}}(\Delta + [\Delta^2 + \Omega^2]^{\frac{1}{2}})}} \quad (2.14)$$

Here, the square of these coefficients give the exciton and cavity fractions, and are sometimes known as the Hopfield coefficients.

Moving back to the atomic model and looking at the eigenstates defined by equation (2.12), even when  $n = 0$  there is a splitting. This is termed the Vacuum Rabi Splitting (VRS) [35] and is the interaction between the atom and the vacuum field. At resonance it is given by,

$$\Omega_0 = \frac{dE_{vac}}{\hbar} = \frac{d}{\hbar} \sqrt{\frac{\omega_{ph}\hbar}{2\epsilon_0 V_{cav}}}. \quad (2.15)$$

In physical terms, what does this split spectrum mean? One way to picture this in the time domain is when an atom in a high finesse cavity emits a photon it is stored by the cavity until it is reabsorbed by the atom. This is sometimes termed Vacuum Rabi Oscillation (VRO). VRS and VRO have been observed in atomic physics [36, 37].

For strong coupling to exist between the cavity mode and the atomic transition the interaction between them must be greater than the damping rate,  $g > \gamma_{ph}, \gamma_{at}$ . The cavity field amplitude damping rate,  $\gamma_{ph}$ , is presumed to be due to the coupling to free space radiation modes and  $\gamma_{at}$  is the atomic dipole damping rate. Another way of viewing this is that if the damping is too fast the system will not have time to oscillate and the system will be in the weak coupling (perturbative) regime. As the new modes of the system are superpositions of the photonic and electronic states then the damping would be expected to be a linear average of the two states, and at resonance the average decay rate of the system is,

$$\frac{1}{\tau} = \frac{1}{2} \left( \frac{1}{\tau_{at}} + \frac{1}{\tau_{ph}} \right) \quad (2.16)$$

where  $\tau_{at}$  is the lifetime of the atom,  $\tau_{ph}$  is the lifetime of the photon<sup>2</sup>. If the system is away from resonance the decay rate will tend towards  $\tau_{at}$  or  $\tau_{ph}$  depending on whether it is atom-like or photon-like.

Increasing the number of atoms,  $N$ , is expected to increase the interaction characterised by an increase in the dipole interaction  $g$  and hence the splitting. The dipole interaction is dependent on the atomic dipole matrix element,  $d$ . By increasing the number of atoms we increase the oscillator strength as  $f_{at} \propto d^2$  [11]. The number of atoms is proportional to the oscillator strength, therefore using equation (2.15) we can state,

---

<sup>2</sup>This is for atomic systems where the added complication of inhomogeneous broadening is not problem due to the small atom densities. There is doppler broadening however this results only in the observation of the VRO being distributed in energy, the states themselves are not inhomogeneously broadened. However, inhomogeneous broadening must be addressed in semiconductor systems.

$N \propto f_{at} \propto d^2 \propto \Omega^2$  thus  $\Omega \propto \sqrt{N}$  or the splitting is dependent on the square root of the number of oscillators.

Hence, despite the large damping of the optical transitions, strong coupling can be seen in semiconductors due to the large number of effective oscillators,  $N$ , enhancing the VRS [10]. To estimate VRS in a semiconductor system using this atomic-CQED model we use oscillator strength instead of dipole moments. For QW excitons in a planar microcavity the oscillator strength per unit area is  $\frac{f}{S}$  ( $= \frac{8f_{at}}{\pi a_0^2}$  in the 2-D limit), so the VRS may be expressed as,

$$\hbar\Omega = \sqrt{\frac{N_q}{2m\epsilon_0 L_{cav}} \left(\frac{f}{S}\right)}, \quad (2.17)$$

where  $N_q$  is the number of QWs and  $L_{cav}$  is the effective cavity length (including penetration into the mirrors). The only reason strong coupling is attainable in semiconductors is due to the large number of oscillators interacting with the cavity, unlike the case of atomic systems where strong coupling is achieved with one atom.

### 2.3.2 Linear dispersion theory

In 1990 Zhu *et al.* [38] demonstrated that linear dispersion theory can be used to obtain VRS. In his model he used  $N$  classical Lorentzian dipole absorbers interacting with a single cavity mode. The dispersive dielectric constant of the oscillators is given by:

$$\epsilon(\omega) = \overline{n(\omega)^2} = \epsilon_\infty + \left(\frac{Nfe^2}{m\epsilon_0}\right) \frac{1}{\omega_{at}^2 - \omega^2 - i\gamma_{at}\omega}. \quad (2.18)$$

Their resonant frequency is given by  $\omega_{at}$  and is assumed to be near the cavity frequency  $\omega_{cav}$ .  $n(\omega)$  is the frequency dependent refractive index,  $f$  is the oscillator strength.  $e$

is the electron charge,  $m$  is the electron mass,  $\gamma_{at}$  is the full width at half maximum homogeneous linewidth of the resonance and  $\epsilon_{\infty}$  is the background dielectric constant. The imaginary component of the refractive index corresponds to the absorption by the atoms. The frequency dependent absorption coefficient and refractive index are given by [38],

$$\alpha(\omega) = \alpha_0 \frac{\gamma_{at}}{4(\omega - \omega_{at})^2 + \gamma_{at}^2}, \quad n(\omega) = n_{\infty} - \alpha_0 \frac{c}{2\pi\omega} \frac{(\omega - \omega_{at})\gamma_{at}}{4(\omega - \omega_{at})^2 + \gamma_{at}^2} \quad (2.19)$$

where

$$\alpha_0 = \frac{2Nfe^2}{mc\gamma_{at}}. \quad (2.20)$$

$\alpha_0$  is the line-centre absorption coefficient and  $n_{\infty}$  is the background refractive index. Then, using standard multibeam interference analysis [39] where  $L$  is the thickness of the two-level atomic system, it can be shown that the transmission ( $T_c$ ), reflection ( $R_c$ ) and Absorption ( $A_c$ ), where  $1=R_c+A_c+T_c$ , is,

$$T_c(\omega) = \frac{(1 - R)^2 \exp(-\alpha L)}{[1 - R \exp(-\alpha L)]^2 + 4R \exp(-\alpha L) \sin^2(\frac{\phi}{2})} \quad (2.21)$$

$$R_c(\omega) = \frac{[1 - \exp(-\alpha L)]^2 R + 4R \exp(-\alpha L) \sin^2(\frac{\phi}{2})}{[1 - R \exp(-\alpha L)]^2 + 4R \exp(-\alpha L) \sin^2(\frac{\phi}{2})} \quad (2.22)$$

$$A_c(\omega) = 1 - T_c(\omega) - R_c(\omega) = \frac{(1 - R)(1 - \exp(-\alpha L))(1 + R \exp(-\alpha L))}{[1 - R \exp(-\alpha L)]^2 + 4R \exp(-\alpha L) \sin^2(\frac{\phi}{2})} \quad (2.23)$$

where  $R$  is the intensity reflection coefficient and  $\phi$  is the round trip phase shift given by,

$$\phi = \frac{2\pi(\omega - \omega_{cav})}{FSR} + \frac{4\pi(n(\omega) - n_{\infty})L\omega}{c} \quad FSR = F\gamma_{cav} = \frac{c}{2L_{cav}} \quad (2.24)$$

$FSR$  is the Free Spectral Range and  $F$  is the cavity finesse.

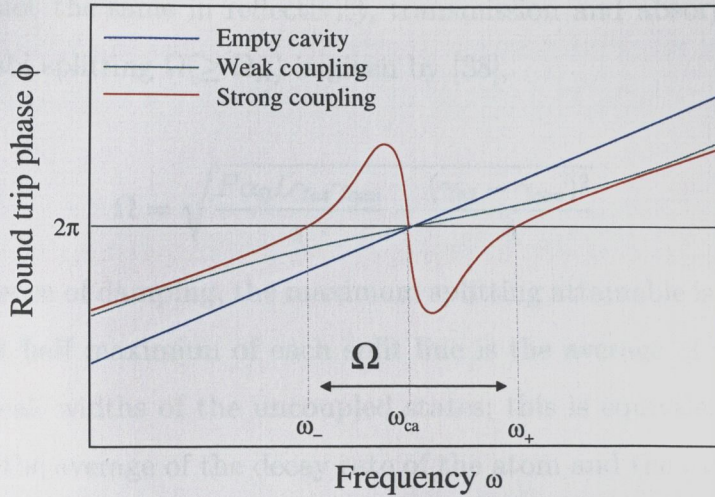


Figure 2.3: Phase advance versus frequency for a bare cavity, a cavity in the weak coupling regime and the strong coupling regime which shows the origin of the two normal modes at  $\omega_-, \omega_+$ .

Looking at the phase can give some insight into the linear dispersion theory. The simplest case is when the input frequency is resonant with the cavity frequency and there is no absorber in the cavity. The background refractive index,  $n_\infty$ , is then 1 and the phase becomes,  $\phi = \frac{4\pi L\omega}{c} = \frac{4\pi L}{\lambda}$ . When the round trip phase is  $2\pi$  a resonance is formed in the cavity and a transmission maximum occurs. This is also apparent from equation (2.21); where it is obvious that the transmission maximum occurs when  $\phi = 2\pi$ . This occurs once in the case of a bare cavity, see figure 2.3. Including absorption in the cavity results in a phase of  $\phi = \left(\frac{4\pi L\omega[n(\omega)-1]}{c}\right)$ . For weak dispersion the phase solution of  $2\pi$  still only occurs once, see figure 2.3. However, for strong dispersion the absorber gives rise to two additional phase solutions ( $\phi = 2\pi$ ), see figure 2.3. Initially one might expect ~~three~~ three transmission maxima, however, the absorption at the central frequency prevents much transmission, resulting in only two transmission peaks. This strong coupling regime requires that the Lorentzian absorber is sufficiently narrow (such that absorption only occurs at  $\omega_{cav}$ ) and also that the cavity finesse is

sufficiently high. This can be intuitively thought of as a requirement that the Rabi oscillation must be faster than the decay rate of the cavity or the excitation.

The splitting is not the same in reflectivity, transmission and absorption [40],  $\Omega_T \geq \Omega_R \geq \Omega_A$ , the Rabi splitting  $\Omega(\geq \Omega_A)$  is given by [38],

$$\Omega = \sqrt{\frac{F\alpha_0 L \gamma_{at} \gamma_{cav}}{\pi} - \frac{(\gamma_{at} - \gamma_{cav})^2}{4}} \quad (2.25)$$

Thus, in the presence of damping, the maximum splitting attainable is when  $\gamma_{cav} = \gamma_{at}$ . The full width at half maximum of each split line is the average of the full width at half maximum peak widths of the uncoupled states; this is equivalent to saying that the decay rate is the average of the decay rate of the atom and the cavity, see equation (2.16). Substituting the oscillator strength ( $f = \frac{2m\omega}{e^2\hbar} d^2$ ), the definition of finesse and equation (2.20) into the maximum Rabi splitting we obtain,

$$\Omega = \frac{d}{\hbar} \sqrt{\frac{\omega_{ph}\hbar}{2\epsilon_0 V_{cav}}} = \frac{dE_{vac}}{\hbar} \quad (2.26)$$

This is the same as equation (2.15) and shows the equivalence of the two models. This result is not surprising as the quantum theory of the interaction of an electromagnetic field and an atom is a well known example where classical and quantum models agree.

The modelling done in this thesis is based on the linear dispersion model. Although more complex models by theorists are drawn on for understanding and comparison, they are beyond the scope of this thesis.

To implement the linear dispersion model we wrote a program based on the transfer matrix method. This is a commonly used method for a dielectric cavity and is well suited to computer implementation. The method is based on solving Maxwell's equations in a multi-layer structure accounting for the boundary conditions (the tangential components, relative to the sample surface, of the resultant electric and magnetic fields

are continuous across the interfaces). The excitons are described by the Lorentz oscillators with a dispersive dielectric constant, *i.e.* they are assumed equivalent to atoms confined in an absorbing layer, of thickness  $L$  as described in equation (2.18). The mathematics is simple and the reader is referred to two good texts [41, 42] and a lecture by Savona [43] who deals specifically with the linear optical properties of cavity polaritons.

Having described two generic strong coupling models we now describe in detail the specific components used in our strong coupling semiconductor samples. Firstly the mirrors, which are distributed Bragg reflectors, and then QW excitons.

## 2.4 Distributed Bragg reflectors

In the above section we discussed some models describing strong coupling. To create strong coupling a large interaction between the atom or electronic excitation and the optical field is needed. Initially we look at confining the optical field with the use of mirrors spaced very closely together. This microcavity confinement of the optical field has already been discussed with respect to the weak coupling regime. It is the strong interaction between the optical field and the electronic excitation which differentiates between the strong and weak coupling regimes. Increased confinement of the optical field is needed in strong coupling samples, this is obtained with extremely high mirror reflectivities.

One possible type of mirror that can be used to create optical confinement is the metallic mirror. These can have high reflectivities of 80-95% over a very wide spectral range (visible to infrared) but unfortunately they have zero transmission, and therefore light cannot be coupled to the outside unless they are exceptionally thin [44]. Total internal reflection can also be used to confine the light, and is generally used when there is more than one dimensional confinement. However total internal reflection





The reflectivity of a DBR is highly dependent on wavelength as it relies on phase differences. The wavelength region around the central Bragg wavelength that has a high reflectivity is termed the stopband [45] and is given as:

$$\Delta\lambda_{stopband} = \frac{2\lambda_{Brg}\Delta n}{\pi n_{eff}}, \quad (2.27)$$

where  $n_{eff}$  is the effective refractive index of the mirror.  $\Delta n = n_H - n_L$  and  $\lambda_{Brg}$  is the wavelength that the layers were designed for. The wavelength range of the stopband is independent of the number of dielectric layers, unlike the reflectivity, which increases with the number of layers: increasing the number of layers will flatten the stopband toward unity. Usually the wavelength stopband is larger than a typical dipole emission width, so leakage due to a drop in reflectivity beyond the wavelength range of the stopband is not a problem. There is however an angular stopband which is comparatively small [29], defined as

$$\Delta\theta_{stopband} = \pm 2\sqrt{\frac{\Delta n}{\pi n_{eff}}}. \quad (2.28)$$

This may allow a dipole inside a distributed Bragg structure to radiate off-axis into 'leaky modes'. The solid angle of the leaky modes is between the end of the DBR stopband and the angle at which the emitted light is totally internally reflected. The fraction of solid angle of the leaky modes is given by [32],

$$\frac{\Omega_{leaky}}{4\pi} \approx 1 - \frac{1}{4n_{eff}^2} - \frac{\Delta n}{\pi n_{eff}} - \sqrt{1 - \left(\frac{n_{eff} - \Delta n}{n_{eff}}\right)^2}. \quad (2.29)$$

This emission loss is a major concern in microcavity design. One can understand why these stopbands occur, as the mirror is a resonant structure and the high reflectivities are due to a series of reflections adding in phase. At shorter or longer wavelengths the reflections will no longer add in phase. With a metallic mirror the reflection phase is

$\pi$ ; however across the Bragg reflector it varies with wavelength and is only  $\pi$  at  $\lambda_{Brg}$ .

When a cavity is placed inside two layers of DBRs there is some penetration into the DBR of the optical mode. This can be visualized as an ideal mirror sitting some distance  $L_{pen}$  into the Bragg mirror.  $L_{pen}$  is approximated by [31]:

$$L_{pen} = \left(\frac{\lambda}{2}\right) \frac{n_L}{2n_{eff} \Delta n} \quad (2.30)$$

From this it is obvious that to decrease the penetration depth one should increase  $\Delta n$  but as mentioned before this can be difficult due to lattice mismatch. This penetration must be taken into account when designing (and understanding) a microcavity.

In this section a method for creating a microcavity which can confine the optical mode has been discussed. We now turn our discussion to an atom-like transition in a semiconductor QW, the exciton.

## 2.5 Quantum well excitons

A QW is a very thin layer whose bandgap energy is smaller than the layers it is sandwiched between. There are two types of QW; our QW is a type-I where both electron and hole are confined in the same material, see figure 2.5(a). Type-II QWs confine the electron and hole in different layers. Although electrons and holes are free to move in the planes of the layers, they are affected by discontinuities normal to the layer. This gives rise to discrete energy states in the QW. The energies of these states (assuming an infinitely deep QW) are given by,

$$E = E_g + \frac{\hbar^2 \pi^2 N^2}{2\mu L^2} \quad (2.31)$$

where  $E_g$  is the bandgap energy of the QW material,  $L$  is the QW thickness,  $N$  is an

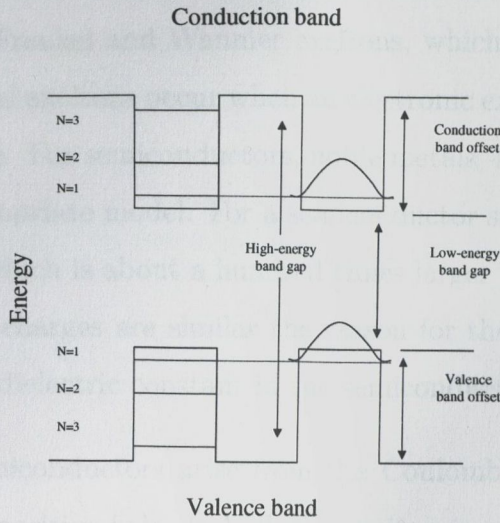


Figure 2.5: Energy diagram of a type-I QW. The minimum energy is not the bottom of the energy band in a QW, the discrepancy is referred to as the zero point energy. A schematic of the wavefunction of the lowest energy exciton is shown.

integer and  $\mu$  is the reduced effective mass,

$$\frac{1}{\mu} = \frac{1}{m_e} + \frac{1}{m_h}, \quad (2.32)$$

where  $m_e$  is the mass of the electron and  $m_h$  is the mass of the hole. From these equations we can appreciate that the minimum energy is not the bandgap energy, the lowest state has a positive zero point energy, see figure 2.5(a).

It should be mentioned that the valence band consists of two different kinds of hole whose angular momentums are,  $j_z = \pm\frac{3}{2}$  and  $j_z = \pm\frac{1}{2}$ , with corresponding masses of  $m_{lh}$  for the light hole and  $m_{hh}$  for the heavy hole.<sup>3</sup> This is important because the energy in the QW depends on the mass.

<sup>3</sup>This is a point of confusion. In bulk the  $m_{hh}$  corresponds to  $j_z = \pm\frac{3}{2}$  and  $m_{lh}$  corresponds to  $j_z = \pm\frac{1}{2}$ . In two dimensions, although the light hole is light in the plane perpendicular to the QW it is heavy in the plane parallel to the QW, and vice versa for the heavy hole. This leads to anti-crossing of the dispersion curves with strong band mixing and non-parabolic dispersion [46].

Excitons can be thought of as a quantum of excitation. Excitons are normally subdivided into two kinds, Frenkel and Wannier excitons, which are two extremes of the same phenomena. Frenkel excitons occur when an electronic excitation is closely bound to an atom or a molecule. For semiconductors, noble metals, and halides, the Wannier exciton is the more appropriate model. For a semiconductor such as ours the diameter is approximately  $100\text{\AA}$  which is about a hundred times larger than the diameter of the hydrogen atom. As the charges are similar the reason for the weakened attraction is due to screening by the dielectric constant in the semiconductor.

Wannier excitons in semiconductors arise from the Coulomb attraction between the negative electron and a positive hole. In bulk the exciton is a crystalline excited state and is free to move about the crystal. The exciton motion can be separated into a centre of mass motion and a relative coordinate of the electron and hole. As we are looking at direct optical excitations, the small wavevector of light results in only excitons with negligible centre of mass motion being optically generated. When this is taken into account we are looking at only the relative motion of an electron and hole and the hydrogen atom analogy becomes appropriate. The Coulomb attraction is of course screened by the dielectric constant and the binding energy is approximately  $5\text{meV}$  compared to the  $13.6\text{eV}$  for the hydrogen atom. The energy of these bound states can then be shown to be [47],

$$R_{3D} = \frac{\mu e^4}{2(4\pi\epsilon_0)^2 \hbar^2} = \frac{e^2}{2(4\pi\epsilon_0)a_{3D}}, \quad (2.33)$$

where  $\mu$  is the reduced mass of the electron and hole,  $\epsilon_0$  is the static dielectric constant of the well material and  $a_{3D}$  is the bulk Bohr radius defined as,

$$a_{3D} = \frac{4\pi\epsilon_0 \hbar^2}{\mu e^2}. \quad (2.34)$$

The atomic analogy of the exciton is common in semiconductor strong coupling models.

However it should be noted that there are important differences between atomic and excitonic systems. For example, when an exciton emits light it is annihilated, unlike an atom, and therefore cannot recoil to conserve momentum. Another difference is that the exciton is a crystalline excitation and as such has dispersion, see section 2.18.

When the exciton is confined to two dimensions, *e.g.* in an ideal QW, the binding energy is given by,

$$R_{2D} = \frac{R_{3D}}{(n - \frac{1}{2})^2}, \quad (2.35)$$

whilst the radius halves,  $a_{2D} = \frac{a_{3D}}{2}$  ( $n$  is an integer). Thus when moving from three to two dimensions there is an increase in the binding energy by a factor of four ( $\approx 20\text{meV}$ ); a relative increase in the separation from the first excited state to the second excited state occurs and the oscillator strength also increases. These changes result in excitonic features being much stronger in two dimensions. A nonintuitive feature of the confinement of the exciton is that by forcing confinement in the  $z$ -direction (this is the direction perpendicular to the QW) the exciton radius also shrinks in the  $x,y$ -direction [47].

Another important effect in moving from two to three dimensions is that the crystal symmetry is broken. Translational symmetry results in conservation of crystal momentum. This is broken in the  $z$ -direction for the QW exciton, enabling excitons to interact with photons without  $k_z$  conservation.

Before moving on to discuss a realistic two dimensional exciton it should be mentioned that the Coulomb interaction between electrons and holes distorts the wavefunction of electrons and holes and enhances the oscillator strength; this not only results in the formation of excitons but also increases the absorption in the bandgap in both two and three dimensions. This is taken into account by the *Sommerfeld factor*.

Models for realistic QW excitons must take into account the finite size of the QW, as the QW size decreases the exciton begins to penetrate into the barrier material. If the QW was of zero thickness the exciton would revert to a three dimensional exciton in the barrier material. The attainable increase in binding energy is nearer a factor of two than the theoretically possible factor of four, and similarly the radius and oscillator strength fall within the predicted two and three dimensional values.

The exciton can be generated from either the light hole or the heavy hole. We do not discuss the rather complicated issue of the relative binding energies of the heavy hole and light hole exciton which depends on the confinement. We only state that in our sample due to strain the heavy hole exciton is at lower energy (more strongly bound) so that we can ignore the interaction with the light hole.

In the next section we present some of the work previously performed on QWs as this will enable us to present comparative studies with some of the work in this thesis. Terminology is presented that is used with regard to QWs that will be used throughout this thesis.

### 2.5.1 Quantum wells summary

Much of the work presented throughout this thesis on cavity polaritons has been previously performed on excitons. In early work on QWs, due to growth phenomena, many excitons were localised in 'islands' [48]. At low energies the excitons are likely to be localised and this would result in a relaxation of the wavevector conservation (the wavevector is no longer a good quantum number). This is not a problem that we will consider in this thesis as the photon component of the polariton will result in a delocalisation of the polariton which allows us to assume that the polariton in plane wavevector is conserved. Many excitonic interactions are now well understood and can help us to understand the strong coupling between QW excitons and photons. The relevant work on excitons is placed within each chapter for comparison but a brief

overview is presented here.

Phonon scattering via the interaction between excitons and longitudinal optical phonons homogeneously broaden [49] the exciton linewidth and longitudinal optical phonons are also an important relaxation channel for excitons with high momentum [50]. However the work done throughout this thesis is at low temperatures where the optical phonon population is negligible, see chapter 5. A more important consideration in this work is the exciton interaction with acoustic phonons, as the acoustic phonon density is sizeable at the low temperatures used in our work (10K). With the exception of scattering due to disorder, acoustic phonons make the strongest contribution to the low temperature linewidth of the excitons at low exciton densities. Acoustic phonon scattering of excitons has been studied using the linewidth dependence on temperature and a linear relationship was observed [51, 52]. This linear relationship was observed down to the lowest temperatures examined ( $\approx 5\text{K}$ ). This linearity requires two conditions: firstly, the acoustic phonon density is approximately linear with temperature at the temperatures studied and secondly, the exciton dispersion curve must be essentially flat in the relevant region.

Another important consideration in the interactions of excitons is the effect of excitation intensity. A considerable amount of work has been performed to examine the effect of excitation intensity on excitons in QWs [53, 54, 55, 56, 57]. We will not enter into the theory here but will give an intuitive explanation of the relevant intensity effects in this thesis and discuss some of the experimental work performed.

As excitation intensity increases, collisional broadening is the first appreciable effect to be encountered in QW excitons under resonant and non-resonant excitation [58]. Collisional broadening is the increase in homogeneous linewidth of the exciton due to exciton Coulomb interaction. It is important to note that when broadening occurs, although the exciton line broadens and the central peak absorption bleaches the integrated absorption remains constant. Collisional broadening was briefly mentioned by

Schmitt-Rink, Chemla and Miller [59]. We review the theory of collisional broadening and study the nonlinear effects on the polariton in detail in chapter 6.

At high intensities the oscillator strength of the exciton becomes saturated. The high intensity nonlinear effects were experimentally investigated by Chemla and Miller [60] and Hegarty and Sturge [48]. They noted two contributions which change the oscillator strength of the exciton. A blocking mechanism which is due to Pauli's exclusion principle and an exciton wavefunction renormalisation due to modification of the electron-hole pairs.

Firstly the blocking which is due to Pauli's exclusion principle results in Phase Space Filling (PSF). Phase space filling is intuitively easy to understand as a result of the fermionic particles, which make up the exciton, filling up the fermion phase space. Band filling is a result of the same principle. This fermionic phase space can be filled either by excitons through resonant pumping or by free electrons and holes which are taking up the same phase space from which the exciton would be made.

Secondly the wavefunction can be renormalised as the bound-state binding energy is weakened in the presence of electron-hole pairs. This results in an increase in the radius of the exciton in real space, with a resulting decrease in oscillator strength. This in turn reduces the probability of finding an electron near a hole and results in a further decrease in oscillator strength. There are two causes of wavefunction renormalisation, exchange effects and long range Coulomb effects.

The long-range direct Coulomb correlations are weak. For exciton excitation they can be thought of as corresponding to Van der Waal's forces between the excitons. For electron hole excitation they are the cause of screening, changing the dielectric constant, which is a small effect in two dimensional excitonic systems.

A more significant cause of saturation of the oscillator strength are the exchange effects. These cause a saturation of the oscillator strength by the gain of energy that parallel



spin particles acquire by avoiding each other and the weakening of attractive electron hole interaction due to the Pauli exclusion principle. They contribute roughly the same amount to the reduction of oscillator strength as PSF, for both resonant and non-resonant excitation [54].

Another effect resulting from pumping above the band edge is Band Gap Renormalisation (BGR). This is a red shift of the bandgap due to screened exchange and Coulomb hole interaction. Generally at moderate intensities the Coulomb hole interaction, that is the energy gain from the charge polarisation of material, is larger.

Another intensity effect seen is a shift in the exciton binding energies. The shift in energy can be a blue or red shift depending on the excitation energy and on the dimensionality. For resonant excitation in two dimensional systems, that is for selective exciton excitation, one generally obtains a blue shift due to weakening of the exciton binding energy [53] from the strong repulsive force due to Pauli's exclusion principle. For non-resonant excitation the blue shift of the exciton can be cancelled by the red shift of the band (BGR) with the result that the exciton energy remains unchanged. This was theoretically predicted to be the case by Zimmermann *et al.* [61] and has been demonstrated experimentally in QW excitons [53].

We have presented a synopsis of strong coupling and the characteristics of the mirrors and electronic excitation used in our sample, DBRs and QWs respectively. We discuss next previous work on polaritons, which are the new states of the system in the strong coupling regime.

## 2.6 Bulk polaritons

We will concentrate on the two dimensional confinement of the exciton-polaritons that will be studied in this thesis. However before continuing our discussion on these we should briefly mention the large amount of research on bulk polaritons (three dimen-

sional), introduced by J. J. Hopfield in 1958 [62] and researched in the 1960s-1970s [8, 9].

The bulk polariton is the result of excitons strongly interacting with the transverse electric field of a photon. The most important difference between the bulk polaritons and the two dimensional polaritons is that the crystal momentum conservation is broken in the two dimensional system. This allows the two dimensional exciton to interact with a continuum of photon states. The bulk exciton however conserves crystal momentum in all three directions. As a result of this the excitons can strongly interact with only one photon. An exciton with a given wavevector and polarisation only interacts with a photon with the same wavevector and polarisation. This is a coupling between two discrete states resulting in a stationary state (ignoring dissipative coupling) as there is no coupling to a density of states into which the polariton can decay.

Once the polariton has been formed the energy oscillates back and forth between the exciton and photon state. In the two-level atomic analogy, this oscillation is equivalent to the atom interacting with only a single mode of the cavity. This results in a splitting of the energy levels as discussed above. The vacuum rabi-splitting (VRS) [63]<sup>4</sup> is,

$$\hbar\omega_c = \hbar e \sqrt{\frac{\pi f}{\epsilon_\infty m_0 V}} \quad (2.36)$$

$V$  is the crystal volume,  $f$  is the oscillator strength,  $\epsilon_\infty$  is the background dielectric constant,  $m_0$  is the free electron mass and  $e$  is the charge on the electron.

The Rabi-splitting in three dimensions will be larger than in two dimensions, even though the exciton binding energy is weaker in three dimensions, due to the discrete state interaction.

The polariton formation does not allow radiative decay of the exciton inside an infinite

---

<sup>4</sup>To be consistent with the previous work presented here  $\omega_c$  is twice the value quoted by Andreani [63].

crystal. Conversely, to form a polariton, the exciton radiation interaction will not be sufficient. Formation at the surface can occur only as a result of the imperfect nature of the surface. Thus, for the polariton to radiatively decay depends on polariton propagation to the surface of the sample. The radiative decay rate then depends on the reflection coefficient at the surface, the polariton group velocity and its distance from the surface. Weisbuch and Ulbrich [9] studied the effects of this following an analogy with carrier diffusion to explain the difference between the photoluminescence between the front and back of a narrow GaAs sample. The radiative recombination of the polariton will also depend on non-radiative decay due to scattering by impurities, and thermalisation processes.

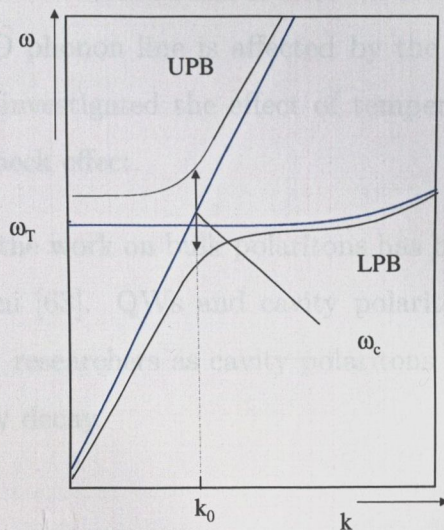


Figure 2.6: Schematic representation of the dispersion of the upper and lower polaritons (black lines). The transverse photon and exciton mode are shown (blue lines).

The fact that the excitonic photoluminescence was not following the expected thermal distribution at low temperatures was important grounds for the acceptance of the polariton picture. The three dimensional polaritons have a bottleneck effect which prevents the emission following a thermal distribution. This bottleneck also occurs in the two dimensional cavity polaritons, and will be discussed in section 2.7.2. Looking

at figure 2.6 the lower branch has a ‘knee’ shaped dispersion curve above the knee the thermalisation processes are very effective due to the large density of states. However, below the knee there is a decrease in the density of states and an increase in the group velocity, resulting in an increase in the radiation rate. This results in a bottleneck effect at the knee.

An excellent paper by Sumi [8] investigates luminescence of bulk polaritons at low temperatures. He showed that the radiative decay rate increased for smaller samples, larger temperatures and lower impurity density as expected within the polariton model. Sumi also investigated the bottleneck effect using the Longitudinal Optical (LO) phonon side-band and the zero LO phonon line. The LO phonon side-band is dependent on the thermalised distribution of excitons above the knee in the dispersion curve whilst the zero LO phonon line is affected by the polariton bottleneck. Using the ratio of these Sumi investigated the effect of temperature, sample thickness and impurities on the bottleneck effect.

A very small amount of the work on bulk polaritons has been presented here, for more information see Andreani [63]. QWs and cavity polaritons systems [10], have been increasingly favoured by researchers as cavity polaritons do not need to propagate to the surface to radiatively decay.

Figure 2.7: Dispersion curves showing the UPE, LPE, uncoupled exciton and uncoupled photon. (a) Dispersion curve at resonance  $\omega_c = \omega_{exc}$  with  $\gamma_{exc} = 0.01\omega_{exc}$ . The uncoupled exciton and photon dispersion is essentially flat in the region we are interested in. (b) The dispersion at resonance with an exciton strength that is decreased by a factor of 10 from part (a). This results in a crossing of the branches at  $k_x = 0$  and the

## 2.7 Cavity polaritons

We now look at two specific properties of the cavity polariton, dispersion and broadening. Dispersion will be discussed first; it is a property of strong coupling in excitonic systems which is not relevant for atomic systems.

## 2.7.1 Dispersion

From the work on the planar microcavity and the ideal QW we realize that the excitons in QWs are translationally invariant in two directions resulting in conservation of in-plane momentum. All photon with finite in-plane momentum couples to excitons in QWs. The exciton dispersion is essentially flat because of coupling to the photon.

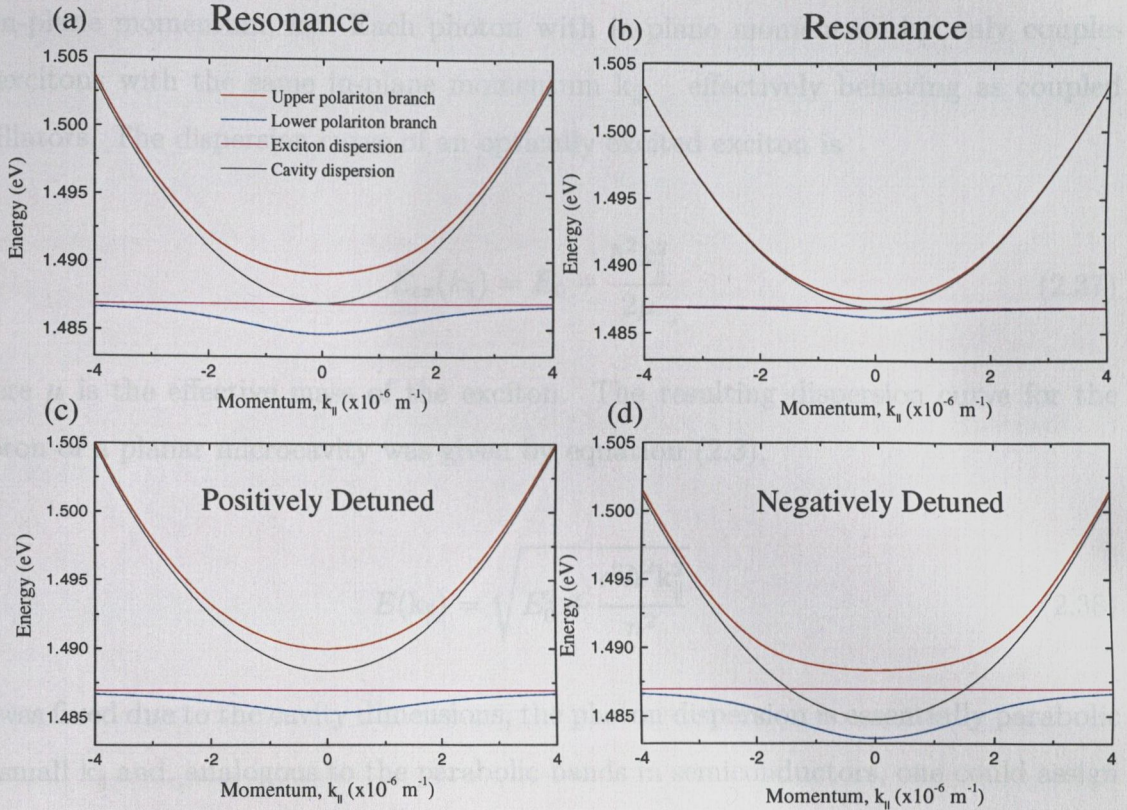


Figure 2.7: Dispersion curves showing the UPB, LPB, uncoupled exciton and uncoupled photon. (a) Dispersion curve at resonance with  $f_{osc} = 9 \times 10^{-6} \text{ cm}^{-2}$ . The uncoupled exciton and photon dispersion curve have the same energy at  $k_{\parallel} = 0$ . The exciton dispersion is essentially flat in the region we are interested in. (b) The dispersion at resonance with an oscillator strength that is decreased by a factor of 10 from part (a). This results in a reduced splitting of the branches at  $k_{\parallel} = 0$  and the recovery of the bare exciton and photon mode more quickly for increasing in-plane wavevector. (c) and (d) show the effect of detuning. (c) A positive detuning, the energy of the cavity is greater than the energy of the exciton. The dispersion curve of the LPB is more weakly coupled to the photon dispersion curve. (d) At a negative detuning the energy of the cavity is less than the energy of the exciton and the upper polariton branch is more strongly coupled to the cavity dispersion.

in detail in chapters 5 and 6.

From the models on the strong coupling regime we expect that for a greater oscillator

## 2.7.1 Dispersion

From the work on the planar microcavity and the ideal QW we realise that the excitons in QWs are translationally invariant in two-directions resulting in conservation of in-plane momentum,  $k_{\parallel}$ . Each photon with in-plane momentum  $k_{\parallel}$  only couples to excitons with the same in-plane momentum  $k_{\parallel}$ , effectively behaving as coupled oscillators. The dispersion curve of an optically excited exciton is

$$E_{ex}(k_{\parallel}) = E_0 + \frac{\hbar^2 k_{\parallel}^2}{2\mu}, \quad (2.37)$$

where  $\mu$  is the effective mass of the exciton. The resulting dispersion curve for the photon of a planar microcavity was given by equation (2.3),

$$E(k_{\parallel}) = \sqrt{E_0^2 + \frac{c^2 \hbar^2 k_{\parallel}^2}{n^2}}. \quad (2.38)$$

$E_0$  was fixed due to the cavity dimensions, the photon dispersion is essentially parabolic for small  $k_{\parallel}$  and, analogous to the parabolic bands in semiconductors, one could assign an effective mass. This would be approximately  $10^4$  times smaller than the effective mass of the exciton. The exciton dispersion is effectively flat in the small  $k_{\parallel}$  region which we are interested in. This is due to its large effective mass compared to that of the cavity photon.

The initial work on the dispersion of the cavity polariton was performed using photoluminescence [64, 65]. The dispersion of the polariton will depend on the strength of the coupling and on the detunings, see figure 2.7. The polariton dispersion curve has a dramatic impact on the scattering processes of the polariton; this will be discussed in detail in chapters 5 and 6.

From the models on the strong coupling regime it is evident that for a greater oscillator

strength there will be a greater splitting in the energy, see figures 2.7(a) and (b). From these figures it can be ascertained that the strong coupling will also lead to large modification in the dispersion curves for the in-plane wavevector; it is unsurprising that larger coupling strengths cause a greater effect on the dispersion curves. Another feature shown in figure 2.7 is the effect of detuning on the dispersion curve, from (c) and (d) it is apparent that the LPB dispersion is more exciton-like at positive detunings and more photon-like at negative detunings.

From equation (2.16) it is obvious that the recombination rate can be engineered to be very fast by modifying the cavity decay. It was originally thought that this could be used in ultrafast switching. However, the nature of the dispersion curve has a profound influence on the recombination rate and gives rise to a bottleneck in the relaxation of polaritons.

## 2.7.2 Bottleneck

We have already briefly discussed the bottleneck effect in bulk polaritons, here we present a more detailed analysis of the bottleneck effect in cavity polaritons. The bottleneck effect results from the dispersion curve of the polariton and is important for non-resonant excitation when looking at emission in the strong coupling regime at  $k_{\parallel}=0$ .

Looking initially at the emission at  $k_{\parallel}=0$  on the LPB, after an initial excitation of electrons-holes, the excitons formed relax down the dispersion curve to the bottom of the exciton-like branch of the lower polariton; there they form a Boltzmann distribution. However after this point there is a bottleneck preventing further relaxation to  $k_{\parallel}=0$ . The bottleneck effect occurs due a decrease in the relaxation rate to  $k_{\parallel}=0$  and an increased radiative rate on reaching  $k_{\parallel}=0$ . The decreased relaxation rate is mainly due to the increased slope of the lower polariton dispersion resulting in a smaller density of states and the decreased scattering rate of polaritons by acoustic phonons with

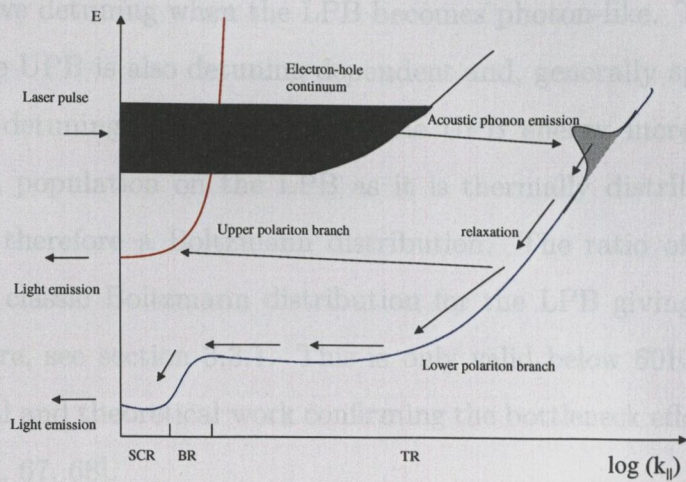


Figure 2.8: Schematic representation of the polariton dispersion, taken from [18]. Illustrating polariton formation from a free-carrier thermal reservoir via absorption or emission of acoustic phonons. SCR: strong coupling region, BR: Bottleneck region and TR: thermal region.

the necessary energy and momentum to relax the polariton from above the bottleneck to  $k_{\parallel}=0$ . The radiative rate at  $k_{\parallel}=0$  does not depend on the intrinsic radiative rate at  $k_{\parallel}=0$  but rather on the relaxation from the bottleneck to  $k_{\parallel}=0$  which depends on the polariton density feeding into the bottleneck [18]. This suggests that the emission from the LPB is less than it would be if there was a thermalised distribution of polaritons along the LPB. This situation only occurs at temperatures  $<60\text{K}$ . Above this temperature longitudinal optical phonons thermalise the polaritons.

The emission at the UPB is generated from a different process. The UPB polaritons are unlikely to be formed at the electron hole continuum energy due to their small exciton content. The upper polaritons are formed by interbranch scattering. The main source of scattering is elastic scattering, from the LPB that is occupied at the same energy as the bottom of the UPB. These horizontal scattering processes are allowed due to the degeneracy of energy, see figure 2.8. The upper polariton population then follows the exciton-like population of the LPB which will have a thermal distribution.



The  $k_{\parallel}=0$  emission from the LPB is detuning dependent; the emission intensity decreases for negative detuning when the LPB becomes photon-like. The  $k_{\parallel}=0$  emission intensity from the UPB is also detuning dependent and, generally speaking, decreases towards positive detuning. This is because the UPB energy increases, resulting in a smaller exciton population on the LPB as it is thermally distributed. The emission ratio is not therefore a Boltzmann distribution. The ratio of emission will be smaller than the classic Boltzmann distribution for the LPB giving an overestimate of the temperature, see section 3.3.1. This is only valid below 60K. There has been both experimental and theoretical work confirming the bottleneck effect in microcavity polaritons [18, 66, 67, 68].

### 2.7.3 Inhomogeneous broadening

Inhomogeneous broadening of excitons in semiconductor QWs is mainly due to inter surface roughness at the QW interface and alloy broadening. Inhomogeneous broadening results in localised excitons which are trapped in islands, as mentioned in section 2.5. The effect of inhomogeneous broadening on the linear properties of polaritons has been extensively carried out, for two review papers see [69, 70], whereas the effect of inhomogeneous broadening on the nonlinear properties of polaritons have been less extensively studied [71]. Presented here is a brief synopsis of the work relevant to this thesis.

Houdré *et al.* [72, 73] initially investigated the effect of inhomogeneous broadening on the linear properties of the polariton and came to two main conclusions (i) the splitting was unaffected by the amount of inhomogeneous broadening and (ii) provided the inhomogeneous linewidth is small compared to the splitting, the linewidths of the polariton are the average of the homogeneous exciton linewidth and the cavity linewidth. This is a very exciting result as it suggests that the linear homogeneous properties can be resolved within the inhomogeneous system. Houdré [74] showed these

results, which were initially derived from an atomic model, could be modelled using a simple LDT model <sup>5</sup>. The first result, showing that the peak separation is unaffected by the broadening, is unsurprising in LDT theory as the refractive index has a linear relationship with the absorption, via the Kramers-Kronig transformation. Thus the order in which the refractive index is summed has no effect, *i.e.* a transformation of a series of different absorption features summed or a sum of a series of the absorption features which have been transformed individually.

The second result is that the linewidth of the polaritons is the average of the exciton homogeneous linewidth and the cavity linewidth, when the splitting is large compared to the inhomogeneous linewidth of the exciton. This is reproduced here in figure 2.9, the interaction strength is characterised by the oscillator strength.

The resulting decrease in linewidth as the oscillator strength increases can be understood on the basis of a convolution of the Lorentzian and Gaussian absorption functions (*i.e.* the Voigt profile) which results in a Gaussian type line-shape in the central region and a Lorentzian type line-shape in the outer regions. The polariton linewidth is determined by the slope of the round-trip phase shift versus energy; the sharper slope seen at the tail ends of the absorption due to the Lorentzian results in a narrow linewidth and conversely the Gaussian central region gives a shallower slope resulting in a broader linewidth. Savona and Weisbuch [69] support Houdré's results, that the linear optical properties of the polariton are unaffected by the inhomogeneous exciton linewidth provided it is small ( $< 1.2\text{meV}$ ), with a simple quantum mechanical model. It should be noted that if the exciton inhomogeneous broadening is large this is not the case.

Another interesting effect regarding the optical linear properties of the polaritons is that the UPB linewidth is broader than the LPB at resonance, see figures 3.4 and 3.5. This has also been explained using a semi-classical approach [75] and LDT [76].

---

<sup>5</sup>It should be mentioned that this model did include dispersion.

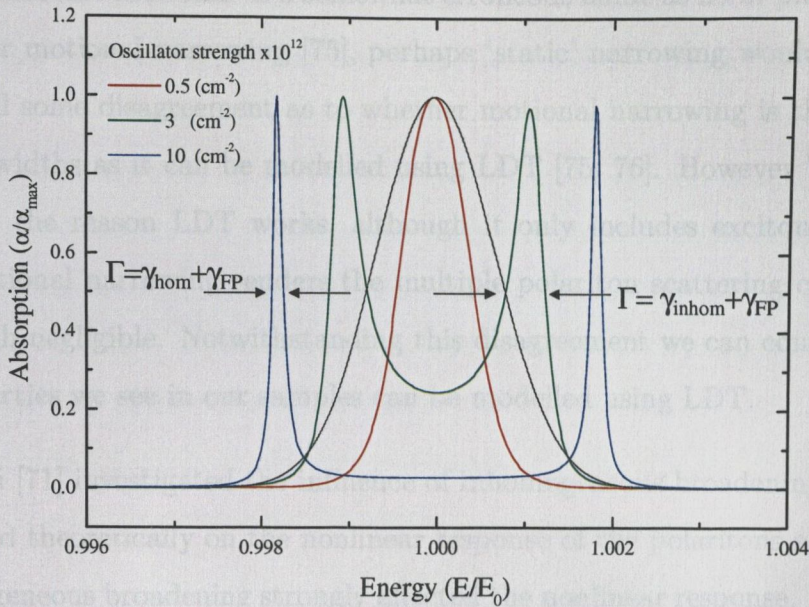


Figure 2.9: Absorption spectra generated using a transfer matrix model showing the homogeneous linewidth resolution for increasing oscillator strengths. This resolution of the homogeneous linewidth within an inhomogeneous system occurs at large oscillator strengths due to the position of the polariton lines. When the polariton lines are in the tail of the convolved (Gaussian and Lorentzian) line functions of the exciton, the dominant absorption lineshape of the exciton will be Lorentzian. The polaritons will be interacting with a homogeneous line function of the exciton. The black line represents the bare exciton, this is spectrally larger than the absorption due to the filtering effect of the cavity.

The explanation using LDT is similar to that used to explain the resolution of the homogeneous linewidth and is due to the asymmetric absorption line of the exciton. The low energy tail decays more quickly resulting in a sharp slope of the round trip phase shift, giving rise to a narrow linewidth, whilst conversely the high energy slope of the round trip phase shift is more gradual resulting in a broader linewidth for the UPB.



These very narrow linewidths and broader UPB linewidths at resonance have been justified on the microscopic scale using ‘motional narrowing’ [77, 78, 79]. ‘Motional narrowing’ is the resolution of the homogeneous linewidth due to the averaging out of

the disorder fluctuation because of the large size of the polariton particle compared to that of the exciton. 'Motional' is a somewhat erroneous name as no in-plane momentum is needed for motional narrowing [75], perhaps 'static' narrowing would be more apt. There is still some disagreement as to whether motional narrowing is the cause of the narrow linewidths as it can be modelled using LDT [75, 76]. However Whittaker [79] asserts that the reason LDT works, although it only includes exciton scattering, is because motional narrowing renders the multiple polariton scattering contribution to the linewidth negligible. Notwithstanding this disagreement we can conclude that the linear properties we see in our samples can be modelled using LDT.

Bongiovanni [71] investigated the influence of inhomogeneous broadening both experimentally and theoretically on the nonlinear response of the polaritons and found that the inhomogeneous broadening strongly affected the nonlinear response. When there is a deep beating at the Rabi frequency in the time-resolved transmission, the nonlinear results (measured using Four Wave Mixing (FWM)) showed little influence of the cavity and the decay time of the time integrated FWM signal was similar to the bare exciton. Although the linear results showed a system in the strong coupling regime the nonlinear results did not exhibit any influence of the cavity on the FWM signal compared to that of the bare exciton. The sample had an inhomogeneous exciton broadening of 4-5meV compared to a splitting of 8meV. Of particular relevance is the decay of the FWM which showed a photon echo, a signature of inhomogeneous broadening, see chapter 4. These results were fitted using numerical solutions to the Maxwell-Bloch equations. Bongiovanni went on to predict that in the limit of Rabi-splitting being greater than four times the inhomogeneous exciton linewidth, the whole exciton population will experience Rabi oscillation; the system is in the strong coupling regime; and a considerable fraction does not show any disorder induced delay. This last consideration implies a considerable amount is homogeneously broadened. This was seen by a large portion of the time resolved FWM occurring at zero time delay, see chapter 4.

## 2.8 Summary

In this chapter we have presented two frameworks within which to view our work. Firstly, that of the strong and weak coupling regimes of optically confined electronic systems and secondly that of previous research carried out on bare quantum wells. We have used two models to illustrate the properties of the strong coupling and have drawn particular attention to the DBR mirrors and the excitons which are the relevant parameters in our semiconductor strong coupling samples. We briefly commented on work performed on three dimensional polaritons. The important features of the microcavity polariton for this thesis were discussed, in particular the dispersion and the broadening type of the polaritons' linewidth.

In this chapter we set out to explain the reasons behind the sample design. We also outline several experiments which were done to investigate the samples' properties. From these investigations important information is obtained and a summary of the information is tabulated at the end of the chapter.

## 3.1 Introduction

To produce a sample in which strong coupling can occur there are two fundamental properties the sample should have: (1) strong optical confinement. This can be created by using high reflectivity mirrors to form a well defined cavity mode as in a Fabry-Pérot interferometer; (2) a well defined excitation with reduced energy levels, such as an atom or a confined exciton. The excitation should be in resonance with the optical resonance.

Growth techniques such as Metal-Organic Chemical Vapour Deposition (MOCVD) [80] and Molecular Beam Epitaxy (MBE) [81] have allowed high quality thin films of semiconductors to be made. Specifically, DBRs (see section 2.4) can be made which have reflectivities of greater than 99.9% [82] enabling strong confinement of the vacuum

field and growth of quantum well structures create near two dimensional excitons which have a well defined excitation level (see section 2.5).

Another factor which makes strong coupling easier to obtain in practice is the freedom to scan the resonant energy of either the cavity mode or the electronic excitation. This gives into and out of resonance and can compensate for growth errors and temperature variation. The detuning of the sample,  $\Delta$ , as stated before is defined by the difference between the cavity energy,  $E_{\text{cav}}$ , and the exciton energy,  $E_{\text{ex}}$ .

## Chapter 3

# Sample characterisation

$$\Delta = E_{\text{cav}} - E_{\text{ex}} \quad (3.1)$$

In this chapter we set out to explain the reasons behind the sample design. We also outline several experiments which were done to investigate the samples' properties. From these investigations important information is obtained and a summary of the information is tabulated at the end of the chapter.

### 3.1 Introduction

The studies in this thesis are on two different samples labelled 1QW and 2QW. To produce a sample in which strong coupling can occur there are two fundamental properties the sample should have: (1) strong optical confinement. This can be created by using high reflectivity mirrors to form a well defined cavity mode as in a Fabry-Pérot interferometer; (2) a well defined excitation with defined energy levels, such as an atom or a confined exciton. The excitation should be resonant with the optical resonance.

Growth techniques such as Metal-Organic Chemical Vapour Deposition (MOCVD) [80] and Molecular Beam Epitaxy (MBE) [81] have enabled high quality thin films of semiconductors to be made. Specifically, DBRs (see section 2.4) can be made which have reflectivities of greater than 99.9% [82] enabling a strong confinement of the vacuum

field and growth of quantum well structures create near two dimensional excitons which have a well defined excitation level (see section 2.5).

Another factor which makes strong coupling easier to obtain in practice is the freedom to scan the resonant energy of either the cavity mode or the electronic excitation. This allows tuning of the energies into and out of resonance and can compensate for growth errors and temperature variation. The detuning of the sample,  $\Delta$ , as stated before is defined by the difference between the cavity energy,  $E_{\text{cav}}$ , and the exciton energy,  $E_{\text{ex}}$ ,

$$\Delta = E_{\text{cav}} - E_{\text{ex}}. \quad (3.1)$$

### 3.1.1 Sample growth and structure

The samples used in this thesis were designed by Ross Stanley and Romuald Houdré and grown by Ursula Oesterle at the Institut de Micro et Opto-électronique, EPFL. The samples possess all the necessary properties for strong coupling and were grown to the highest standard to date. The samples comprise of a DBR which confines the vacuum field and creates a cavity mode and QWs which confine the exciton.

The studies in this thesis are on two different samples labelled 1QW and 2QW. The samples were grown on a GaAs substrate using MBE [81]. The samples consist of 20 DBR pairs at the front and 23.5 DBR pairs at the back (attached to the substrate). The DBR pair is made of alternating AlAs/ $\text{Al}_{0.1}\text{Ga}_{0.9}\text{As}$ , each of length  $\frac{\lambda}{4}$ , where  $\frac{\lambda_0}{n}$  is the wavelength,  $n$  is the refractive index and  $\lambda_0$  is the resonant wavelength in air. Enclosed within these DBR mirrors for the 1QW sample is a  $\lambda$ -cavity containing one QW and for the 2QW sample is a  $\frac{3\lambda}{2}$  cavity containing two QWs. Each QW is 80Å in thickness and is placed at an antinode of the electric field, this is illustrated for the 1QW sample in figure 3.1. In sample 2QW the  $\frac{3\lambda}{2}$  cavity supports two antinodes, one QW is grown at each of the antinodes. The QWs are made from  $\text{In}_{0.05}\text{Ga}_{0.95}\text{As}$ .

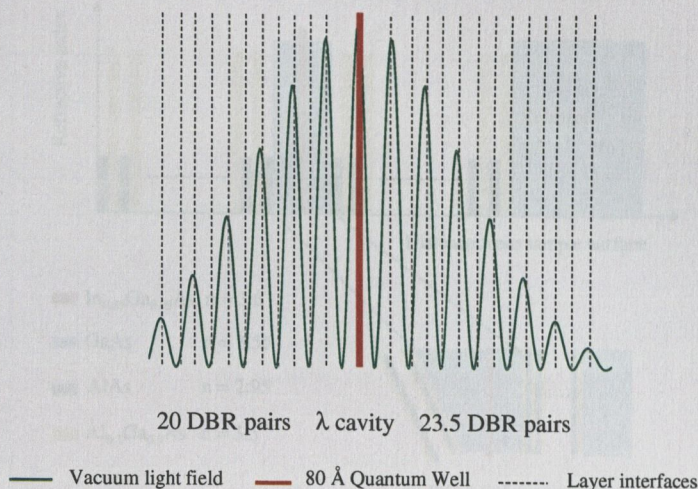


Figure 3.1: A schematic representation of the vacuum field intensity for the 1QW sample. The quantum well is placed at the antinode of the electric field in the centre of the one  $\lambda$  cavity. The interfaces represented are of the alternating DBR pairs consisting of AlAs/ $\text{Al}_{0.1}\text{Ga}_{0.9}\text{As}$ .

The refractive index change across the sample is illustrated in figure 3.2. In GaAs the heavy hole and light hole are normally degenerate at the zone centre, however the low indium content creates a compressive strain in the QW as the lattice constant of InAs is greater than the lattice constant of GaAs. The shear component of the compressive strain causes a splitting of the heavy hole and light hole energies. In our sample the splitting is  $\approx 23.4\text{meV}$  [83].

The sample was wedged to enable scanning of the cavity energy across the exciton energy; the detuning of the sample changes with position on the sample. MBE growth [1] in its simplest form can be described as a wafer, in our case GaAs, heated in a ultra-high vacuum with shuttered canisters which open and close allowing different concentrations of substances such as aluminium, arsenide, gallium and indium to form layers on the wafer substrate. The thickness of the layers grown are controlled by temperature and by the time duration that the canisters are open. During this process the wafer is normally rotated to ensure uniform growth of the layers. However, in



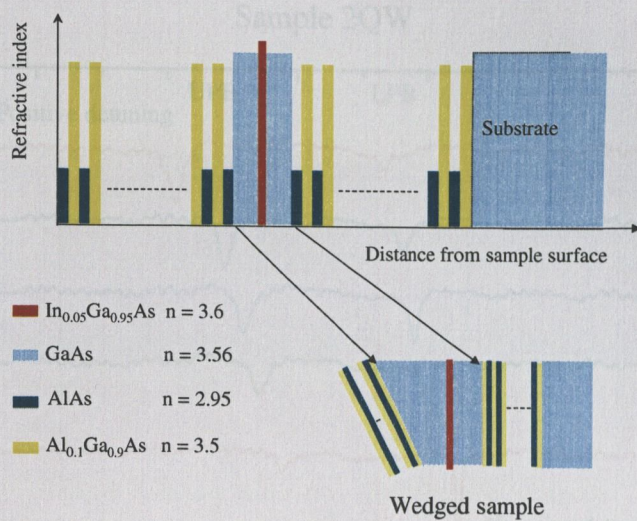


Figure 3.2: A schematic representation of refractive index across the 1QW sample from the surface down. The cavity is wedged due to the uneven growth (see text), an exaggerated wedge is shown, this allows a scanning of the cavity mode (energy) across the exciton absorption line.

the growth of our samples this rotation was stopped during the growth of the cavity resulting in a wedge shaped cavity, see figure 3.2.

For a given absolute change in the thickness, the resulting percentage change in the exciton confinement energy is approximately twice the resulting percentage change of the cavity energy. However due to the larger size of cavity energy compared to the exciton confinement energy, the cavity varies in energy more quickly across the wedge than the quantum well.

## 3.2 Sample properties

Throughout this thesis we assume that our sample is homogeneously broadened. As already stated, there are two main factors that cause inhomogeneous broadening in semiconductor microcavities: the alloy concentration and the interface roughness. The very low concentration of indium (five atoms in a hundred) reduces the alloy broaden-

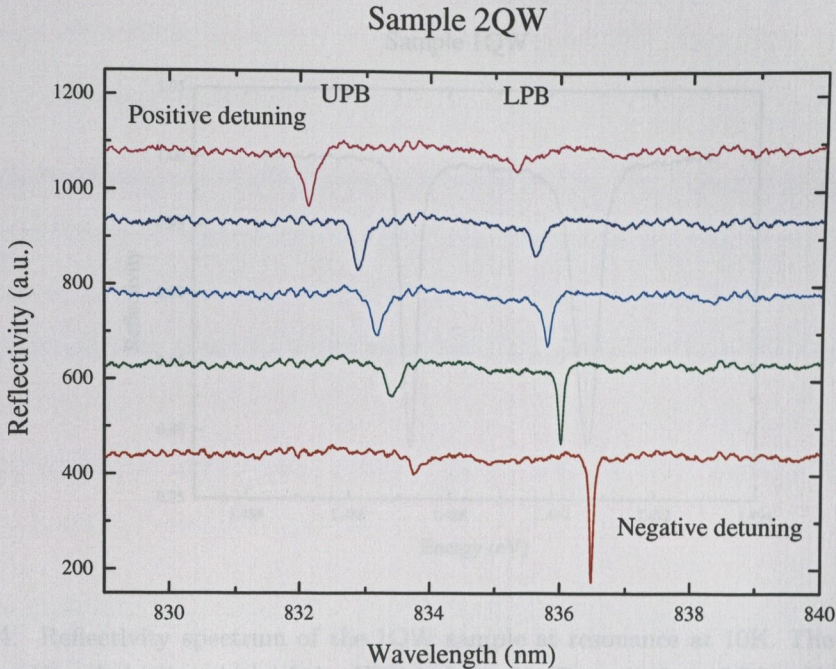


Figure 3.4: Reflectivity spectrum of Sample 2QW at resonance at 10K. The linewidth of the LPB is 0.04meV and the linewidth of the UPB is 0.06meV. The splitting of 3.5meV is over five times the estimated inhomogeneous linewidth of the system. Courtesy of R. Stanley [84].

Figure 3.3: Reflectivity spectrum across the 2QW sample at different positions on the sample. This illustrates how the sample was detuned. It is clearly apparent that the cavity photon mode scans across the exciton energy, this is because the cavity energy changes more quickly than the exciton energy due to the wedge. The reflectivity dip is not as low as theory predicts due to the linewidth resolution of our experimental setup.

ing; the majority of the inhomogeneous broadening is caused by interface roughness in our samples. The narrow linewidths, see figures 3.4 and 3.5, imply that the samples have a very small amount of inhomogeneous broadening.

It can be seen from the extremely narrow linewidths (sub meV) and large splitting that our systems are well described by Houdré's theory [72]; the samples have small inhomogeneous broadenings and a strong exciton photon interaction resulting in polariton linewidths that are the average of the homogeneous linewidth of the exciton and the cavity linewidth. With a cavity linewidth taken from the transfer matrix theory of  $\approx 0.06\text{meV}$  (this is in good agreement with Hayes' [85] measurement made on the 1QW sample of  $0.07\text{meV}$ ), we can estimate an exciton linewidth of  $\approx 0.6\text{-}0.8\text{meV}$  for

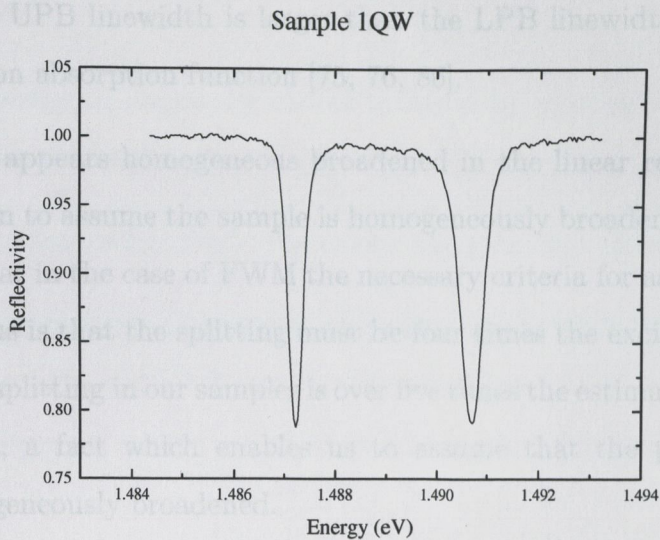


Figure 3.4: Reflectivity spectrum of the 1QW sample at resonance at 10K. The linewidth of the LPB is 0.3meV and the linewidth of the UPB is 0.5meV. The splitting of 3.5meV is over five times the estimated inhomogeneous linewidth of the exciton. Courtesy of R. Stanley [84].

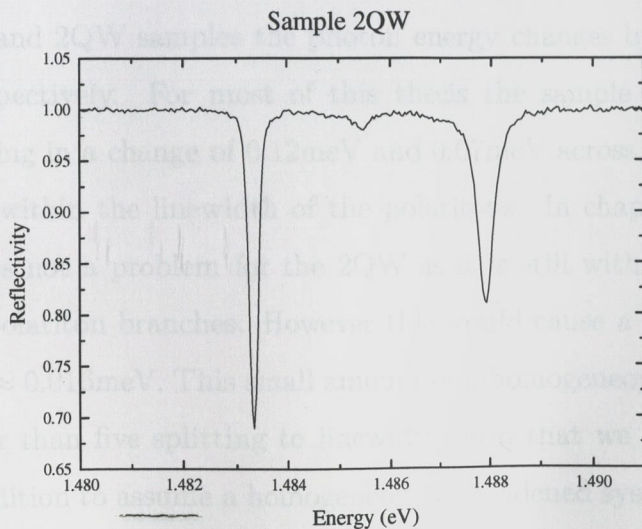


Figure 3.5: Reflectivity spectrum of the 2QW sample at resonance at 15K. The linewidth of the LPB is 0.4meV and the UPB linewidth is 0.6meV. The splitting of 4.6meV is over five times the estimated inhomogeneous linewidth of the exciton. Courtesy of R. Stanley [84].

the samples [85]. Figures 3.4 and 3.5 demonstrate the large splitting to linewidth ratio. As predicted, the UPB linewidth is larger than the LPB linewidth; this is due to an asymmetric exciton absorption function [75, 76, 86].

The sample then appears homogeneous broadened in the linear regime; this is not a sufficient condition to assume the sample is homogeneously broadened. Bongiovanni *et al.* [71] showed that in the case of FWM the necessary criteria for assuming the sample to be homogeneous is that the splitting must be four times the exciton inhomogeneous broadening. The splitting in our samples is over five times the estimated inhomogeneous exciton linewidth, a fact which enables us to assume that the polariton is almost exclusively homogeneously broadened.

Another sample characteristic that might contribute to inhomogeneous broadening is the in built wedge of the cavity. As discussed above, the wafer was rotated during growth resulting in a slight cavity wedge, this could result in different modes being pumped across the sample. The photon energy changes more quickly with thickness than the exciton energy and thus would give rise to greater homogeneous broadening. Across the 1QW and 2QW samples the photon energy changes by  $3.7\text{meVmm}^{-1}$  and  $1.7\text{meVmm}^{-1}$  respectively. For most of this thesis the sample was excited with a  $40\mu\text{m}$  spot, resulting in a change of  $0.12\text{meV}$  and  $0.07\text{meV}$  across the 1QW and 2QW respectively, well within the linewidth of the polaritons. In chapter 5 a  $110\mu\text{m}$  spot size is used; this is not a problem for the 2QW as it is still within the homogeneous linewidth of the polariton branches. However this would cause a slight broadening of the 1QW sample  $\approx 0.016\text{meV}$ . This small amount of inhomogeneous broadening would still give a greater than five splitting to linewidth ratio that we have assumed to be the necessary condition to assume a homogeneously broadened system in the nonlinear regime.

To summarise, the main characteristics are:

- Excellent samples with extremely narrow linewidth.

- Large ratio of splitting to linewidths enables us to assume the polariton is homogeneously broadened.
- The resonant energy of the cavity can be changed by moving sample position, this allows detuning across the sample.
- Inhomogeneous broadening due to the cavity wedge is negligible.

In figure 3.6 we have presented a pictorial representation of the 2QW sample properties: part (a) shows the LPB and UPB dips in the reflectivity spectra at different positions on the sample; these correspond to different detunings. Marking a position on the graphs in (a), and labelling the corresponding detuning, the reflectivity is then shown at that position in (b). From this it is evident that the cavity energy changes with the sample position. The corresponding transfer matrix reflectivity, transmission and absorption are shown in (c). We do not use an asymmetric exciton absorption in our model so it does not account for the larger linewidth and decreased reflectivity of the UPB. It is worth noting the transmission is very small. In 3.6 (d) the corresponding dispersion is shown at each detuning. At negative detunings, when the cavity energy is less than the exciton energy at  $k_{\parallel}=0$ , the LPB is cavity-like and the dispersion curve is steep at  $k_{\parallel}=0$ . When the cavity energy is resonant with the exciton energy the splitting of the UPB and LPB is 4.6meV. At positive detunings the exciton energy is greater than the cavity energy at  $k_{\parallel}=0$ , the LPB is more exciton-like than at negative detunings and the dispersion curve is less steep.

### 3.3 Experimental characterisation of the samples

Having discussed some of terminology we will encounter in the following section, we now turn to a series of short experiments with which we characterise our samples namely: photoluminescence, pump-probe and femtosecond reflectivity.

### 3.3.1 Photoluminescence

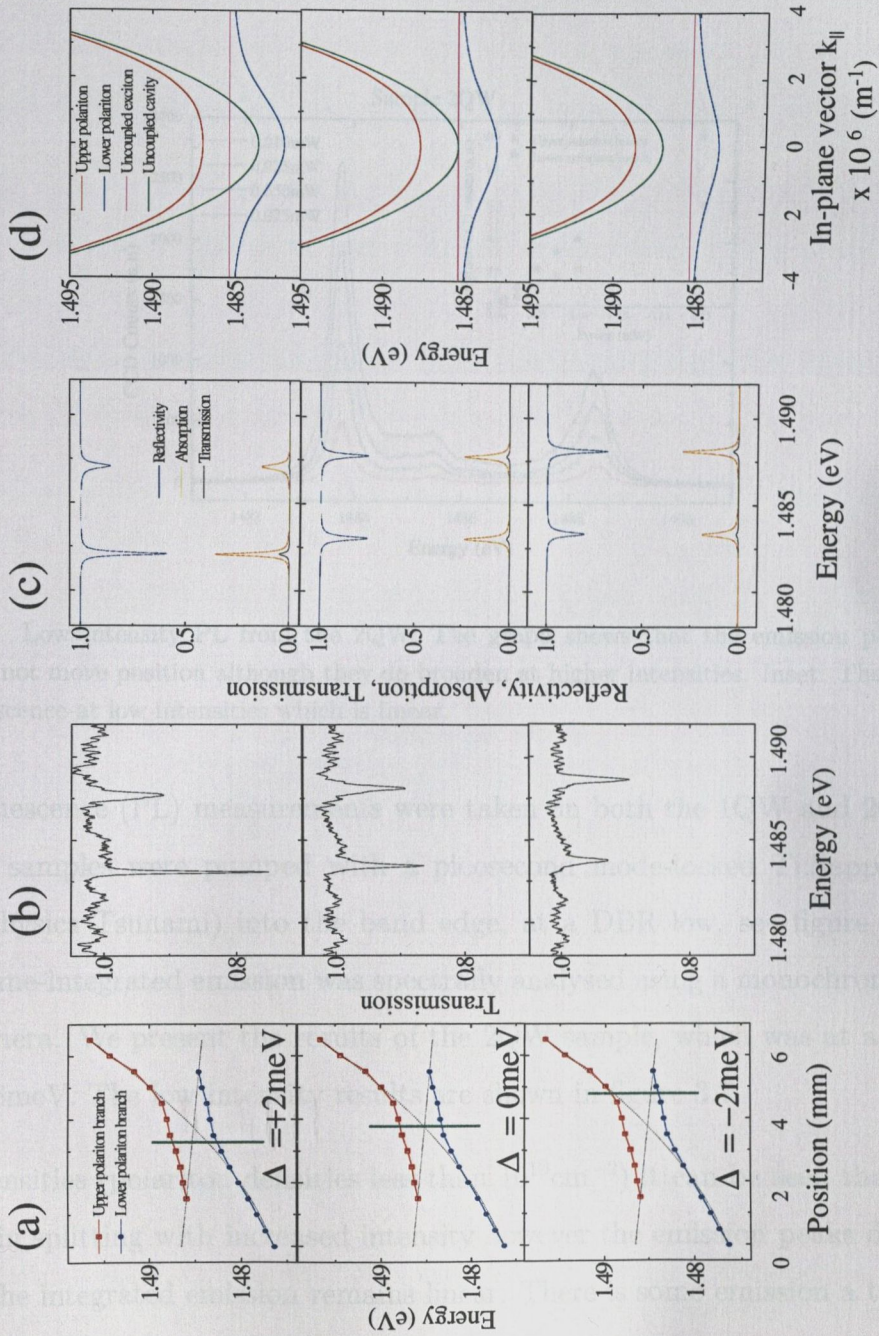


Figure 3.6: (a) Reflectivity dips of the UPB and LPB at different positions on the sample illustrating the three different detunings where the data is taken,  $\Delta = -2 \text{ meV}$ ,  $\Delta = 0$ ,  $\Delta = +2 \text{ meV}$ . (b) Reflectivity data at the three detunings. (c) Modelled reflectivity, absorption and transmission. (d) Dispersion at three different detunings, showing the large decoupling of the LPB from the uncoupled exciton branch at negative detunings compared to positive detunings. At resonance the uncoupled exciton and cavity energy are degenerate.

### 3.3.1 Photoluminescence

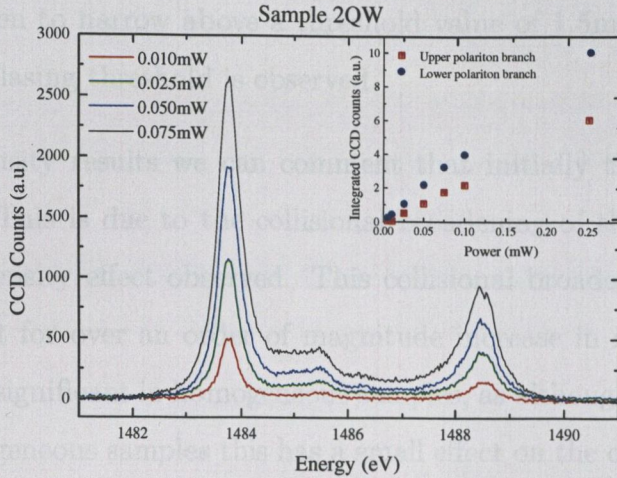


Figure 3.7: Low intensity PL from the 2QW. The graph shows that the emission peaks of the polariton do not move position although they do broaden at higher intensities. Inset: The integrated photoluminescence at low intensities which is linear.

Photoluminescence (PL) measurements were taken on both the 1QW and 2QW samples. The samples were pumped with a picosecond mode-locked Ti:Sapphire laser (Spectra Physics Tsunami) into the band edge, at a DBR low, see figure 2.4. The collected time-integrated emission was spectrally analysed using a monochromator and a CCD camera. We present the results of the 2QW sample, which was at a detuning of  $\Delta = -0.6\text{meV}$ . The low intensity results are shown in figure 3.7.

At low intensities (polariton densities less than  $10^{10}\text{cm}^{-2}$ ) it can be seen that there is no change in splitting with increased intensity however the emission peaks do become broader. The integrated emission remains linear. There is some emission at the uncoupled exciton wavelength  $1.4855\text{eV}$ . At the very lowest intensity the populations were measured and analysed to see if the polaritons showed a Boltzmann distribution. We calculated the temperature using the Boltzmann distribution and found the value to be larger than the cryostat reading by 30K, this verifies Tassone's predictions [18] as discussed in section 2.7.2.

The PL at high intensities was then measured, see figure 3.8. At higher intensities the emission at 1486.5eV increases relative to the polariton emission. This emission at the central region is seen to narrow above a threshold value of 1.5mW. From the inset it can be seen that a lasing threshold is observed.

From the low intensity results we can comment that initially there is a broadening of the polaritons. This is due to the collisional broadening of the uncoupled exciton and is the first intensity effect observed. This collisional broadening continues to be the dominant effect for over an order of magnitude increase in intensity. Collisional broadening is only significant in homogeneous samples, as although the individual lines broaden in inhomogeneous samples this has a small effect on the overall linewidth [87]. This confirms our assessment that our samples are homogeneous in the linear regime, according to Houdré [73].

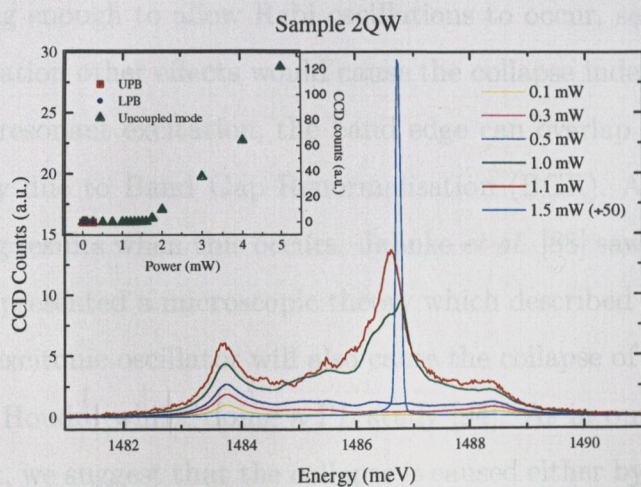


Figure 3.8: High intensity PL from the 2QW sample. At high intensities, emission from the uncoupled mode between the two polariton branches can be seen. There is a narrowing of the emission line at the onset of lasing. Inset: The PL intensity versus power showing a clear threshold at the onset of lasing.

There is no change in the spectral positions of the polariton lines, implying that the interaction strength does not weaken. Thus, although there is a broadening of the exciton absorption line, the strength of the interaction between the exciton and the



cavity remains the same. This behaviour of broadening with no change in splitting has been reported before [88, 89, 90].

At high intensities emission at 1486.5eV becomes dominant. Although emission is also apparently coming from the polariton branches this does not imply that all three exist at the same time but rather that the detection is time integrated [91]. At high intensities the picosecond pulse collapses the polariton. The strong coupling regime moves to the weak coupling regime, and then the weak coupling response recovers to the strong coupling response in the 12ns between the ps pulses.

There are three causes of the collapse from the strong coupling to the weak coupling regime through excitation. (1) If the collisional broadening becomes very large the increase in dephasing rate collapses the strong coupling regime [92, 93]. This is because one of the conditions for strong coupling is that the dephasing rate of the individual states must be long enough to allow Rabi oscillations to occur, see section 2.3. With non-resonant excitation other effects would cause the collapse independent of this first effect. (2) In non-resonant excitation, the band edge can overlap the exciton absorption line, primarily due to Band Gap Renormalisation (BGR). A sudden collapse of the strong coupling results when this occurs. Jahnke *et al.* [88] saw this in a cw PL experiment and also presented a microscopic theory which described the results well. (3) Saturation of the excitonic oscillator will also cause the collapse of the strong coupling regime as seen by Houdré whilst doing a PL study [94]. As in our measurements the PL is non-resonant, we suggest that the collapse is caused either by BGR or saturation of the excitonic oscillator.

At a threshold intensity of 1.5mW there is the onset of lasing. This lasing occurs after the polariton collapses and effectively becomes an optically pumped microcavity laser.

### 3.3.2 Pump-probe

Resonant pump-probe was investigated on the 2QW sample near zero detuning. The experimental setup is shown in figure 3.9.

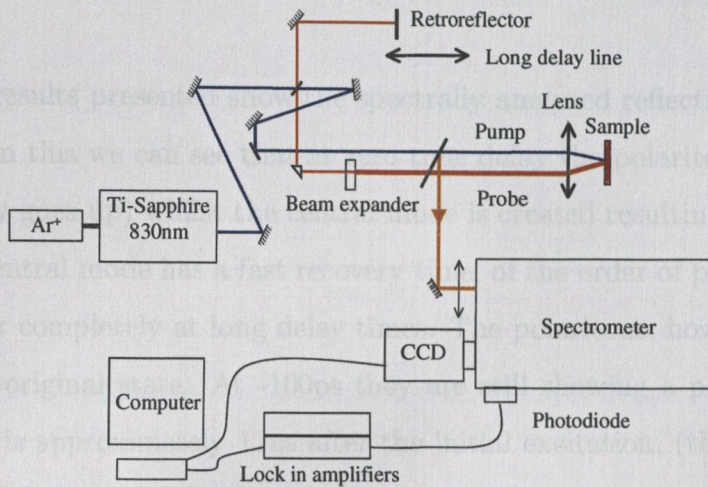


Figure 3.9: Experimental pump-probe setup. The femtosecond Ti:Sapphire beam was split into two, the pump and the probe beams. The probe was delayed with respect to the pump using a retroreflector. Then both beams were focused onto the sample. The reflected probe was spectrally analysed using a spectrometer and then analysed both via a CCD camera and using a dual lock-in detection system and a photodiode.

A femtosecond pulse (500fs) with a spectral width of approximately 12meV ( $\approx 7\text{nm}$ ) from the Ar<sup>+</sup>-pumped Ti:Sapphire was split into two beams, namely the pump and the probe. The probe was delayed with respect to the pump using a retroreflector and a stepper motor driven translation stage. After the delay, the probe was then expanded; a larger beam diameter results in a smaller spot size. Expanding the beam ensures that only the central region of the pump was probed. Both beams were then focused onto the sample, through a linear polariser and a quarter wave plate which controlled the polarisation; the pump was focused at normal incidence onto the sample and the probe was focused at an angle of  $3^\circ$ . The reflected probe was then analysed

initially using a CCD camera ( $\text{LN}_2$ ). This enabled the spectrally resolved differential reflectivity to be measured at various times. The second measurement was made using a dual lock-in with photodiode to detect the reflected probe. This allowed us to probe the differential reflectivity with respect to time, at three positions the LPB, UPB and uncoupled mode. The collapse and recovery of the polariton was recorded using this setup.

The first set of results presented show the spectrally analysed reflectivity changes, see figure 3.10. From this we can see that at zero time delay the polariton peaks collapse (their reflectivity goes up) whilst the central mode is created resulting in a reflectivity decrease. The central mode has a fast recovery time, of the order of picoseconds and is shown to recover completely at long delay times. The polaritons, however, never fully recover to their original state. At -100ps they are still showing a positive change in reflectivity; this is approximately 12ns after the initial excitation, (the repetition rate of the laser is 82Mhz). At -100ps there is a negative reflectivity around the outer edges of the polariton, this can be seen more clearly in the inset of figure 3.10.

The results from the lock-in photodiode detection system measure the recovery time of the LPB, UPB and uncoupled mode. The LPB and UPB recover steadily but have not fully recovered in 12ns, whilst the uncoupled mode recovers quickly, in the first 100ps.

These results give a measured decay of  $12.1 \pm 2\text{ns}$  for the UPB and  $9.5 \pm 1\text{ns}$  for the LPB and the fast decay of the uncoupled mode is  $11 \pm 1\text{ps}$ . The change in reflectivity is less in the UPB, compared to the LPB, because the reflectivity dip of the UPB is smaller at resonance, this was discussed in chapter 2.

The fast recovery time of the uncoupled mode is apparent in both sets of data. This fast recovery time is a result of the decay time of the cavity; once the polariton has collapsed due to the femtosecond pulse the light in the cavity will decay with the cavity decay time, which we measure to be  $11 \pm 1\text{ps}$ . This value is in good agreement with the decay time based on the linewidth predicted by the linear dispersion model using the

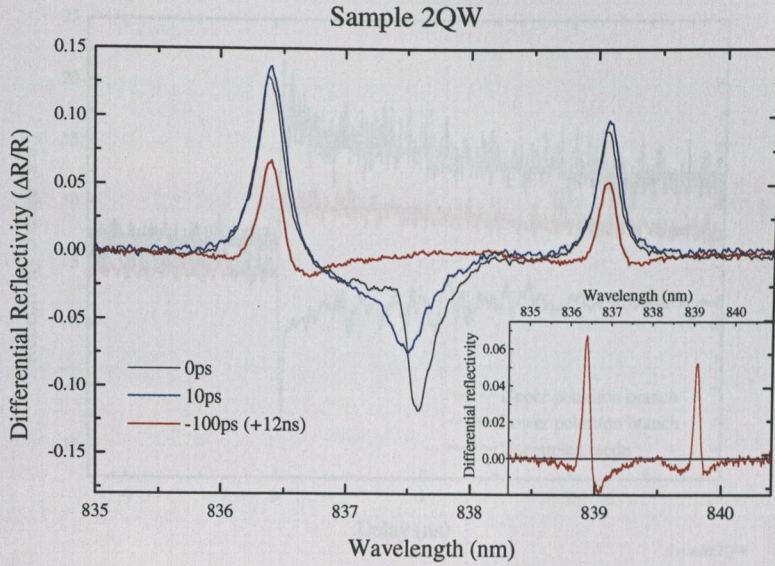


Figure 3.10: Spectrally resolved pump-probe data. At zero delay there is the collapse of the polariton regime and the uncoupled mode comes into existence. The recovery time of the uncoupled mode is fast, unlike that of the two polariton modes. There is no change in the position of the polariton lines as they recover. The inset is a reprint of the +12ns data to show more clearly the collisional broadening effect on the differential reflectivity.

transfer matrix method, of 10.6ps. It is also in agreement with other measurements done on these samples which suggest a decay time of 10ps [85]. The collapse of the strong coupling regime may be caused by the broadening of the exciton line due to exciton-exciton interaction. When the linewidth of the cavity becomes too large, then the decay rate of the system exceeds the interaction rate and the weak coupling regime is recovered, see section 2.3. Another possible reason for the collapse is due to saturation of exciton oscillator strength.

We believe the long recovery time of the UPB and LPB is due to electron-hole pair recombination recombination which would be of the order of nanoseconds [95]. Spectrally we have a very wide femtosecond pulse FWHM of 12meV. This appreciable pulse width overlaps with the band edge as the exciton binding energy, is around 8meV. However, due to the large stop band in the DBR of  $\approx 65\text{meV}$  between the central region to

### 3.3.3 Femtosecond reflectivity

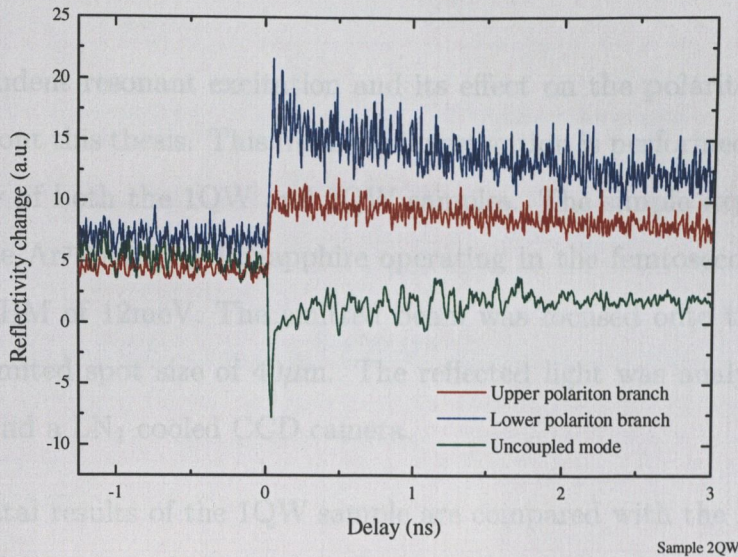


Figure 3.11: The change in reflectivity with respect to time at three different position; UPB, LPB and uncoupled mode.

the first leaky mode, with a reflectivity of  $>99\%$ , only a small amount of electrons and holes (approximately  $1 \times 10^9 \text{ cm}^{-2}$ ) are being generated through the DBRs. The spectral tail of the excitation is extremely small, at  $65 \text{ meV}$  from the centre, but still might contribute to the electron hole generation. The low temperatures would result in a very small amount of electron-holes being created from thermalised excitons.

From the inset of figure 3.10 at long time delays ( $\approx 12 \text{ ns}$ ) after the central mode has recovered the polaritons have not recovered their original reflectivities. However the central mode has disappeared and the strong coupling regime has recovered. This effect is due to the collisional broadening. The polaritons are broader with the result that the peak reflectivities have diminished whilst the tail ends have broadened. The resulting change in reflectivity is a positive change at the peak and a negative change at the edges. This can be seen clearly in the inset of figure 3.10. The polaritons have not shifted position towards the middle suggesting the overall exciton oscillator strength which is interacting with the cavity mode has not diminished.

### 3.3.3 Femtosecond reflectivity

Intensity dependent resonant excitation and its effect on the polariton is a recurring theme throughout this thesis. This intensity investigation is performed using femtosecond reflectivity of both the 1QW and 2QW samples. The simple experimental setup consisted of the  $\text{Ar}^+$ -pumped Ti:Sapphire operating in the femtosecond regime, with a spectral FWHM of 12meV. The emitted beam was focused onto the samples with a diffraction limited spot size of  $40\mu\text{m}$ . The reflected light was analysed using a 1m spectrometer and a  $\text{LN}_2$  cooled CCD camera.

The experimental results of the 1QW sample are compared with the results modelled from the transfer matrix calculation, see figure 3.12.

The model was discussed in section 2.3.2 however it should be noted that to specifically model the effect of intensity, a saturation function was added to the oscillator strength. The fitted saturation density,  $N_{\text{sat}}$ , are displayed on the modelled results to compare with the experimentally obtained values. Also to obtain good agreement between experimental and modelled data it was necessary to account for the Gaussian intensity distribution over the spot size by separating the excitation spot into a minimum of three different intensity regions.

The following effects occur with increasing intensity on the 1QW sample: a broadening of the line and a decrease in reflectivity ( $R$ ) although the integrated area remains the same ( $1-R$ ) and there is no change in splitting. This is followed by a blue shift of the LPB. At high intensities the polariton then collapses completely. At the low energy side of the collapsed mode there is some emission. Some of these experimental features are well reproduced by our model though not all. The broadening of the linewidth with a decrease in peak reflectivity whilst the integrated area ( $1-R$ ) remains constant are well reproduced. However, there is no shift in the polariton positions with intensity in the model. The absorption versus the carrier density was plotted to obtain an estimation of the saturation density,  $N_{\text{sat}}$  (see figure 3.13) using [57],

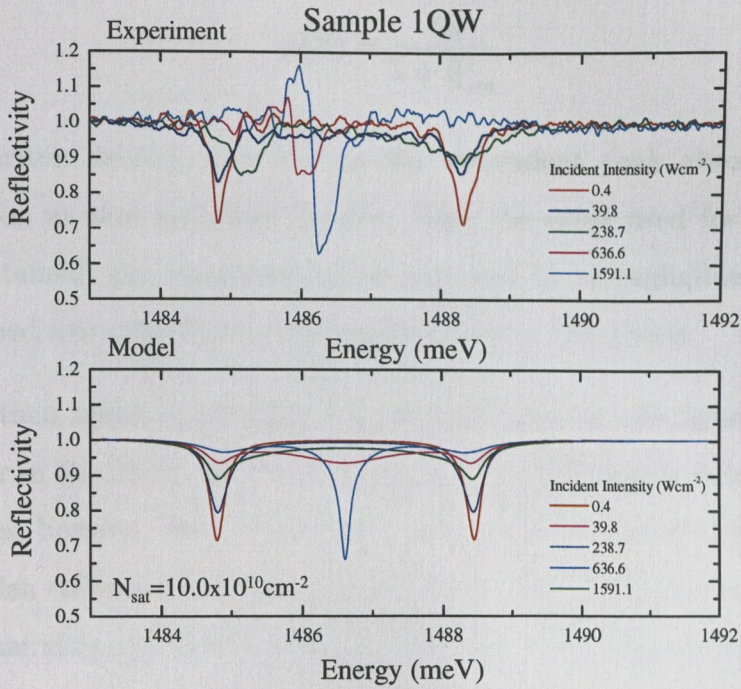


Figure 3.12: Femtosecond reflectivity of the 1QW sample at resonance. At low intensities the model and experimental data agree well, collisional broadening can be seen with increased intensity. As the intensity increases the LPB blue shifts and then collapses into the weak coupling regime. The blue shift is not apparent in the modelled results.

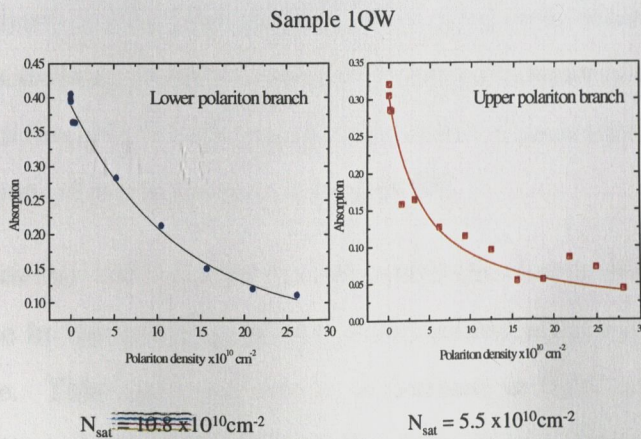


Figure 3.13: Absorption taken from the reflectivity spectrum (assuming no transmission) versus polariton density. The polariton saturation density is obtained using a simple saturation function, see equation 3.2.

$$\alpha(N) = \frac{\alpha_0}{1 + \frac{N}{N_{\text{sat}}}} \quad (3.2)$$

$N$  is the polariton density,  $\alpha$  is the density dependent peak absorption,  $\alpha_0$  is the peak absorption at zero polariton density. Here the value used for  $\alpha_0$  is the largest absorption obtained, the transmission was assumed to be negligible. The saturation density obtained from this fitting will be used later in this thesis.

Results were then taken at resonance in the 2QW sample, see figures 3.14 and 3.15. The behaviour in the 2QW sample is similar to the 1QW sample at low intensities. At high intensities, however, there is no shift in the energies of either polariton branches, until the sudden collapse. Looking specifically at a polariton density of  $78.5^{10}\text{cm}^{-2}$  it can be seen that although there is some collapse due to the high intensity at the centre of the excitation spot there is also a contribution from the outer area of the excitation spot where the polariton is still in the strong coupling regime.

Data was also taken on the 2QW sample at detunings of  $+5\text{meV}$  and  $-5\text{meV}$  and good agreement is shown between experiment and theory, see figures 3.16 and 3.17.

At low intensities both of the samples show good agreement between experiment and theory, exhibiting a decrease in peak reflectivity and an increase in linewidth, whilst the overall area of the reflectivity (1-R) remains the same. This is similar to the collisional broadening behaviour of the bare quantum well [58].

At higher intensities the 1QW results do not match the theory as well, see figure 3.12. There is a decrease in the splitting of the polariton and a blue shift in the LPB just before the collapse. This could be due to a decrease in interaction strength of the cavity and the exciton along with a blue shift of the exciton energy.

The 2QW sample, see figure 3.14, does not show any decrease in oscillator strength before a sudden collapse, suggesting that the collapse is due to; a rapid saturation



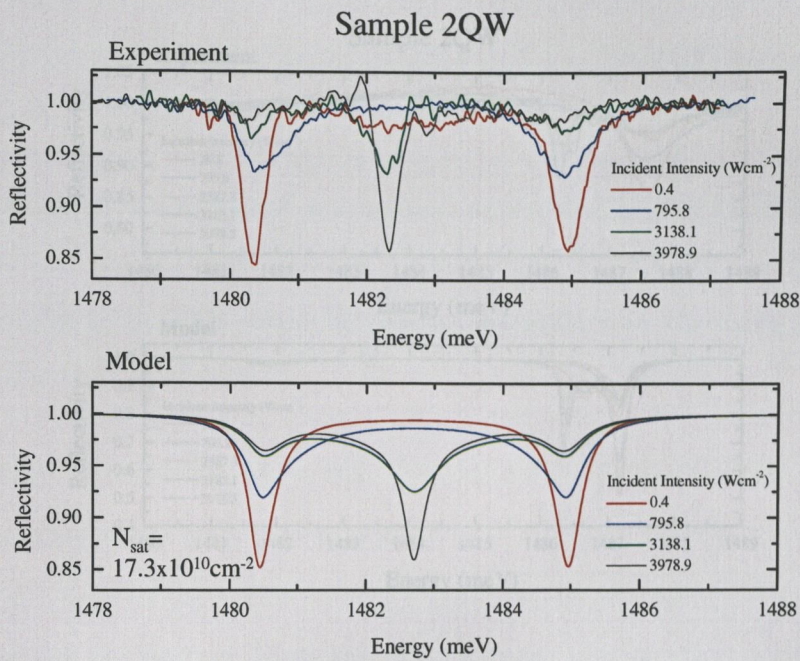


Figure 3.14: Experimental and modelled femtosecond reflectivity showing good agreement. The collisional broadening is reproduced well. At high intensities there is a sudden collapse of the polariton. There is no shift in the polariton lines.

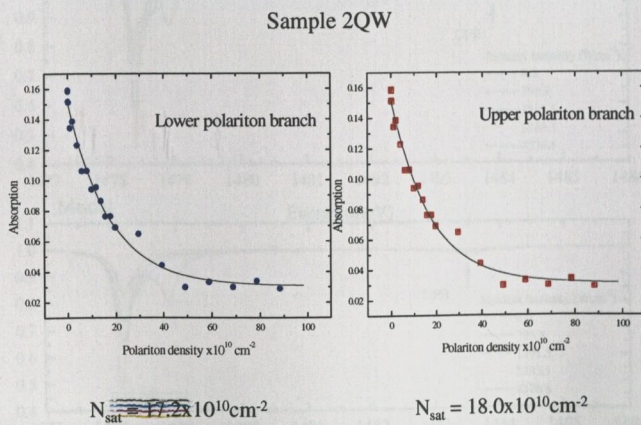


Figure 3.15: Absorption taken from the reflectivity assuming no transmission with polariton density. The data was fitted with a simple saturation formula, see equation (3.2), to obtain a saturation density.

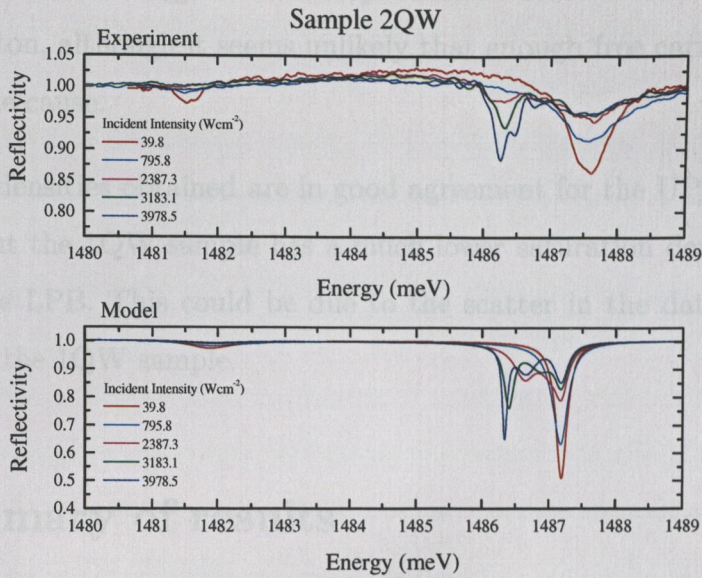


Figure 3.16: Experimental and modelled femtosecond reflectivity data at a detuning of +5meV.

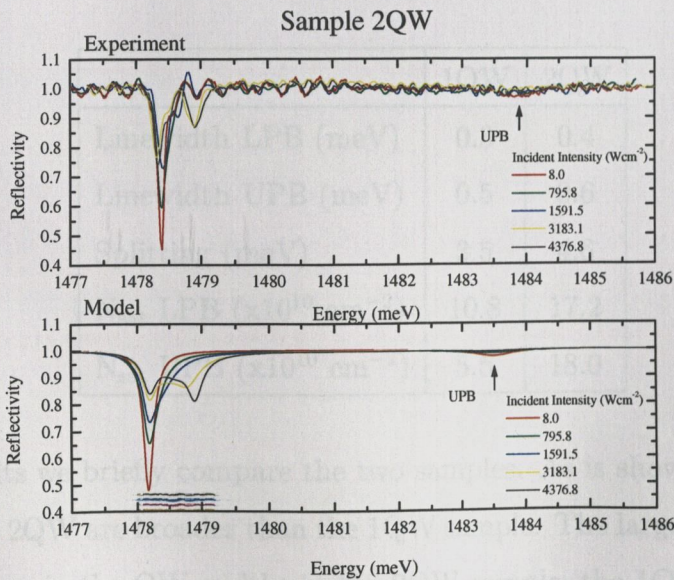


Figure 3.17: Experimental and modelled femtosecond reflectivity data at a detuning of -5meV.

of oscillator strength; a rapid increase in the collisional broadening, or the bandgap overlapping the exciton energy. This overlap would be attributed to BGR and the blue shift of the exciton, although it seems unlikely that enough free carriers are generated for this to be the cause.

The saturation densities obtained are in good agreement for the UPB and LPB in the 2QW sample but the 1QW sample has a much lower saturation density for the UPB compared to the LPB. This could be due to the scatter in the data points which is much larger for the 1QW sample.

### 3.4 Summary of results

Summarising the conclusions from the experiments, the samples are assumed to be homogeneously broadened. At low intensities the only appreciable intensity effect is collisional broadening. The cavity decay time is  $\approx 10\text{ps}$  and the electron-hole pair recombination time  $\approx 10\text{ns}$ . All other results are summarised in the table below.

	1QW	2QW
Linewidth LPB (meV)	0.3	0.4
Linewidth UPB (meV)	0.5	0.6
Splitting (meV)	3.5	4.6
$N_{\text{sat}}$ LPB ( $\times 10^{10} \text{ cm}^{-2}$ )	10.8	17.2
$N_{\text{sat}}$ UPB ( $\times 10^{10} \text{ cm}^{-2}$ )	5.5	18.0

From these results we briefly compare the two samples. As is shown in the table, the linewidths of the 2QW are broader than the 1QW sample. The larger linewidth may be due to fluctuations in the QW widths in the 2QW sample; the 1QW sample contains only one QW and as such would not suffer from this problem. The different QW widths would result in different exciton energies resulting in an inhomogeneous broadening of

the exciton lines <sup>1</sup>.

The splitting of the 2QW sample is larger than the 1QW sample. This is unsurprising as the 2QW sample contains two QWs and the oscillator strength increases with the number of QWs. The saturation density of the 2QW sample is also approximately twice that of the 1QW sample because the polariton density is spread over two QWs.

Another interesting difference is that in the 2QW sample there is a node at the centre of the cavity, whilst in the 1QW sample there is an antinode at the centre of the cavity, see figure 3.1. Thus guided modes which move along the cavity, with their peak intensity in the centre of the cavity, will strongly overlap with the 1QW sample electric field and QW. Whilst, the guided modes will not overlap strongly with the QWs or electric field in the 2QW sample.

In this chapter we have demonstrated that our model provides good agreement with the samples in the linear regime.

## 4.1 Introduction

Since the development of ultrafast lasers, linear and nonlinear spectroscopy such as pump-probe, luminescence, interferometry and FWM have become important tools in studying the fast dynamics of semiconductors.

The simplest FWM setup, that of Degenerate-FWM (DFWM) is shown in figure 4.1(b). DFWM uses two pulsed beams from the same laser, the pump beam with wavevector  $k_1$  and the probe beam with wavevector  $k_2$ . The probe beam is delayed with respect to the pump beam by time  $\tau_d$ . The pump pulse generates a macroscopic coherence which begins to decay via various relaxation processes. When the probe beam arrives after the pump, if there is any coherence left in the system, a grating will be formed. The probe beam itself can then

---

<sup>1</sup>Looking at figure 3.5 a small dip in the reflectivity at 1.4855meV is apparent. This may be the result of some excitons not strongly coupling to the field.

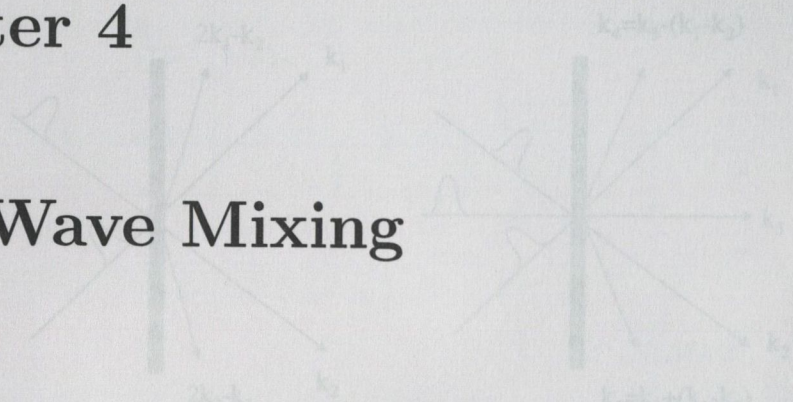
how it varies with the delay time can give an estimation of the time scale of the coherence destroying processes also known as the 'dephasing' time.

(a) Degenerate-FWM

(b) Three beam FWM

## Chapter 4

# Four Wave Mixing



In this chapter we discuss the technique of Four Wave Mixing (FWM), a nonlinear process which can be used to measure the dephasing time (loss of coherence) of a QW excitonic system. The time integrated degenerate FWM signal is estimated using a two-level model, and its limitations are stated in view of recent improved models.

### 4.1 Introduction

Since the development of ultrafast lasers, linear and nonlinear spectroscopy such as pump-probe, luminescence, interferometry and FWM have become important tools in studying the fast dynamics of semiconductors.

The simplest FWM setup, that of Degenerate-FWM (DFWM) is shown in figure 4.1(a). DFWM uses two pulsed beams from the same laser, the pump beam with wavevector  $k_1$  and the probe beam with wavevector  $k_2$ . The probe beam is delayed with respect to the pump beam by time  $\tau_d$ . The pump pulse generates a macroscopic coherence which begins to decay via various relaxation processes. When the probe beam arrives after the pump, if there is any coherence left in the system, a grating will be formed. The probe beam itself can then diffract off the grating (self-diffraction). A study of the intensity of the diffracted signal and

how it varies with the delay time can give an estimation of the time scale of the coherence destroying processes also known as the ‘dephasing’ time.

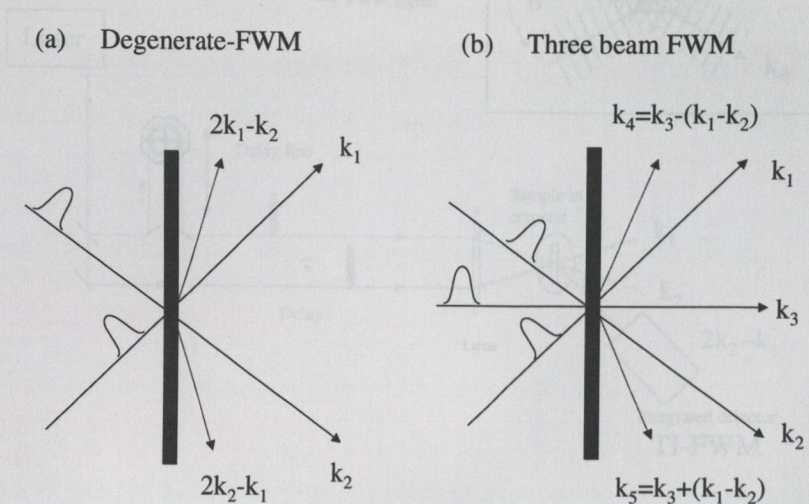


Figure 4.2: The degenerate TI-FWM setup. The inset shows a schematic for a grating produced inside a sample.

Figure 4.1: Schematic showing the wave vectors of two different FWM configurations. (a) Degenerate or self-diffracted FWM and (b) three beam FWM.

We use DFWM although three beam FWM is more versatile, see figure 4.1(b). From three beam FWM the population decay time of the excitons and the nature of the broadening, homogeneous or inhomogeneous, can be ascertained. The spectral relaxation and non-Markovian effects<sup>1</sup> can also be investigated. The FWM signal collected in the work done in this thesis is time-integrated (TI-FWM). However, the FWM signal can be temporally resolved using up conversion (TR-FWM), and this can provide new information. For example, in the DFWM configuration it can be used to find the broadening nature (see below) and it can give insight into some of the interaction effects which go beyond the two-level model which is regularly used to analyse FWM results [96].

FWM is thus a powerful tool in the study of coherence in excitonic systems in semiconductors.

<sup>1</sup>A non-Markovian effect is one where the dephasing time is not an instantaneous function of the environment but depends on the history of the environment. The so called ‘memory’ is taken in to account.

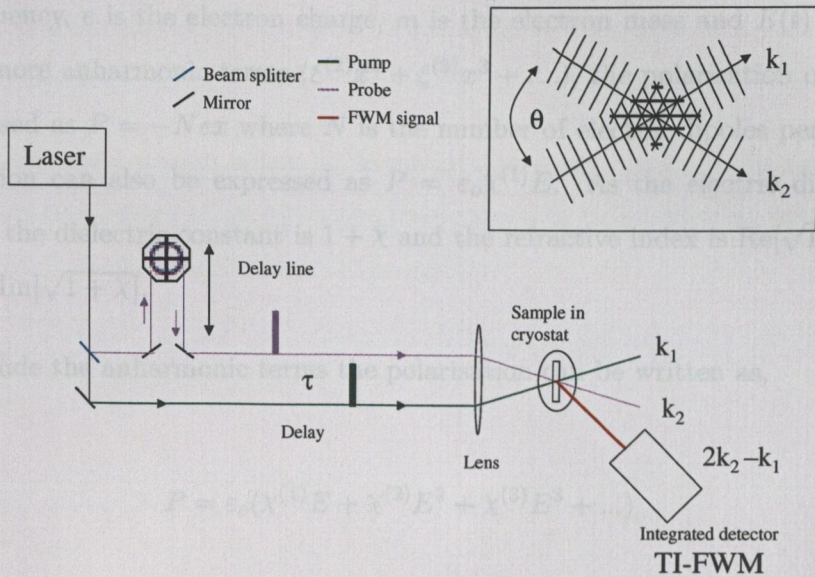


Figure 4.2: The degenerate TI-FWM setup. The inset shows a schematic for a grating produced inside a sample.

Two of the main reasons why coherence is important are, firstly that the intrinsic relaxation and recombination time of photoexcited excitons are important parameters to be considered when using QWs in a commercial device such as high speed modulators. Secondly, a deep insight into the fundamental relaxation processes of excitons such as: collisions with other excitons, scattering from crystal defects, interaction with phonons and free electron-hole pairs, can be obtained. For a review of some of the work done using three beam FWM and DFWM in semiconductor GaAs/AlGaAs QW excitons see Cundiff and Steel [97] and Kuhl, Honold, Schulthies and Tu [98].

FWM is a nonlinear  $\chi^{(3)}$  process, it arises from the anharmonic response to the field. The response of an electron moved by an electric field can be mathematically represented by the equation of motion of a driven oscillator,

$$m \left[ \frac{d^2 x}{dt^2} + 2\Gamma \frac{dx}{dt} + \omega_0^2 x - (\xi^{(2)} x^2 + \xi^{(3)} x^3 + \dots) \right] = -eE(t). \quad (4.1)$$

Where  $x$  is the displacement from the mean position,  $\Gamma$  is the damping constant,  $\omega_0$  is the response frequency,  $e$  is the electron charge,  $m$  is the electron mass and  $E(t)$  is the electric field. If we ignore anharmonic terms ( $\xi^{(2)}x^2 + \xi^{(3)}x^3 + \dots$ ), the polarisation of the material can be expressed as  $P = -Nex$  where  $N$  is the number of electric dipoles per unit volume. The polarisation can also be expressed as  $P = \varepsilon_0\chi^{(1)}E$ . As the electric displacement is  $D = \varepsilon_0E + P$  the dielectric constant is  $1 + \chi$  and the refractive index is  $\text{Re}[\sqrt{1 + \chi}]$  and the absorption is  $\text{Im}[\sqrt{1 + \chi}]$ .

When we include the anharmonic terms the polarisation can be written as,

$$P = \varepsilon_0(\chi^{(1)}E + \chi^{(2)}E^2 + \chi^{(3)}E^3 + \dots), \quad (4.2)$$

where  $\chi^{(2)}$  and  $\chi^{(3)}$  are the nonlinear susceptibilities of the material. The process we are going to study is FWM and this is a result of the cubic polarisation  $P^{(3)} = \varepsilon_0\chi^{(3)}E^3$ . One way to view a cubic process is to think of it as replacing the effective value of  $\chi^{(1)}$  with  $\chi^{(1)} + \chi^{(3)}E^2$ , in other words the dielectric constant is changed by an amount proportional to the optical intensity. This dielectric constant includes both the imaginary and real parts which gives the absorption and refractive index respectively.

Looking at the nonlinear optics with this perspective gives an intuitive understanding of the grating, see figure 4.2 (inset). Two waves interfere to form fringes, and the fringes induce changes in the absorption and refractive index of the material. The modulation of the refractive index and absorption constitutes a grating. This grating will exist for as long as there is coherence in the system. Either beam can then self-diffract off the grating.

## 4.2 Two-level model

To find an expression for  $\chi^{(3)}$  we initially use the independent two-level model [99, 100, 101]. In this model we assume that the exciting photon is nearly resonant with a two-level transition. We also assume that there is no interaction between the two-level oscillators,



and that the two-level resonance is far away from all other resonances. Each exciton in a semiconductor can be considered two-level in its simplest approximation; this is in keeping with the atomic analogy.

Considering a two-level system where  $E_a$  is the ground state and  $E_b$  is the excited state. If the exciton is in the ground state, the energy eigenstate  $u_a$  is determined by the eigenvalue equation, where  $H_0$  is the Hamiltonian of the system:

$$H_0 u_a = E_a u_a. \quad (4.3)$$

The state of the system evolves according to Schrödinger's equation,

$$i\hbar \frac{d\psi}{dt} = H\psi. \quad (4.4)$$

$H$  is the Hamiltonian of the system. The wavefunction that describes the system without any perturbation is

$$\psi = \exp\left(\frac{-iE_a t}{\hbar}\right) u_a. \quad (4.5)$$

Here an arbitrary phase factor has been set to zero. Alternatively if the system is in the excited state then the subsequent unperturbed evolution of the wavefunction would be,

$$\psi = \exp\left(\frac{-iE_b t}{\hbar}\right) u_b. \quad (4.6)$$

However, the general case is when the wavefunction for the system is a coherent superposition of the two states.

$$\psi = a \exp\left(\frac{-iE_a t}{\hbar}\right) u_a + b \exp\left(\frac{-iE_b t}{\hbar}\right) u_b, \quad (4.7)$$

where  $a$  and  $b$  are complex numbers. The probability that the system is to be found in either

the lower or upper energy level is  $|a|^2$  or  $|b|^2$  respectively. Therefore  $|a|^2 + |b|^2 = 1$ . Having examined a single two-level system case we now study an ensemble of these two-level systems, using the density operator,  $\rho$ . The equation of motion for the density operator is given by the commutator [102],

$$\begin{pmatrix} \rho_{aa} & \rho_{ab} \\ \rho_{ba} & \rho_{bb} \end{pmatrix} = \begin{pmatrix} |a|^2 & 0 \\ 0 & |b|^2 \end{pmatrix} \quad (4.13)$$

$$i\hbar \frac{d\rho}{dt} = [H, \rho]. \quad (4.8)$$

The density operator can also be written as

$$\rho = \sum_{\psi} p_{\psi} P(\psi), \quad (4.9)$$

where the projection operator is

$$P(\psi) = \psi \int d\zeta \psi^*, \quad (4.10)$$

and  $p_{\psi}$  is the probability that the two-level system is in a particular superposition state  $\psi$ . The density operator can be specified in terms of a  $2 \times 2$  matrix whose (ij)th element is defined by,

$$\rho_{ij} = \int d\zeta u_i^* \rho u_j. \quad (4.11)$$

$$\begin{pmatrix} \rho_{aa} & \rho_{ab} \\ \rho_{ba} & \rho_{bb} \end{pmatrix} = \sum_{\psi} P_{\psi} \begin{pmatrix} |a|^2 & ab^* \exp(i\Omega_{ba}t) \\ a^*b \exp(-i\Omega_{ba}t) & |b|^2 \end{pmatrix}, \quad (4.12)$$

$\Omega_{ba} = (E_b - E_a)/\hbar$ , is the resonant frequency of the system,  $\rho_{aa} + \rho_{bb} = 1$ , and  $\rho_{ba} = \rho_{ab}^*$ , as expected for a Hermitian operator. If all the two-level systems were in the same state,  $P_{\psi} = 1$  and the system would be coherent. However if  $|a|^2$  and  $|b|^2$  were constant but the

phase angle of the coherent superposition is randomly distributed between 0 and  $2\pi$  then the density operator could be represented by,

$$H_I(t) = \begin{pmatrix} \delta E_a & -er_{ab} \cdot E(t) \\ -er_{ba} \cdot E(t) & \delta E_b \end{pmatrix} = \begin{pmatrix} 0 & \Delta_{ab} \\ \Delta_{ab}^* & 0 \end{pmatrix} \quad (4.12)$$

$$\begin{pmatrix} \rho_{aa} & \rho_{ab} \\ \rho_{ba} & \rho_{bb} \end{pmatrix} = \begin{pmatrix} |a|^2 & 0 \\ 0 & |b|^2 \end{pmatrix} \quad (4.13)$$

The diagonal components are non-zero, indicating that there is no macroscopic coherence in the ensemble. Having found the density matrix, equation (4.12), we now describe the Hamiltonian used to obtain the equation of motion, see equation (4.8).

The Hamiltonian operator of the system we are studying is given by,

$$H = H_0 + H_I(t) + H_R, \quad (4.14)$$

where  $H_0$  is the Hamiltonian describing the system when external forces are absent,

$$H_0 = \begin{pmatrix} E_a & 0 \\ 0 & E_b \end{pmatrix} \quad (4.15)$$

The perturbation Hamiltonian  $H_I(t)$  is the operator representing the energy of the interaction between the two-level system and the applied electric field  $E(t)$ .  $H_R$  represent the various relaxation processes that return the ensemble to thermal equilibrium.

When the two energy levels are coupled by an electric-dipole transition, the dipole moment of the two-level system is denoted by  $er$  and its energy in the applied optical field is  $-er \cdot E(t)$ .

The Hamiltonian is then given by

$$H_I(t) = \begin{pmatrix} \delta E_a & -er_{ab} \cdot E(t) \\ -er_{ba} \cdot E(t) & \delta E_b \end{pmatrix} \quad (4.16)$$

<sup>2</sup>It should be mentioned that in our FWM experiments the light is circularly polarised and for these conditions the rotating wave approximation is inadequate since terms containing  $\omega + \Omega_{ab}$  vanish.

$$H_I(t) = \begin{pmatrix} \delta E_a & -er_{ab} \cdot E(t) \\ -er_{ba} \cdot E(t) & \delta E_b \end{pmatrix} \equiv \begin{pmatrix} 0 & \Delta_{ab} \\ \Delta_{ab}^* & 0 \end{pmatrix} \quad (4.16)$$

The diagonal components are due to the optically induced Stark shifts of the energy levels  $E_a$  and  $E_b$ . In the simplest approximation these are considered negligible. When the rotating wave approximation<sup>2</sup> is applied, the states with terms that oscillate at  $\omega + \Omega_{ba}$  are neglected.

The relaxation Hamiltonian represents the processes which relax the ensemble back to thermal equilibrium, such as phonon collisions, interaction with other electronic states or recombination. A simple phenomenological approach is taken. Two relaxation rates are assigned,  $T_1$  and  $T_2$ .  $T_1$  represents the processes that restore the population in the excited state back to the ground state.  $T_1$  is then effectively the lifetime of the excited state,

$$[H_R, \rho]_{bb} = \frac{-i\hbar\rho_{bb}}{T_1} \quad (4.17)$$

The ground state lifetime of the two-level system is assumed to be infinite.  $T_2$  is the lifetime of the coherent superposition state  $\psi$  and is often referred to as the ‘dephasing’ time for the dipole oscillator.  $T_2$  is a measure of the coherence which depends on both the lifetime of the excited state  $T_1$  and on the pure dephasing  $T_2^*$ .

$$\frac{1}{T_2} = \frac{1}{2T_1} + \frac{1}{T_2^*} \quad (4.18)$$

$T_2$  is then the lifetime of the dipole moments and the corresponding off-diagonal elements of the relaxation operator are

$$[H_R, \rho]_{ab} = \frac{i\hbar\rho_{ab}}{T_2} \quad \text{and} \quad [H_R, \rho]_{ba} = \frac{i\hbar\rho_{ba}}{T_2} \quad (4.19)$$

<sup>2</sup>It should be mentioned that in our FWM experiments the light is circularly polarised and for these conditions the rotating wave approximation is unnecessary since terms containing  $\omega + \Omega_{ba}$  vanish.

The relaxation-time approximation is valid if the response of the medium, in which the system under study is embedded, is either very fast or slow compared to the system-medium interactions [101]. Schmitt-Rink *et al.* [103] have shown that in the limit of a very fast response of the medium the linear absorption is Lorentzian (homogeneously broadened) and in the very slow response the linear absorption is Gaussian (inhomogeneously broadened).

The coupled equations of motion for the polarisation and the population of an ensemble of independent two-level systems are known as the optical Bloch equations. An alternative representation of the density matrix can be rewritten as

$$E(R, t) = B_1 A(R, t) \exp(i(k_1 \cdot R - \omega t)) + B_2 A(R, t - \tau_2) \exp(i(k_2 \cdot R - \omega t)), \quad (4.23)$$

$$\rho = \begin{pmatrix} n & \varrho \\ \varrho^* & 1 - n \end{pmatrix} \quad (4.20)$$

The optical Bloch equation can then be written as [101],

$$\frac{dn}{dt} + g_r n + \frac{i}{\hbar} (\Delta_{ab} \varrho^* - \varrho \Delta_{ab}^*) = 0, \quad \frac{d\varrho}{dt} + g\varrho + \frac{i}{\hbar} \Delta_{ab} (1 - 2n) = 0 \quad (4.21)$$

where  $g_r = 1/T_1$  and  $g = i\Omega_{ba} + 1/T_2$ . The optical Bloch equation cannot be solved analytically. A Taylor series in the incident field amplitudes is used; we formally write the density and polarisation as,

$$n = n^{(0)} + n^{(1)} + n^{(2)} + \dots \quad \text{and} \quad \varrho = \varrho^{(0)} + \varrho^{(1)} + \varrho^{(2)} + \dots \quad (4.22)$$

The solutions of third order polarisation were presented by Yajima and Taira in 1979 [99]. We study the relevant configuration used in this thesis, DFWM, see figure 4.1(a), where one of the two beams self diffracts off the grating. Both pulses are from the same mode-locked laser. Pulses one ( $k_1$ ) and two ( $k_2$ ) interfere to create a grating; pulse two then self-diffracts from this grating creating a signal in the direction,  $k_3 = 2k_2 - k_1$ . The TI-FWM gives a measure of the total energy diffracted in this direction whereas, the TR-FWM gives a measure of

the temporal evolution of the diffracted signal. The optical Bloch equations must be solved iteratively for two incident electric fields along  $k_1$  and  $k_2$  to obtain a third order polarisation along  $k_3$ .

The electric fields from a mode-locked laser cannot be approximated by monochromatic plane waves. The pulse along  $k_2$  is delayed by time  $\tau_d$  and the relative phase is set to zero. Assuming both pulses have the same linear polarisation and they are in line with the dipole moment and using the rotating wave approximation, then the electric field can be expressed as

$$E(R, t) = B_1 A(R, t) \exp[i(k_1 \cdot R - \omega t)] + B_2 A(R, t - \tau_d) \exp[i(k_2 \cdot R - \omega t)], \quad (4.23)$$

where  $B_1$  ( $B_2$ ) are the amplitude of the field of the first (second) pulse.  $A(R, t)$  is the electric field pulse shape at  $R$ , and  $\omega$  is the frequency at the peak of the mode-locked laser. Solving the third order polarisation in the  $k_3$  direction, assuming the pulse is a Dirac delta function, and assuming a thin sample (neglecting propagation effects) [99, 101],

$$\begin{aligned} \rho_{221}^{(3)} = & -i \left( \frac{e|r_{abl}|}{\hbar} \right)^3 \exp(-i\omega t) \exp[i(2k_2 - k_1) \cdot R] B_1 B_2^2 \\ & \times \Theta(\tau_d) \Theta(t - \tau_d) \exp[-Gt + (G - G^*)\tau_d]. \end{aligned} \quad (4.24)$$

$\Theta$  is the Heaviside function and  $G = (1/T_2) + i(\Omega_{ba} - \omega)$ . Therefore at resonance,  $\omega = \Omega_{ba}$ , the third-order polarisation in the direction  $k_3$  when  $\tau_d \geq 0$  and  $t \geq \tau_d$  decays with the dephasing time constant  $T_2$ .

The time-resolved and time-integrated FWM signal is then given as,

$$S_{221^*}^{(3)}(t) = |\rho_{221}^{(3)}|^2 \quad \text{and} \quad I_{221^*}^{(3)}(\tau_d) = \int_{-\infty}^{\infty} S_{221^*}^{(3)}(t) dt \quad (4.25)$$

respectively. These results are normally analysed in two limits, the homogeneous and inhomogeneous limits.

In the homogeneous limit for a Dirac pulse the TR-FWM peak will occur at  $t = \tau_d$ . For a

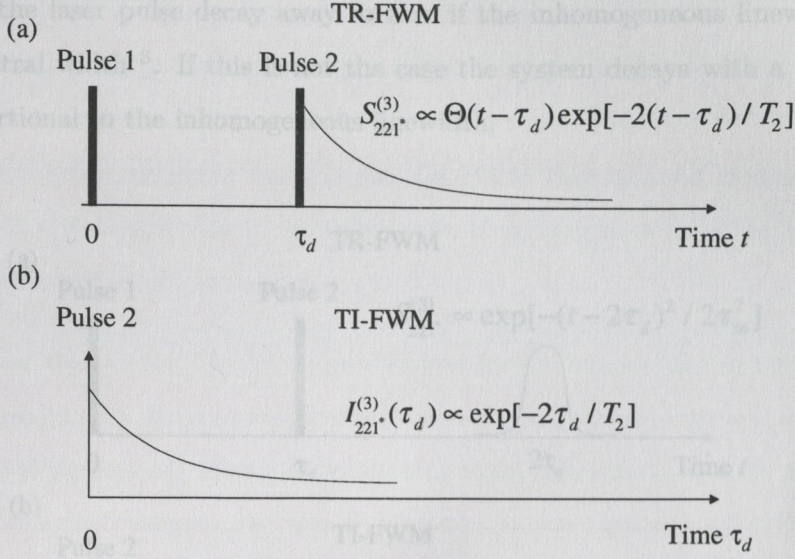


Figure 4.3: Representation of the TR-FWM as a function of time and the TI-FWM as a function of time delay for a homogeneously broadened two-level system and a Dirac delta pulse function [101].

real pulse, of pulse width  $\tau_p$  the peak will occur at  $t = \tau_d + \tau_p$  and for either case it will decay with a decay constant  $\tau_{decay} = T_2/2$ , see figure 4.3. The TI-FWM as a function of  $\tau_d$  is just the integration of the TR-FWM and decays as,

$$I_{221}^{(3)}(\tau_d) = I_{\text{hom}} \propto \exp\left(-\frac{2\tau_d}{T_2}\right) \quad (4.26)$$

This equation, giving a dephasing time from the TI-DFWM signal for a homogeneous system, is a very important result that we will be using throughout the thesis. The coherence time can then be used to work out the linewidth via,

$$\Gamma_{\text{hom}} = \frac{2\hbar}{T_2} \quad (4.27)$$

Using equations (4.26) and (4.27) in the next two chapters we measure the effect of exciton-phonon and exciton-exciton interactions on the coherence of the polariton.

For an inhomogeneously broadened system the phases of different frequency components excited within the laser pulse decay away to zero if the inhomogeneous linewidth ( $\Gamma_{inh}$ ) is within the spectral width <sup>3</sup>. If this is not the case the system decays with a time constant inversely proportional to the inhomogeneous linewidth.

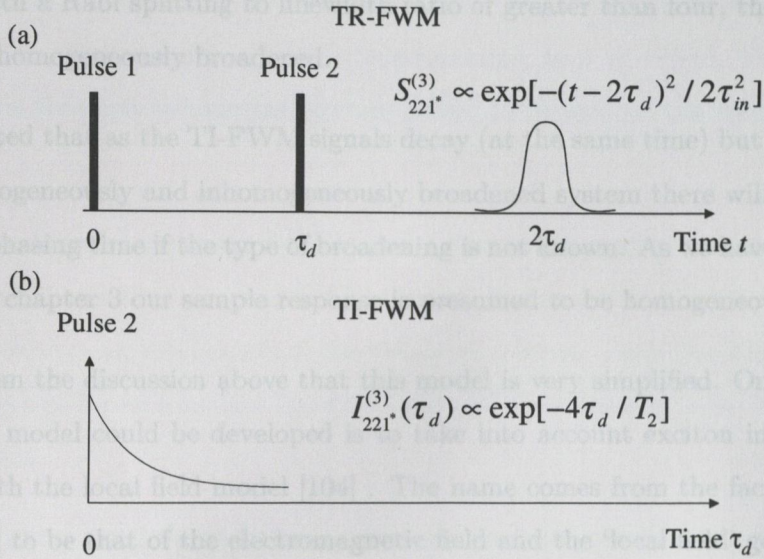


Figure 4.4: Representation of the TR-FWM as a function of time and the TI-FWM as a function of time delay for a inhomogeneously broadened two-level system and a Dirac delta pulse function [101].

If the second pulse arrives in a time which is short compared to  $T_2$  then this reverses the phase evolution and the phase is restored at time  $2\tau_d$  from the initial pulse, this is known as the photon echo, see figure 4.4. The width of the photon echo is determined by  $\tau_d$  and  $\Gamma_{inh}$  and the intensity of the photon echo is  $\propto \exp(-\frac{4\tau_d}{T_2})$ . The TI-FWM case is again the integration of the TR-FWM and decays as

$$I_{221}^{(2)}(\tau_d) = I_{inh} \propto \exp\left(\frac{-4\tau_d}{T_2}\right) \quad (4.28)$$

From equations (4.26) and (4.28) it is evident that the TI-FWM signal for an inhomogeneous

<sup>3</sup>Each individual phase decays with a rate which is inversely proportional to it's homogeneous linewidth.



system decays with a factor of two smaller than the homogeneous system,  $\frac{T_2}{4}$  compared with  $\frac{T_2}{2}$ . Another difference in the homogeneous and inhomogeneous systems is where the signal appears in the TR-FWM. In a homogeneous system the signal begins to decay at  $\tau_d$  whereas in an inhomogeneous system the system decays at  $2\tau_d$  (the photon echo). It was the large proportion of the decay occurring at  $\tau_d$  in the TR-FWM that allowed Bongiovanni [71] to deduce that, with a Rabi splitting to linewidth ratio of greater than four, the sample can be assumed to be homogeneously broadened.

It should be noted that as the TI-FWM signals decay (at the same time) but with a different rates for a homogeneously and inhomogeneously broadened system there will be some ambiguity in the dephasing time if the type of broadening is not known. As we have already stated and justified in chapter 3 our sample response is presumed to be homogeneously broadened.

It is evident from the discussion above that this model is very simplified. One way in which a more general model could be developed is to take into account exciton interactions, this can be done with the local field model [104]. The name comes from the fact that the total field is assumed to be that of the electromagnetic field and the 'local field' generated by the polarisation of the electron-hole pairs. This does not affect  $\tau_d$  of the FWM, however it does result in a rise-time where [101],

$$I_{221}^{(3)}(\tau_d) = I_{\text{FWM}} \propto \exp\left(\frac{4\tau_d}{T_2}\right). \quad (4.29)$$

Several other improvements have been made on this simple two-level model. These include theoretically modelling the FWM for a smooth transition from the homogeneous to inhomogeneous broadening regime [103], and improvements using the semiconductor Bloch equations including Coulomb coupling and exchange self-energy effects [96, 105].

The initial work on FWM in QW excitons was pioneered by Hegarty *et al.* [106]. Since then a large amount of FWM on QW excitons has been carried out on phonon scattering, exciton scattering and free carrier scattering [97, 98, 107, 108] and on the polarisation dependence of exciton dephasing [109, 110, 111, 112].

More recently there has been work on FWM in semiconductor microcavities [113, 114, 115, 116, 117], this work will be discussed in more detail in the next two chapters.

## 4.3 Conclusion

In this chapter we discussed the nonlinear spectroscopic tool of FWM. The properties of excitonic systems that can be ascertained were shown to depend on the configuration of the FWM.

A simple two-level model assuming DFWM and a Dirac delta pulse was described for both the time integrated and time resolved FWM setups. It was shown that the TR-FWM can determine the broadening mechanism of the two-level system. Both the TR-FWM and TI-FWM were shown to be an excellent spectroscopic tool for measuring the coherence time of a two-level system.

The limitations of the two-level model were discussed and improved models were commented upon. Reference was made to the extensive amount of FWM research carried out on QW excitons and microcavities, the work relevant to this thesis will be discussed in more detail in the following chapters.

Measuring the coherence of the excitonic system enables us to study fundamental interactions such as exciton-exciton and exciton-phonon interactions. In such interactions the linewidth which can be ascertained from the coherence of the system, see equation (4.27), is the characteristic parameter used.

## Chapter 5

# Acoustic phonon broadening of the lower polariton

In this chapter we discuss the acoustic phonon broadening of the Lower Polariton Branch (LPB) linewidth. The effect of acoustic phonon broadening on the homogeneous linewidth of the LPB is unlike that of the bare exciton, due to the modified dispersion curve [64], which was discussed in chapter 2. The modified polariton dispersion curve leads to a suppression of the acoustic phonon broadening that becomes more pronounced as the LPB becomes increasingly negatively detuned, and thus more photon-like. Four Wave Mixing (FWM) data is presented which clearly demonstrates this suppression at different detunings.

### 5.1 Introduction

The description of the cavity polariton in chapter 2 shows that although  $k_{\perp}$  symmetry is broken there is a conservation of the in-plane wave vector  $k_{\parallel}$ . There are three main scattering mechanisms which affect  $k_{\parallel}$ .

Firstly there is scattering of QW excitons by static disorder of the QW due to alloy fluctuations and interface roughness, which create fluctuations in the potential. The interaction of

excitons with a series of different potentials results in a range of different energies and gives rise to an inhomogeneously broadened system. As the scattering is from a weak disorder potential the process conserves kinetic energy and as a result of this it is not strongly affected by the cavity polariton dispersion curve. Scattering due to structural disorder has been extensively investigated [72, 76, 77, 78, 79, 118] and used to explain ‘motional narrowing’. This was discussed in detail in section 2.7.3.

The second scattering mechanism is polariton-phonon scattering which differs from the scattering due to structural disorder in that the kinetic energy of the polariton is not conserved. There are two types of polariton-phonon scattering, acoustic and optic. Acoustic phonon scattering, which is the subject of this chapter, is dominant at low temperatures whereas the optical phonons become the main scattering mechanism at high temperatures ( $> 80\text{K}$ ) [52]. In view of the large energy of GaAs optical phonons, approximately  $36\text{meV}$ , compared to the splitting of the cavity polaritons, approximately  $4\text{meV}$ , it can be assumed that the optical phonon scattering is unlikely to be significantly affected by the strong coupling [119]. However, it should be noted that work by Pau [66], who used longitudinal optical phonons to bypass the slow thermalisation of ‘hot excitons’, *i.e.* the bottleneck (see section 2.7.2), found the emission to exhibit a strong angular dependence due to the nature of the polariton dispersion curve.

Polariton-polariton scattering, the third scattering mechanism which affects  $k_{\parallel}$ , is strongly affected by the dispersion curve. This is due to the fact that the kinetic energy of the individual polariton is not conserved; of course overall energy conservation of the polaritons is not broken. This scattering mechanism, is the topic of chapter 6 and so we will not dwell on the details here.

We study the effect of acoustic phonon scattering by extracting a homogeneous linewidth for the LPB from a FWM experiment. We then investigate the effect of temperature on this linewidth as the temperature defines the number of the acoustic phonons; this is discussed in more detail below.

The chapter is set out as follows: firstly a succinct reminder of the physics of acoustic phonons is given before a short summary of the theory is presented. This is followed by a

brief description of the sample and details of the experimental setup. The results are then compared with the literature and finally conclusions are drawn.

## 5.2 Acoustic phonons

In solids, lattice vibrations take the ions of the lattice away from their positions of minimum energy. Only certain vibrational frequencies occur in crystalline solids due to the periodicity of the lattice. Phonons are the quanta associated with these frequencies whose characteristics depend on the material. We consider only long wavelength phonons, much greater than the lattice constant, a fact which enables us to treat the phonons classically. The phonons discussed in this section, are that of an idealised case. A real crystal would require a fourth-order stiffness tensor which is not necessary for the analysis here. The simplest way in which to view these crystal vibrations is by looking at an idealised 1D case, *i.e.* that of a linear chain of ions linked together by springs which obey Hooke's law [120]. A vibration along the monatomic chain has two possible transverse degrees of freedom and one longitudinal degree of freedom. In a structure with more than one atom per primitive cell such as GaAs the ions may combine to generate the same wave, as in the case of acoustic phonons, or each set may individually create their own wave, as in the case of optical phonons, see figure 5.1(a).

The longitudinal acoustic phonon in one dimension along the x-direction, with atoms of mass  $m$  separated by a distance  $a$ , and the displacement of atom  $j$  by  $u_j$  due to the phonon is substituted into Newton's second law to give [120],

$$m \frac{d^2 u_j}{dt^2} = R[(u_{j-1} - u_j) - (u_j - u_{j+1})]. \quad (5.1)$$

The solution to the equation can be written as  $u_j = U_0 \cos(qx - \omega_q t)$  where  $x = ja$ ,  $U_0$  is a constant,  $R$  is the elastic spring constant and  $q$  is the wave vector of the phonon;  $q$  is used to distinguish the phonon wave vector from the exciton wave vector which will be called  $k$ . Substituting this solution back into the equation of motion gives the dispersion relation

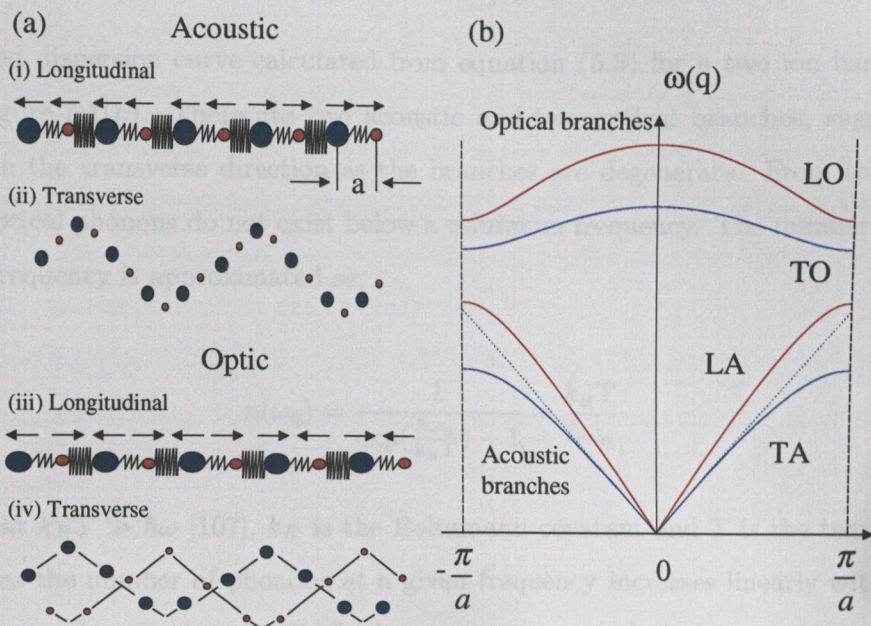


Figure 5.1: (a) A pictorial representation of (i) longitudinal acoustic (ii) transverse acoustic (iii) longitudinal optic (iv) transverse optic phonons. The second degree of freedom for the transverse waves is perpendicular to the page. (b) An idealised phonon dispersion showing the longitudinal and degenerate transverse optical and acoustic modes. It can clearly be seen that the optical modes have a minimum non-zero frequency at which they exist. This corresponds to a temperature of  $\approx 100\text{K}$  in GaAs. The linear approximation of the transverse acoustic mode is also shown on the diagram.

$$\omega_q = 2\sqrt{\frac{R}{m}} \left| \sin \frac{qa}{2} \right|, \quad (5.2)$$

where  $\omega_q$  is the phonon frequency at a given wave vector. In the case of a two ion system, using the same formalism as above and assuming the ions are identical, but with two different spring constants,  $K$  and  $R$ , we arrive at,

$$\omega_q^2 = \frac{K + R}{m} \pm \frac{1}{m} \sqrt{K^2 + R^2 + 2KR \cos(qa)}. \quad (5.3)$$

The +ve is the solution for the optical phonons whilst the -ve is the solution for the acoustic

phonons.

The idealised dispersion curve calculated from equation (5.3) for a two ion basis crystal is shown in figure 5.1(b). There are two acoustic and two optical branches, suggesting a  $q$ -symmetry in the transverse direction as the branches are degenerate. From this it can be seen that optical phonons do not exist below a minimum frequency. The number of phonons at a given frequency is approximated as;

$$n(\omega_q) = \frac{1}{\exp(\frac{\hbar\omega_q}{k_B T}) - 1} \approx \frac{k_B T}{\hbar\omega_q}, \quad (5.4)$$

provided that  $k_B T \gg \hbar\omega$  [107],  $k_B$  is the Boltzmann constant and  $T$  is the temperature in Kelvin. Thus the number of phonons at a given frequency increases linearly with temperature. This approximation is not valid for low temperature optical phonons due to their large frequency but is a valid approximation for low frequency acoustic phonons.

The optical phonon energy in bulk GaAs is approximately equal to 36meV [121]. This energy corresponds to a phonon occupation of only 0.015 at a temperature of 100K, via equation (5.4), which is considered to be negligible [122]. The maximum temperature used in our experiment was 80K, a fact which allows us to ignore optical phonon effects.

Acoustic phonons, unlike optical phonons, cannot be neglected at low temperatures (energies), see figure 5.1. At low temperatures we assume that high energy (large  $q$ ) acoustic phonons are negligible. This assumption enables a linear approximation of the acoustic phonon dispersion curve. This linear approximation  $\omega_q = c_s q$ , where  $c_s$  is the speed of sound  $\simeq 5000 \text{ ms}^{-1}$  in GaAs [123], is shown for the transverse acoustic branch in figure 5.1(b). This approximation is used in the theoretical work discussed later [118, 124].

The parameters of bulk GaAs have been used, rather than a modified phonon description to take into account the two dimensional phonon field and surface phonon effects. The reason for this is that, due to the very low indium content of the QW ( $\text{In}_{0.05}\text{Ga}_{0.95}\text{As}$ ) there is a small lattice mismatch between the QW and surrounding GaAs material; we have assumed the phonons in the QW are equivalent to the phonons in the GaAs cavity [125]. This

negates the need for any special treatment of the phonon field. In essence we have a three dimensional phonon interacting with a two dimensional exciton. Crystal momentum will only be conserved in the plane. The same approximation has been made in the theoretical papers investigating this topic [122, 124]. As the phonon, to a good approximation, 'sees' the same crystal structure in all directions, crystal momentum is conserved in all directions. However the QW affects the crystal structure that the exciton 'sees', it is broken in the perpendicular direction but remains periodic in the direction parallel to the QW. Thus crystal momentum is only conserved parallel to the QW. As the QW exciton does not conserve crystal momentum in the perpendicular direction it can interact with an arbitrary phonon momentum in the perpendicular direction. This gives rise to an enhancement of the phonon scattering rate by two orders of magnitude [126].

The acoustic phonons interact with excitons via the deformation potential. The phonons produce compression and rarefaction of alternating sections of the crystal which cause the edge of the electronic band to move up and down by an amount which is proportional to the strain. The constant of proportionality is called the deformation potential. The deformation potential interaction expressed as a Hamiltonian,  $H_{\text{exc-ph}}$ , used in Fermi's golden rule gives a transition rate for the absorption or emission of a phonon. Piezoelectric scattering also occurs in GaAs, as it is a polar material, however it has a negligible contribution to exciton dynamics [127].

### 5.3 Theory of exciton and polariton scattering by acoustic phonons

Several groups have worked on the theory of exciton and polariton scattering by acoustic phonons [51, 124, 126]. Lee *et al.* [51] presented detailed experimental and theoretical work on the effects of phonon broadening in exciton QWs, showing the linewidth to vary linearly with temperature when assuming acoustic phonon scattering to be the only broadening mechanism. The temperature dependent homogeneous linewidth, taking into account acoustic phonon scattering only, is given by,



$$\Gamma_h = \Gamma_0 + \gamma T, \quad (5.5)$$

$\Gamma_0$  is the linewidth at 0K and  $\gamma$  is the linear scattering coefficient. This linear relationship is indicative of a one phonon process and can be related back to the phonon number equation (5.4) which is approximately linear with temperature at these frequencies and temperatures. Lee *et al.* measured a linear scattering coefficient of  $7.5\mu\text{eVK}^{-1}$  by analysing the luminescence linewidths in a 20 period GaAs/AlGaAs bare QW at low temperatures ( $<150\text{K}$ ).

In 1986 a dynamic study, using FWM, of the effect of acoustic phonon scattering on the QW exciton linewidth was undertaken by Schultheis *et al.* [52]. A linear dependence on linewidth with temperatures from 5K to 80K in a single QW (GaAs/Al<sub>0.3</sub>Ga<sub>0.7</sub>As) was demonstrated. The value of the linear scattering coefficient,  $\gamma$ , measured for the heavy hole bare QW exciton is  $10\mu\text{eVK}^{-1}$ .

The theoretical work by Savona and Piermarocchi [118, 122, 128], calculates the polariton states and includes scattering by phonons as a perturbation. This is a simplified theory taking into account only the acoustic phonon scattering via the deformation potential. It does not take into account exciton (or electron) optical phonon scattering, limiting the validity to temperatures  $< 100\text{K}$ , and it also ignores exciton-exciton and exciton-free carrier scattering, constraining it to low carrier densities. Here we illustrate only the main points of the acoustic phonon scattering theory and the reader is referred to the original texts for the full analysis. We begin with the analysis of the exciton acoustic phonon interaction, and this is later extended to the polariton interaction with acoustic phonons. The deformation potential interaction for an exciton-longitudinal acoustic phonon is

$$U(\mathbf{r}_e, \mathbf{r}_h) = \Delta(\mathbf{r}_e)\Xi_e - \Delta(\mathbf{r}_h)\Xi_h, \quad (5.6)$$

where  $\Delta(\mathbf{r}_e)$  and  $\Delta(\mathbf{r}_h)$  are the relative deformations of the lattice at the points where the electrons and holes are located.  $\Xi_e$  and  $\Xi_h$  are the bulk deformation potentials which are experimentally measured. The exciton-phonon Hamiltonian is then given by,

$$H_{\text{exc-ph}} = \sum_{q_z} \sum_{q_{\parallel}, k_{\parallel}, k'_{\parallel}} G(q_{\parallel}, q_z) \delta_{k'_{\parallel}, k_{\parallel} + q_{\parallel}} (\hat{c}_{q_{\parallel}, q_z} - \hat{c}_{-q_{\parallel}, q_z}^{\dagger}) \hat{A}_{k'_{\parallel}}^{\dagger} \hat{A}_{k_{\parallel}}, \quad (5.7)$$

where  $\hat{A}_{k_{\parallel}}^{\dagger}$  ( $\hat{A}_{k_{\parallel}}$ ) is the creation (annihilation) operator of the two dimensional exciton system with in-plane wave vector  $k_{\parallel}$  and  $\hat{c}_{q_{\parallel}, q_z}^{\dagger}$  ( $\hat{c}_{q_{\parallel}, q_z}$ ) is the creation (annihilation) of three dimensional phonons with wave vector  $(q_{\parallel}, q_z)$ . Translational invariance along the QW plane means there is momentum conservation represented by the Kronecker delta function,  $\delta$ . However the  $z$  component of the wave vector is not conserved and hence the summation across all  $q_z$  appears. The  $G(q_{\parallel}, q_z)$  contains all the parameters of the interaction:

$$G(q_{\parallel}, q_z) = i \sqrt{\frac{\hbar(|q_{\parallel}|^2 + q_z^2)^{\frac{1}{2}}}{2\rho c_s \Omega}} [\Xi_e I_e^{\parallel}(|q_{\parallel}|) I_e^{\perp}(q_z) - \Xi_h I_h^{\parallel}(|q_{\parallel}|) I_h^{\perp}(q_z)], \quad (5.8)$$

$\Omega$  is the quantisation volume and  $\rho$  is the density of GaAs. The terms  $I_{e(h)}^{\parallel}(|q_{\parallel}|)$  and  $I_{e(h)}^{\perp}(q_z)$  are the superposition integrals of the exciton envelope function and the phonon wavefunction in the in-plane and the  $z$  direction respectively.

The importance of this equation is that the integrals introduce cut-offs in  $G(q_{\parallel}, q_z)$  for  $|q| > \frac{1}{a_B}$  where  $a_B$  is the exciton bohr radius and  $q_z > \frac{3\pi}{L_{\text{QW}}}$  where  $L_{\text{QW}}$  is the QW width. For a complete expression please refer to Savona [128]. The latter expression corresponds to an energy cut-off  $E_{\text{cut}} = \hbar c_s q_z$  perpendicular to the QW. The excitons can be thought of as being able to interact with phonons of longer wavelength than their radii. The localisation of the electrons and holes in the QW decreases the size of the exciton radius and enables it to interact with shorter wavelength (*i.e.* higher energy) phonons. Thus the narrower the QW, the greater the interaction between exciton and phonon and this effect becomes important in narrow QWs such as our own. It is important not to underestimate the size of the QW as there will be penetration into the barrier material. If the size of the well is underestimated, the broadening will be over-estimated.

In summary, phonons can be treated as three dimensional due to the low indium content in the QW, resulting in a weak modification of the phonon dispersion due to the QW. Nevertheless

from the argument above it can be seen that the size of the QW which leads to a confinement of the exciton determines which phonons the exciton can interact with; thus the two dimensional nature of the exciton is important and must be taken into account.

The dependence of phonon scattering on the QW width was suggested by Schmitt-Rink *et al.* [57] and has been experimentally investigated [108, 129]. However further experimental work on the recently available high quality samples would add greatly to this work; as yet only a rough agreement has been seen at low temperatures.

When the exciton phonon Hamiltonian interaction is substituted into Fermi's golden rule it is subdivided into absorption  $W^{\text{abs}}$  and emission  $W^{\text{ems}}$  terms where  $W_{a,k_{\parallel} \rightarrow b,k'_{\parallel}} = W_{a,k_{\parallel} \rightarrow b,k'_{\parallel}}^{\text{abs}} + W_{a,k_{\parallel} \rightarrow b,k'_{\parallel}}^{\text{ems}}$ .

Savona [118], when investigating the effect of acoustic phonon scattering in the polariton system, used the basis of this model and summed over the transition rate given by Fermi's golden rule to derive homogeneous linewidths for both the UPB and the LPB. These included the scattering by acoustic phonons via the deformation potential at  $k_{\parallel}=0$ , still subject to the restrictions of low temperatures and low densities:

$$\begin{aligned} \gamma_{a,0} &= \sum_{k_{\parallel},b} W_{a,0 \rightarrow b,k_{\parallel}} \\ &= \frac{1}{2} C \sum_b \int_0^{\infty} k_{\parallel} dk_{\parallel} \left( \frac{E_b(k_{\parallel})}{\hbar c_s} \right)^2 \frac{|X_b(k_{\parallel})|^2}{|\hbar c_s q_z^0|} |I_{\parallel}(k_{\parallel})|^2 |I_{\perp}(q_z^0)|^2 \frac{1}{\exp\left(\frac{E_b(k_{\parallel})}{k_B T}\right) - 1}, \end{aligned} \quad (5.9)$$

where  $C$  is the interaction constant and  $q_z^0$  is the exchange component of the wave vector, see [122].  $E_b(k_{\parallel})$  is the polariton dispersion. This equation cannot be solved analytically and its solution is beyond the scope of this thesis.

From this equation the main points of polariton-acoustic phonon interaction can be gathered. Clearly the broadening depends on the dispersion of the polaritons which in turn depend on their interaction with the photon field and this can be characterised by an oscillator strength, Pau does this explicitly [124]. The dispersion will contain the energy of the polariton and the density of states available for it to scatter into, both of which are relevant for the broadening.

The broadening depends on several factors: the Hopfield coefficient; the number of phonons; and the superposition integrals of the exciton envelope function and the phonon wavefunction. The square modulus of the Hopfield coefficient,  $X_b(k_{\parallel})$ , gives the exciton fraction of the polariton state in both the initial and final scattering states. The number of phonons is given by equation (5.4). The dependence of the scattering efficiency on the exciton envelope function results in a dependence on the size of the QW.

The solution of this equation shows a strong suppression of acoustic phonon scattering of the LPB for non-zero temperatures compared to the bare QW exciton. This is the result of the reduced exciton fraction of the lower polariton and the modified LPB dispersion curve compared to the bare QW exciton. At  $k_{\parallel}=0$  the LPB has only a small number of density of states to scatter into unless the energy is large enough to allow scattering to the large density of states at large  $|k_{\parallel}|$ ; the large  $|k_{\parallel}|$  states are energetically decoupled from  $k_{\parallel}=0$ . Even when high enough energies are obtained to allow scattering to the large density of states, Savona predicts, a reduced linear scattering coefficient compared with the bare QW exciton due to the energy step, a result of the modified dispersion curve. The UPB, however, begins to scatter from  $T=0\text{K}$  and the scattering efficiency is predicted to be 10 times larger than the LPB due to the interbranch scattering process. This scattering mechanism is unavailable to the LPB [118].

Thus, it is theoretically predicted [118], that collisional broadening of the lower cavity polariton fundamentally differs from collisional broadening of the bare QW exciton [52, 107]. To experimentally investigate this we use FWM.

## 5.4 Sample and experimental setup

The sample used in this experiment, which is described in more detail in chapter 3, is the one QW sample (1QW). The single QW ( $\text{In}_{0.05}\text{Ga}_{0.95}\text{As}$ ) is at the antinode of a  $1\lambda$  GaAs cavity which is bounded by 20 front and 23.5 back distributed Bragg reflector pairs ( $\text{AlAs}/\text{Al}_{0.1}\text{Ga}_{0.9}\text{As}$ ). The cavity is wedged to allow detuning of the photon mode across the exciton resonance. This allows measurements to be made at several different detunings. The

quality of the sample is attested to by the narrowness of the UPB and LPB linewidths of 0.5meV and 0.3meV at 10-15K.

Dephasing times were measured using time integrated degenerate FWM in transmission geometry, see figure 5.2. A 10W Ar<sup>+</sup>-pumped Ti:Sapphire (Spectra Physics Tsunami) laser was directed through an optical isolator, two glass slides reflected a fraction of the beam into a spectrum analyser and a mini autocorrelator respectively. The setup was mode-locked to give a pulse width of 1.1ps. This allowed us to spectrally resolve the LPB from the UPB. The laser pulse was split into two parts of equal power. One pulse was delayed by time  $\tau_d$  with respect to the other using a retro-reflector on a translation stage with a computer controlled stepper motor. The two pulses were then brought parallel to each other and their polarisation was set by a linear polariser and a 830nm quarter wave plate. The pulses were then focussed onto the sample, using a 15cm focal length lens, to a measured

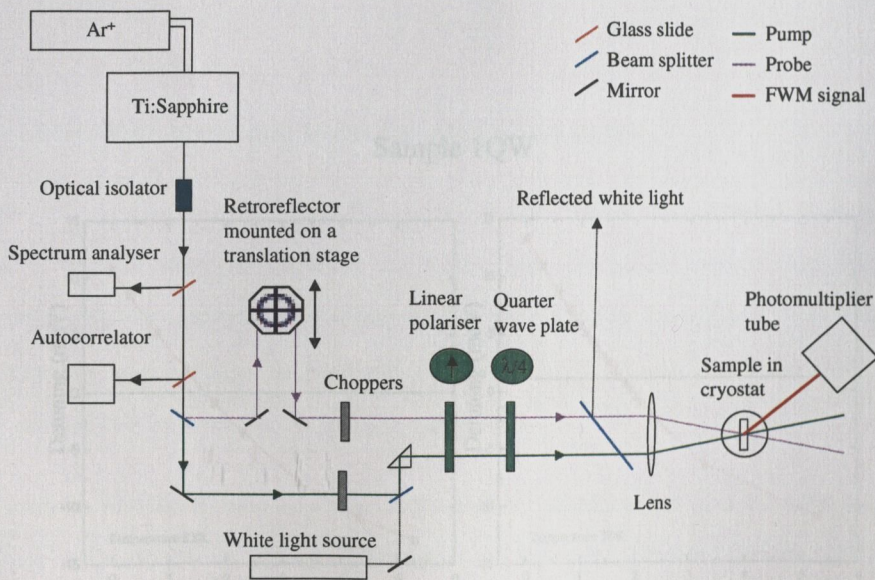


Figure 5.2: A schematic representation of the FWM setup. The pulsed light from the Ti:Sapphire was split into two beams, the pump and the probe. The probe was delayed with respect to the pump by a retroreflector. Both beams were focussed onto the sample, the transmitted diffracted signal was time integrated by a photomultiplier tube.

The pulses were then focussed onto the sample, using a 15cm focal length lens, to a measured

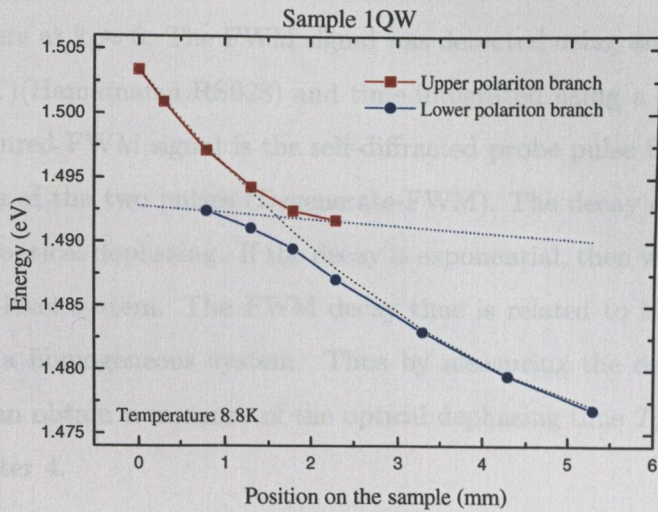


Figure 5.3: The positions of the reflectivity minimum of the UPB and LPB at different positions on the sample.

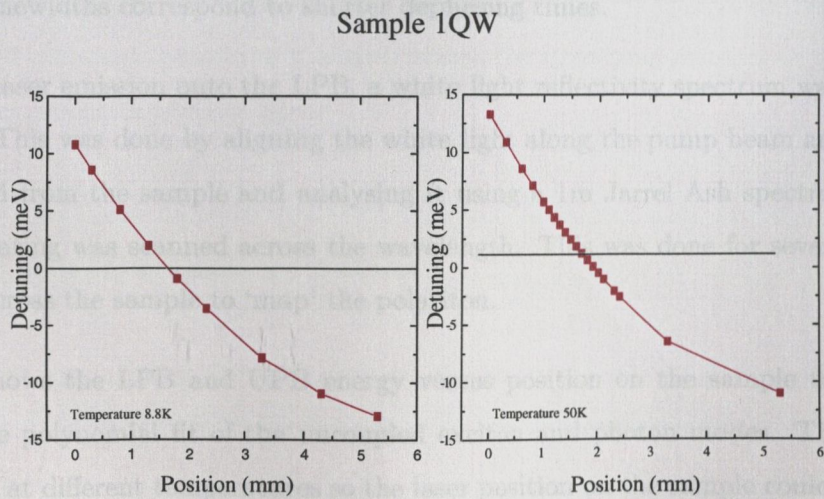


Figure 5.4: The detuning at different positions on the sample for 8.8K and 50K. The temperature dependence of the exciton energy is greater than the cavity, resulting in the detuning across the sample changing with temperature. To track a fixed detuning with temperature a detuning versus position map was made of the sample at each temperature for which data was taken. Above are two illustrative examples.

spot size of  $110\mu\text{m}$ . The angle between the two beams was less than  $3^\circ$  to ensure the excited polariton states were at  $k_{\parallel} \approx 0$ . The FWM signal was detected using an air cooled PhotoMultiplier Tube (PMT)(Hamamatsu RS928) and time integrated using a dual lock-in detection system. The measured FWM signal is the self-diffracted probe pulse from a grating created by the interference of the two pulses (Degenerate-FWM). The decay of the FWM signal in principle is due to optical dephasing. If the decay is exponential, then we assume a dephasing time  $T_2$  for a two-level system. The FWM decay time is related to the dephasing time by  $T_{(\text{FWM})} = \frac{2}{T_2}$  for a homogeneous system. Thus by measuring the decay of the diffracted FWM signal we can obtain a measure of the optical dephasing time  $T_2$ . This was discussed more fully in chapter 4.

From the dephasing time the homogeneous linewidth ( $\Gamma_h$ ) can be determined using

$$\Gamma_h = \frac{2\hbar}{T_2}, \quad (5.10)$$

thus larger linewidths correspond to shorter dephasing times.

To tune the laser emission onto the LPB, a white light reflectivity spectrum was taken from the sample. This was done by aligning the white light along the pump beam and taking the light reflected from the sample and analysing it using a 1m Jarrel Ash spectrometer and a PMT; the grating was scanned across the wavelength. This was done for several detunings (positions) across the sample to ‘map’ the polariton.

Figure 5.3 shows the LPB and UPB energy versus position on the sample taken at 8.8K with a simple polynomial fit of the uncoupled exciton and photon modes. This procedure was repeated at different temperatures so the laser position on the sample could be changed, if necessary, to remain at the same detuning whilst the temperature changed. An example showing the change in detuning with temperature is given in figure 5.4 for 8.8K and 50K. The change in detuning was due to the larger effect of temperature on the exciton energy, which scales with the bandgap, compared to the energy of the cavity which scales with the refractive index [130].

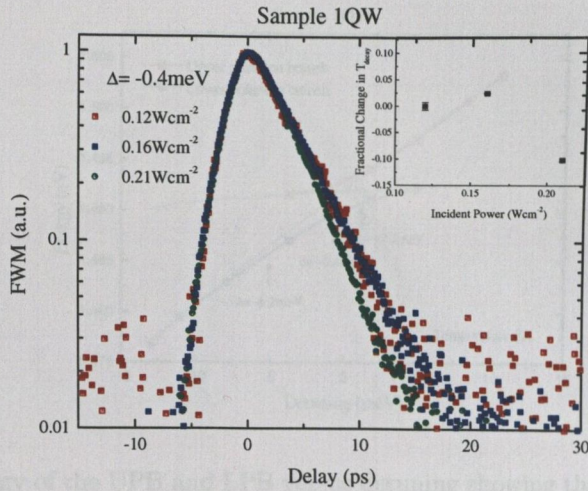


Figure 5.5: The FWM results for three intensities at a detuning of  $-0.4\text{meV}$ .

To specifically measure acoustic phonon broadening, the temperature of the sample was kept below  $80\text{K}$  and low excitation densities were used (polariton densities less than  $10^{10}\text{cm}^{-2}$ ) to prevent exciton-exciton and exciton-free carrier interactions, as discussed above. As a further test that no collisional broadening was occurring,<sup>1</sup> the FWM data was taken at several intensities and then kept below the intensity where the dephasing rate began to change due to exciton-exciton scattering, see figure 5.5.

## 5.5 Experimental results

The FWM data was taken on the LPB at three detunings on the sample;  $\Delta = -6.2\text{meV}$ ,  $\Delta = -0.4\text{meV}$  and  $\Delta = +2.1\text{meV}$ . These detunings are marked on figure 5.6.

The first temperature dependent FWM results were taken at  $\Delta = -6.2\text{meV}$ . These results showed no change in the FWM decay up to  $40\text{K}$ , as illustrated by figure 5.7. This is in

<sup>1</sup>To ensure the data was taken in the density independent regime the intensity independence of the decay of the FWM signal was checked. Another possible method to ascertain if the signal was intensity independent was to calculate the polariton density. However, as the spot size was known to be overestimated an accurate polariton density could not be obtained using this method and the polariton density would have been underestimated.



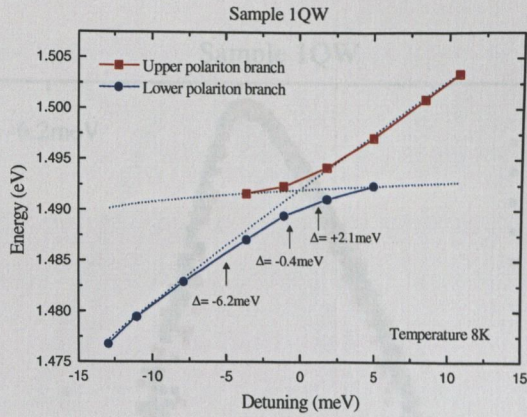


Figure 5.6: The energy of the UPB and LPB versus detuning showing the three positions where the FWM data was taken on the LPB. Simple polynomial fits have been made to the bare exciton and cavity.

contrast with the behaviour of a bare QW which shows a linear increase in linewidth from 5K.

At this large negative detuning the LPB is photon-like. Photons weakly interact with the deformation potential and hence with acoustic phonons. The FWM signal was observed to be weak, due to the increased photon-like behaviour at negative detunings *i.e.* low absorption.

The second temperature dependent FWM results were taken at  $\Delta = -0.4\text{meV}$ . This position is very close to resonance where the polariton can be thought of as half-exciton half-photon. The results show no change up to a temperature of 20K, whereupon the FWM signal decays more quickly with increasing temperature, as seen in figure 5.8. The FWM is less noisy here, near resonance, than at negative and positive detunings as there is a strong exciton content which gives rise to a strong grating, and there is also transmission which allows the diffracted probe to be detected.

The third FWM results were taken at  $\Delta = +2.1\text{meV}$ . Here the LPB is more exciton-like than the previous detunings and the FWM results are affected by acoustic phonon scattering at a lower temperature somewhere between 10K and 15K. The FWM, once again, is shown to decay more quickly above these temperatures. The large exciton content of the polariton results in a strong grating, but, it is hard to obtain a good signal at low intensities due to

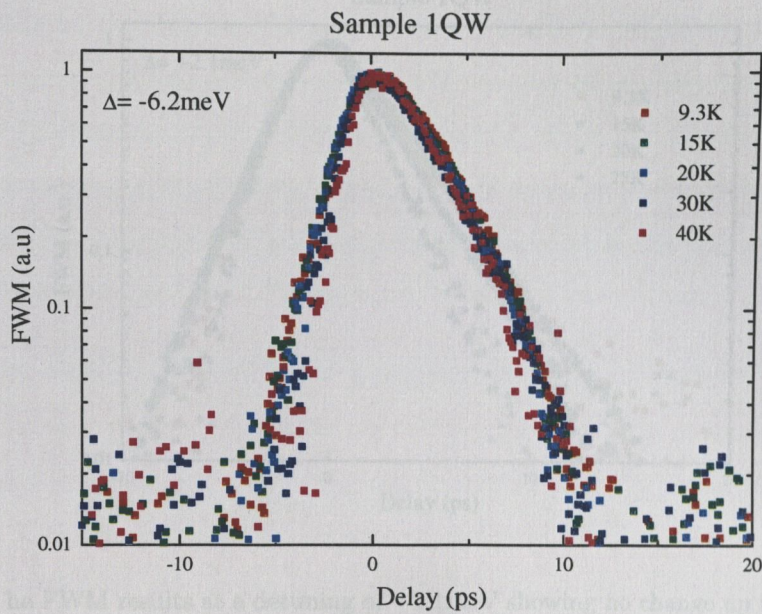


Figure 5.7: The FWM results at a detuning of  $-6.2 \text{ meV}$  showing no change up to a temperature of  $40 \text{ K}$ .

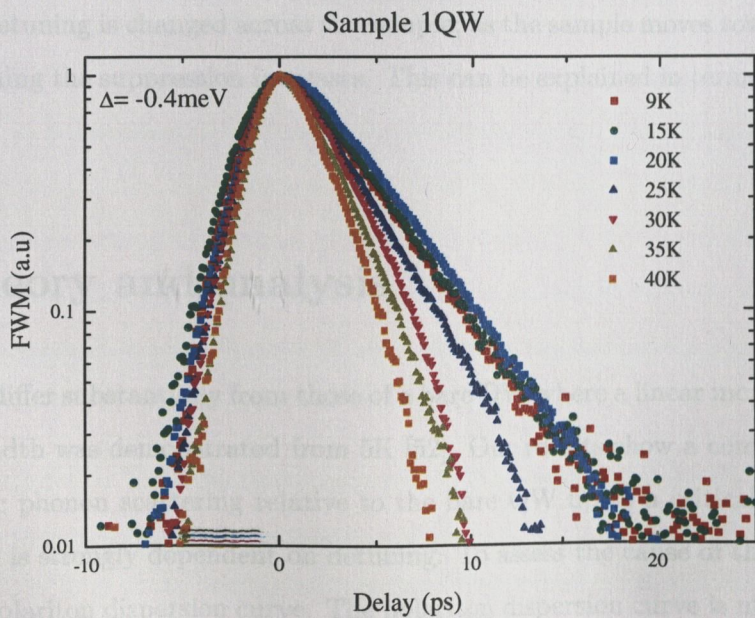


Figure 5.8: The FWM results at a detuning of  $-0.4 \text{ meV}$  showing no change up to a temperature of  $20 \text{ K}$ . Above  $20 \text{ K}$  the FWM decay rate increases as the temperature is increased.

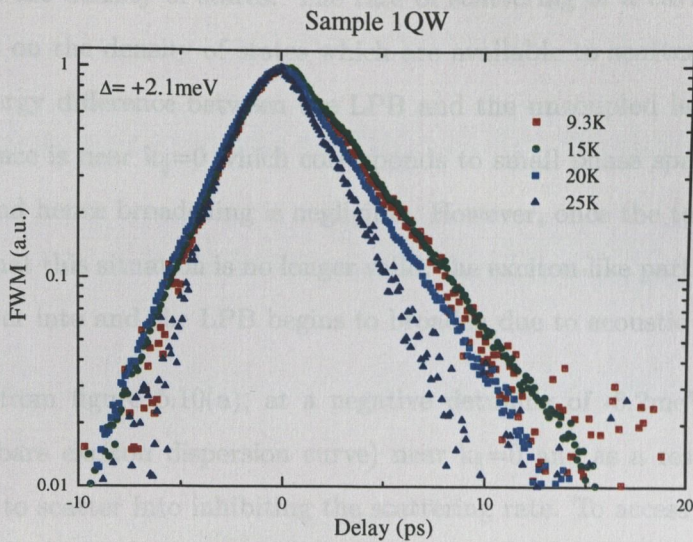


Figure 5.9: The FWM results at a detuning of +2.1meV showing no change up to a temperature of 10-15K.

the low transmission.

These results show the suppression of acoustic phonon scattering on the LPB. The suppression varies as the detuning is changed across the sample; as the sample moves towards increasingly negative detuning the suppression increases. This can be explained in terms of the dispersion curve.

## 5.6 Theory and analysis

These results differ substantially from those of a bare QW where a linear increase of the homogeneous linewidth was demonstrated from 5K [52]. Our results show a complete suppression of the acoustic phonon scattering relative to the bare QW up to a critical temperature the value of which is strongly dependent on detuning. To assess the cause of this suppression we examine the polariton dispersion curve. The polariton dispersion curve is modified compared to the bare QW dispersion curve, which is effectively flat over the region of interest. The polariton dispersion curve also varies at different detunings. The gradient of the dispersion

curve determines the density of states. The rate of scattering of a cavity polariton created at  $k_{\parallel}=0$  depends on the density of states which are available to scatter into. When  $k_B T$  is less than the energy difference between the LPB and the uncoupled large  $k_{\parallel}$  reservoir, the only available space is near  $k_{\parallel}=0$  which corresponds to small phase space and the resulting scattering rate and hence broadening is negligible. However, once the temperature increases to a point such that this situation is no longer valid, the exciton-like part at large  $k_{\parallel}$  becomes available to scatter into and the LPB begins to broaden due to acoustic phonon scattering.

As can be seen from figure 5.10(a), at a negative detuning of  $-6.2\text{meV}$  the LPB is steep (relative to the bare exciton dispersion curve) near  $k_{\parallel}=0$  and as a result there is a small density of states to scatter into inhibiting the scattering rate. To access the large density of states at large  $k_{\parallel}$  the cavity polaritons require an energy of  $>6.8\text{meV}$ . This energy corresponds to a temperature of  $80\text{K}$ . We see the suppression of acoustic phonon scattering up to  $40\text{K}$ , see figure 5.11. Close to resonance at a detuning of  $-0.4\text{meV}$ , the gradient of the LPB still results in an inhibition of the scattering due to the decreased density of states. However, the energy difference between the LPB and the reservoir of states at large  $k_{\parallel}$  has decreased to  $1.7\text{meV}$ , see figure 5.10(b). This corresponds to a temperature of  $20\text{K}$  and as can be seen in figure 5.11 this is in excellent agreement with the experimentally measured temperature of  $20\text{K}$  where the homogeneous linewidth increases due to acoustic phonon scattering. For the final position corresponding to a detuning of  $+2.1\text{meV}$ , even though the gradient is significantly less than the more negative detunings, it decreases the density of states enough to inhibit scattering. However the smaller energy difference of  $0.8\text{meV}$  between the LPB and the reservoir states, as shown in figure 5.10(c), reduces the temperature to which the scattering is inhibited.  $0.8\text{meV}$  corresponds to a temperature of  $10\text{K}$  which is in moderately good agreement with our measurement of between  $10\text{-}15\text{K}$ , see figure 5.11.

It should be noted that once the temperature is high enough the acoustic phonon scattering rate is directly proportional to temperature, see figure 5.11. However there is still a difference from the bare QW in that the scattering rate is smaller compared to the case of the bare QW. At a negative detuning of  $-6.2\text{meV}$  the value for  $\gamma$  is negligible,  $0.16\mu\text{eVK}^{-1}$ , as opposed to  $7\mu\text{eVK}^{-1}$  near resonance and a value of  $9.2\mu\text{eVK}^{-1}$  at a detuning of  $+2.1\text{meV}$ .

## Dispersion curves for three different detunings

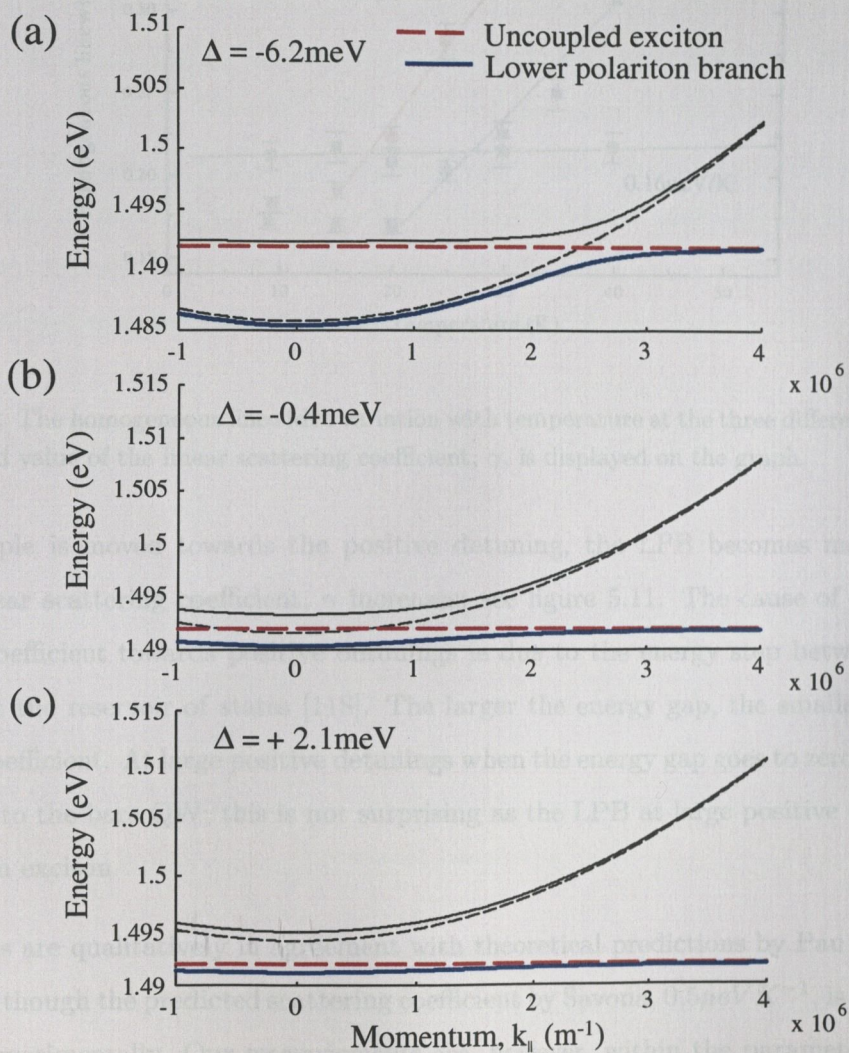


Figure 5.10: Dispersion curve at three different detunings  $\Delta = -6.2 \text{ meV}$ ,  $\Delta = -0.4 \text{ meV}$  and  $\Delta = +2.1 \text{ meV}$ . — Uncoupled cavity line - - - uncoupled exciton line.

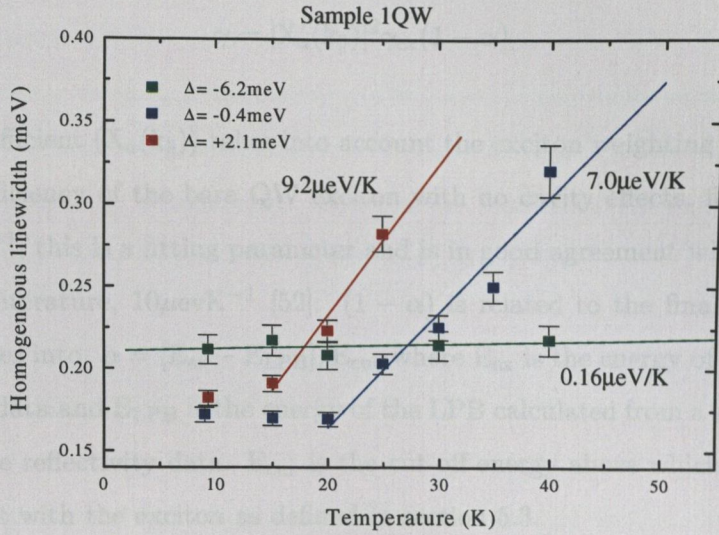


Figure 5.11: The homogeneous linewidth variation with temperature at the three different detunings. The measured value of the linear scattering coefficient,  $\gamma$ , is displayed on the graph.

As the sample is moved towards the positive detuning, the LPB becomes more exciton-like, the linear scattering coefficient,  $\gamma$  increases; see figure 5.11. The cause of the reduced scattering coefficient towards positive detunings is due to the energy step between LPB at  $k_{\parallel}=0$  and at the reservoir of states [118]. The larger the energy gap, the smaller the linear scattering coefficient. At large positive detunings when the energy gap goes to zero,  $\gamma$  becomes comparable to the bare QW; this is not surprising as the LPB at large positive detunings is effectively an exciton.

These results are qualitatively in agreement with theoretical predictions by Pau and Savona [118, 124], although the predicted scattering coefficient by Savona,  $0.5\mu\text{eV K}^{-1}$ , is less than we measured experimentally. Our measurements are, however, within the parameters reported in the literature, for similar samples for example  $8\mu\text{eV K}^{-1}$  determined by photoluminescence linewidth measurements [131].

A simple phenomenological model suggested by Piermarocchi [132] is used to fit the data, see figure 5.12. Following this model, the scattering by acoustic phonons induces a dephasing given by:

$$\gamma = |X_a(k_{\parallel})|^2 \gamma_{\text{ex}} (1 - \alpha). \quad (5.11)$$

The Hopfield coefficient ( $X_a(k_{\parallel})$ ) takes into account the exciton weighting of the LPB.  $\gamma_{\text{ex}}$  is the scattering efficiency of the bare QW exciton with no cavity effects, for which we use a value of  $11 \mu\text{eV K}^{-1}$ ; this is a fitting parameter and is in good agreement with previous values reported in the literature,  $10 \mu\text{eV K}^{-1}$  [52].  $(1 - \alpha)$  is related to the final density of states available to scatter into.  $\alpha = [E_{\text{ex}} - E_{\text{LPB}}]/E_{\text{cut}}$  where  $E_{\text{ex}}$  is the energy of the exciton taken from reflectivity data and  $E_{\text{LPB}}$  is the energy of the LPB calculated from a simple polynomial fit taken from the reflectivity data.  $E_{\text{cut}}$  is the cut-off energy above which the phonons can no longer interact with the exciton as defined in section 5.3.

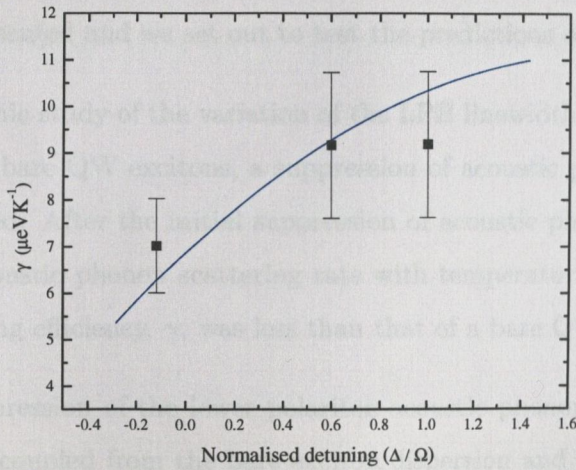


Figure 5.12: Phenomenological fitting of the scattering efficiency at different detunings using Piermarocchi's theory.

We use a value of  $80 \text{ \AA}$  for our QW thickness, but there would be a penetration into the barriers in such a narrow QW sample which we have not included in our fitting. This would actually decrease the broadening as  $E_{\text{cut}} \propto \frac{1}{L_{\text{QW}}}$ . Our scattering coefficient is thus slightly larger than expected. There is however a substantial uncertainty in our measurements and more points would be needed to improve the error margin in the results. This simple model breaks down when the bare energy of the exciton is greater than the energy of the LPB by an amount  $E_{\text{cut}}$ , ( $3.9 \text{ meV}$ ), after this a negative broadening effect is predicted.

It should be noted that since the first dynamic measurements showing the suppression of acoustic phonon scattering by ourselves and Baumberg [115, 133, 134], there has been some excellent experimental work by several groups who have subsequently shown suppression and  $\gamma$  variation with detuning. It should also be noted that there is some variation in the literature between quoted values of  $\gamma$  at resonance, from  $1\mu\text{eVK}^{-1}$  obtained by Cassabois [132, 135] to  $16\mu\text{eVK}^{-1}$  as measured by Renucci and Marie [136, 137, 138].

## 5.7 Conclusions

In this chapter we outlined the physics of acoustic phonons and reviewed some of the experimental and theoretical work on acoustic phonons in bare QW excitons. The theoretical work on polaritons was presented and we set out to test the predictions of this work.

We presented a dynamic study of the variation of the LPB linewidth with temperature using FWM. In contrast to bare QW excitons, a suppression of acoustic phonon scattering of the LPB was demonstrated. After the initial suppression of acoustic phonon scattering a linear dependence of the acoustic phonon scattering rate with temperature was verified. However the measured scattering efficiency,  $\gamma$ , was less than that of a bare QW exciton.

The cause of the suppression of the lower polariton-acoustic phonon interaction is twofold. Firstly, the LPB is decoupled from the bare exciton dispersion and has a larger gradient at  $k_{\parallel} \approx 0$  resulting in a decreased density of states which can be scattered into. Secondly, the LPB at  $k_{\parallel} \approx 0$  is an admixture of the exciton and the photon and the photonic part of the lower polariton is less efficient at interacting with the deformation potential.

The effect of detuning on the suppression was investigated. The suppression was found to increase to higher temperatures as the LPB was more negatively detuned. This was shown to be due to the larger decoupling in energy of the LPB from the exciton-like states at large  $k_{\parallel}$  which have a greater density of states. A larger acoustic phonon energy, from Boltzmann's constant and temperature, was needed to access the large density of states at  $k_{\parallel} \neq 0$ . At large negative detuning the lower polaritons Hopfield coefficient of the photon part is greater;



the LPB is more photon than exciton, this also causes an increase in the suppression of the acoustic phonon scattering.

Once the energy needed to access the larger density of states at  $k_{\parallel} \neq 0$  was achieved, the linear scattering coefficient was measured. The effect of detuning on the scattering coefficient was examined. It was found that at increased negative detunings, as the photon nature of the LPB increases, the scattering efficiency decreases. The reason for this is due to the energy step needing to be overcome in order to enable scattering to the large density of states at large  $k_{\parallel}$  [118]. The energy step increases for negative detunings.

A simple phenomenological model was used to fit the data, there was reasonable agreement for realistic fitting parameters. The scattering efficiencies of the LPB were also shown to be in good agreement with recent publications. This fundamental change in the acoustic phonon scattering rate of the polariton compared to the bare exciton is not indicative of an exciton filtered system.

In this chapter we discuss collisional broadening, i.e. the density dependent broadening of the homogeneous linewidth of the Lower Polariton Branch (LPB), due to polariton-polariton scattering. Once again, as in the case of acoustic phonon scattering, the broadening is different from that of a bare Quantum Well (QW) exciton due to the modified dispersion curve of the LPB and the photonic nature of the lower polariton. The nature of the dispersion curve again leads to a pronounced suppression of the polariton broadening at negative detunings. The nature of the suppression, however, is qualitatively different to that of the acoustic phonon scattering in that it is a threshold effect. Four Wave Mixing (FWM) data is presented in this chapter which clearly demonstrates this suppression in the 1QW and 2QW samples.

## 6.1 Introduction

At the beginning of chapter 5 we discussed the three main scattering mechanisms which affect the in-plane wave vector of the polariton. It was pointed out that the nature of the dispersion curve of the LPB strongly affects the scattering mechanisms that do not conserve

kinetic energy: there are two such processes, phonon scattering, discussed in the previous chapter, and polariton-polariton scattering which is the topic of this chapter. It should be noted once again that the conservation of kinetic energy of the total polariton-polariton scattering process is maintained although conservation of individual polariton kinetic energy is not.

## Chapter 6

Collisional broadening was also discussed in chapter 5 as one of the three main effects caused by resonant excitation of the polariton branches. Collisional broadening occurs at much lower intensities than other intensity effects in homogeneous samples. Throughout the work collisional broadening is only an appreciable effect, unless otherwise stated. This effect can only be studied on homogeneous samples, such as Quantum Wells (QWs), as bulk samples do not exhibit significant collisional broadening effects with resonant excitation [10]. Although the individual homogeneous lines do show collisional broadening this does not significantly increase the overall inhomogeneous linewidth. FWM is used to measure the effect of collisional broadening on the homogeneous linewidth of the

In this chapter we discuss collisional broadening, *i.e.* the density dependent broadening of the homogeneous linewidth of the Lower Polariton Branch (LPB), due to polariton-polariton scattering. Once again, as in the case of acoustic phonon scattering, the broadening is different from that of a bare Quantum Well (QW) exciton due to the modified dispersion curve of the LPB and the photonic nature of the lower polariton. The nature of the dispersion curve again leads to a pronounced suppression of the polariton broadening at negative detunings. The nature of the suppression, however, is qualitatively different to that of the acoustic phonon scattering in that it is a threshold effect. Four Wave Mixing (FWM) data is presented in this chapter which clearly demonstrates this suppression in the 1QW and 2QW samples.

### 6.2 Background and theory

#### 6.1 Introduction

A large amount of experimental work predominantly on FWM has been done to date. At the beginning of chapter 5 we discussed the three main scattering mechanisms which affect the in-plane wave vector of the polariton. It was pointed out that the nature of the dispersion curve of the LPB strongly affects the scattering mechanisms that do not conserve collisional broadening is bulk [10, 14] and in QWs [9], due

kinetic energy; there are two such processes, phonon scattering, discussed in the previous chapter, and polariton-polariton scattering which is the topic of this chapter. It should be noted once again that the conservation of kinetic energy of the total polariton-polariton scattering process is maintained although conservation of individual polariton kinetic energy is not.

Collisional broadening was also discussed in chapter 3 as one of the three main effects caused by resonant excitation of the polariton branches. Collisional broadening occurs at much lower intensities than other intensity effects in homogeneous samples. Throughout the work in this chapter we are within the regime where collisional broadening is the only appreciable effect, unless otherwise stated. This effect can only be studied on homogeneous samples, such as ours, as inhomogeneous samples do not exhibit significant collisional broadening effects with resonant excitation [87]. Although the individual homogeneous lines do show collisional broadening this does not significantly increase the overall inhomogeneous linewidth. FWM is used to measure the effect of collisional broadening on the homogeneous linewidth of the LPB. By varying the intensity of the FWM pulses we are able to see a strong suppression and threshold behaviour of the collisional broadening of the LPB as compared to a bare exciton.

The chapter is set out as follows: firstly a brief summary of the background work and theory is presented on the collisional broadening of bare QWs and polaritons; this is followed by a brief description of the samples and details of the FWM experimental setup; the results showing the threshold effect in the 2QW sample are presented and analysed. The effect of detuning is investigated using the 1QW sample. Finally, we draw comparisons between our results and the work published in the literature.

## 6.2 Background and theory

A large amount of experimental work (predominantly using FWM) has been done to ascertain the dephasing time of excitons due to processes such as exciton-exciton scattering and exciton-electron scattering both in bulk [139] and QWs [55, 140, 141]. Initially there was some confusion about the amount of collisional broadening in bulk [139, 142] and in QWs [55], due

to inhomogeneous broadening which as discussed has been shown to have a negligible carrier density dependence [87]. Bulk investigations also had the added problems of thickness and spatial inhomogeneities of the system. Investigations of collisional broadening in homogeneous samples caused by exciton-exciton scattering show the broadening to be linear with density [55, 141]. This agrees with more recent work by Litvinenko [143] whose work on QWs shows a linear dependence on the broadening of the linewidth with intensity due to exciton-exciton broadening and a square root dependence on the broadening of the linewidth with intensity due to free carrier-exciton broadening. It should be mentioned at this point that the collisional broadening we are investigating is near ( $k_{\parallel}=0$ ). At large  $k_{\parallel}$ , in both bare QWs and polaritons, the collisional broadening will be inhibited. This is due to the exciton dispersion curve at large  $k_{\parallel}$ ; it is difficult for the excitons to satisfy energy and momentum conservation when they scatter off each other.

The theoretical work, as in the previous chapter, is heavily computational and we will only discuss it for a qualitative understanding and to highlight a few interesting properties of excitons. The excellent work done by Tassone and Jahnke [88, 89, 67] should be mentioned although we do not discuss their theoretical work here as they examine non-resonant excitation. We will follow the work of Ciuti [144, 145] in which he specifically analyses the effect of broadening by resonant excitation of the 1s heavy hole exciton state, first in a QW and then in a strongly coupled microcavity.

Theoretical work has been published by several groups [146, 147, 148] however these papers either neglect exciton-exciton exchange, which has subsequently been proven to be a significant effect [144], or they do not work out the dependence of the scattering matrix elements on the exciton wavefunction. Ciuti in his initial work [144], analyses the exciton-exciton scattering due to Coulomb interaction in a two dimensional system, taking into account inter-exciton exchange of carriers and spin degrees of freedom as well as exciton-exciton exchange and dipole interactions. The scattering matrix elements are derived from a four carrier Hamiltonian and it is shown that the most important interaction is inter-exciton exchange of carriers, *i.e.* electron-electron and hole-hole exchange, and not the classic exciton-exciton or dipole interactions. The collisional broadening is calculated within the Born approximation and then shown to be in good agreement with experimental data [56] at specific densities.

Ciuti [144, 145] makes several approximations which should be mentioned. For example, valence band mixing is ignored, this is justified if the splitting between the light hole and heavy hole is comparable to or larger than the binding energy of the exciton. For our two samples we obtain a light hole heavy hole splitting of 23.4meV and the exciton binding energy is approximately 8meV [125]. Thus our samples characteristics are with the specified limits in which Ciuti's approximations hold.

A second assumption, discussed below, is to ignore spin scattering states and bi-excitons as the sample is assumed to be resonantly excited with co-circularly polarised light. There are four heavy hole exciton states in GaAs, two of which are optically active. Once optically active excitons are generated they can scatter into the optically inactive *i.e.* 'dark' exciton states. The four heavy hole exciton states arise from the angular momentum associated with the conduction and valence bands. The quantisation of the angular momentum in the z-direction,  $J_z$  gives an angular momentum of  $s_e = \pm\frac{1}{2}$  for the conduction band, as the conduction band has spherical symmetry and so the angular momentum is just given by the spin. The heavy hole valence band has total angular momentum  $j_h = \pm\frac{3}{2}$ . Thus the two optically active exciton states are  $|J_z = \pm 1\rangle = |s_e = \mp\frac{1}{2}; j_h = \pm\frac{3}{2}\rangle$  and the two dark states are  $|J_z = \pm 2\rangle = |s_e = \pm\frac{1}{2}; j_h = \pm\frac{3}{2}\rangle$ . When the excitons are generated with elliptically polarised light both the  $J_z \pm 1$  states are created. These states can relax into  $J_z \pm 2$  dark states, which are approximately 0.1meV [144] less in energy than the optically active states. However, collisions between excitons generated with co-circularly polarised light do not lead to relaxation as the only scattering mechanism is  $(\pm 1, \pm 1) \rightarrow (\pm 1, \pm 1)$ . Thus excitons created from the co-circularly polarised light will not scatter into the cross-circularly polarised light or into the forbidden dark states. As a consequence of this, no spin scattering is allowed in this regime. Bi-exciton effects can also be ignored, see appendix A for a justification.

Another assumption of Ciuti's was that only the scattering of 1s excitons by 1s excitons are taken into account. This is justified as the excitons are created with a small amount of kinetic energy, due to the resonant excitation, and the next excited state has a binding energy of  $\frac{1}{9}$  of the 1s exciton. The valence band mixing due to spin-orbit interactions are also ignored, these cause spin flips but are on a long time scale (50-100ps) compared to the dynamics we are looking at and can thus be neglected.

Ciuti's theory of exciton-exciton broadening predicts a sub-linear dependence of the linewidth with respect to exciton density. This does not agree with published experimental data where most experiments show a linear dependence with exciton density [55, 141]. However, this could be due to the excitation region over which the experimental data was taken. Ciuti also predicted a larger broadening for the circularly polarised light as compared to linearly polarised light. To the author's knowledge this has not yet been investigated experimentally.

By taking into account the cavity mode coupling, and assuming the LPB mixing with the UPB is negligible due to the energy separation, Ciuti [145] derived the collisional broadening of the LPB in a strongly coupled microcavity system for resonant excitation with circularly polarised light as:

$$\Gamma_1 = \Gamma_0 + \left(\frac{2}{\pi}\right)^4 \left(\frac{\hbar^2}{2\mu}\right)^2 n \int_0^\infty dk k |I(k)|^2 |X_1(0)|^4 |X_1(k)|^4 \times \mathcal{L}(2E_1(k) - 2E_1(0), 4\Gamma_1), \quad (6.1)$$

where

$$\mathcal{L}(E, \gamma) = \frac{1}{\pi} \frac{\gamma/2}{E^2 + (\gamma/2)^2}. \quad (6.2)$$

When the linewidth  $\gamma \rightarrow 0$  the Lorentzian  $\mathcal{L}(e, \gamma) \rightarrow \delta(e)$ , ( $\delta$  is the Dirac delta function) and equation (6.2) reduces to the usual Fermi's golden rule in the limit of very small damping. The quantity  $I(k)$  is proportional to the matrix element corresponding to the scattering of two excitons generated at  $k_{\parallel}=0$  which scatter to  $-k_{\parallel}$  and  $+k_{\parallel}$  and is defined by Ciuti [144]. The Hopfield coefficient of the LPB takes into account the excitonic fraction of the initial and final states,  $(X_1(0), X_1(k))$  of the polariton-polariton collision.  $\Gamma_0$  is the homogeneous broadening of the polariton in the limit of zero intensity. In the range of  $\Gamma_0 = 0.01 - 0.10\text{meV}$  the collisional broadening  $\Gamma - \Gamma_0$  is insensitive to  $\Gamma_0$ .  $\mu$  is the reduced mass of the electron-hole pair and  $n$  is the polariton density on the LPB, per unit area. When equation (6.1) is numerically solved a remarkable threshold behaviour is evident, see figure 6.2.

An intuitive understanding of the threshold can be gained by the following argument. As the intensity increases, collisional broadening of the LPB linewidth occurs. The portion of  $k_{\parallel}$  states available increases with excitation due to this broadening of the polariton linewidth.

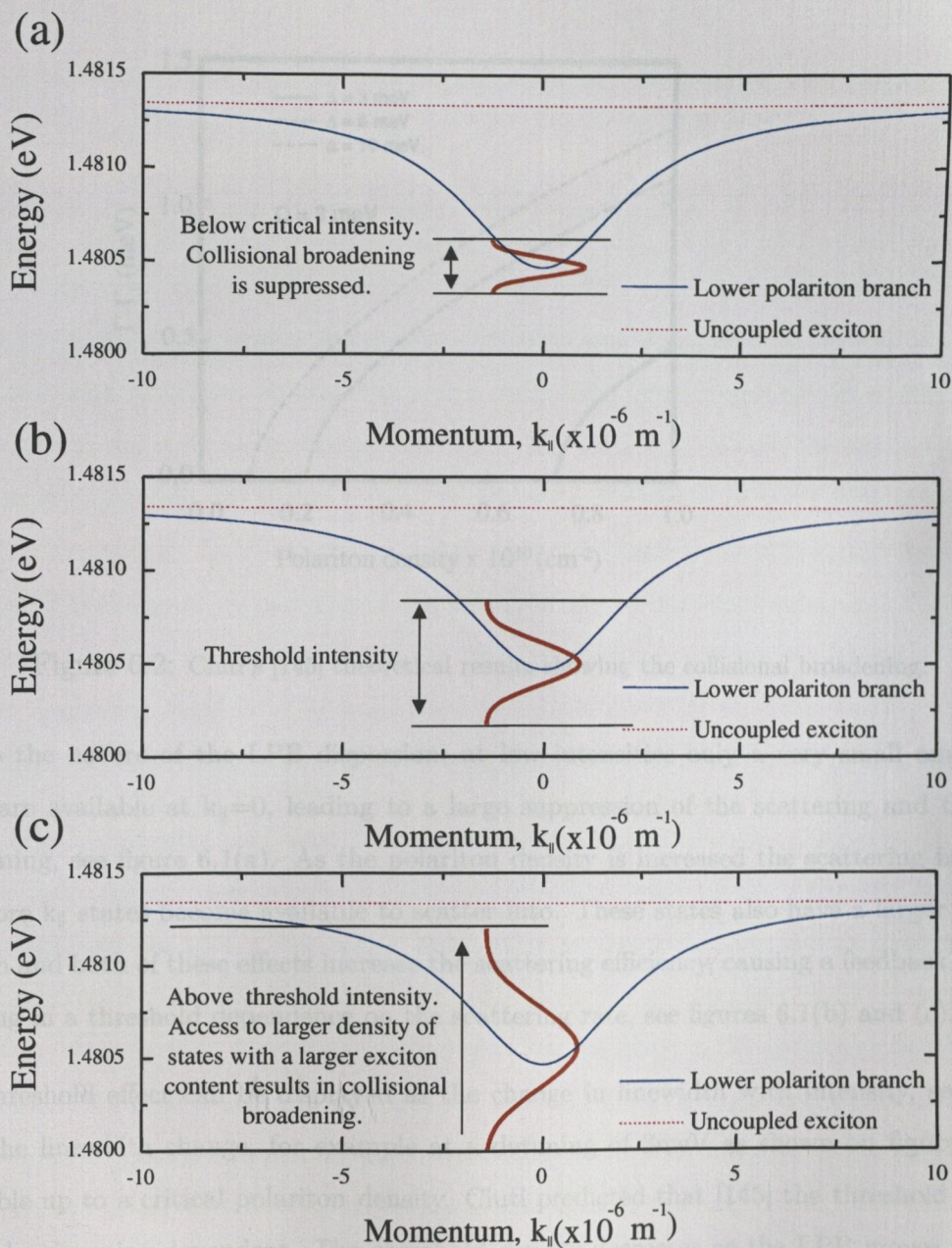


Figure 6.1: An illustration of the threshold dependence of the collisional broadening,  $\Delta = +4.9 \text{ meV}$ . (a) Below threshold the collisional broadening is suppressed. The linewidth represented by the red line (not to scale) only has access to a small density of states and the polaritons have a large photon component. Both of these effects suppress the collisional broadening. (b) At a critical density the linewidth increases enough to allow access to a greater density of states with an increased exciton component. This gives rise to a rapid increase in the collisional broadening and results in a threshold effect. (c) Above the critical density there is access in the tail of the linewidth to a large density of states with an increased exciton component.

### 6.3 Samples and experimental setup

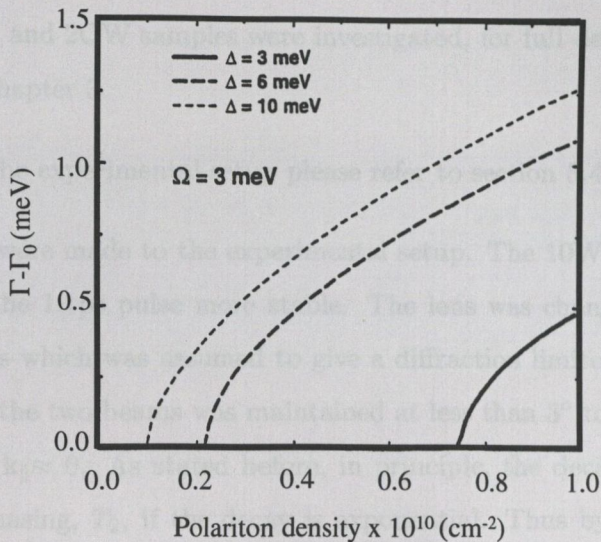


Figure 6.2: Ciuti's [145] theoretical results showing the collisional broadening.

Due to the nature of the LPB dispersion, at low intensities only a very small amount of states are available at  $k_{\parallel}=0$ , leading to a large suppression of the scattering and thus the broadening, see figure 6.1(a). As the polariton density is increased the scattering increases and more  $k_{\parallel}$  states become available to scatter into. These states also have a larger exciton fraction and both of these effects increase the scattering efficiency, causing a feedback process resulting in a threshold dependence on the scattering rate, see figures 6.1(b) and (c).

This threshold effect can be displayed as the change in linewidth with intensity, see figure 6.2. The linewidth change, for example at a detuning of 3meV as shown on figure 6.2, is negligible up to a critical polariton density. Ciuti predicted that [145] the threshold density should be detuning dependent. The threshold density decreases as the LPB moves towards positive detunings and becomes more exciton-like with a flatter dispersion curve. Conversely, the threshold should increase towards negative detuning, see figure 6.2. At resonance, Ciuti predicts the threshold density is of the order of the saturation density of the polariton. To test these predictions experimentally we investigate the effect of collisional broadening on the linewidth of the LPB using FWM.



## 6.3 Samples and experimental setup

Both the 1QW and 2QW samples were investigated, for full details of the sample the reader is referred to chapter 3.

For details of the experimental setup please refer to section 5.4.

Some changes were made to the experimental setup. The 10W Ar<sup>+</sup> was replaced by a 20W Ar<sup>+</sup> to make the 1.1ps pulse more stable. The lens was changed to a 12.5cm focal length achromatic lens which was assumed to give a diffraction limited spot size of  $\simeq 40\mu\text{m}^1$ . The angle between the two beams was maintained at less than 3° to ensure the excited polariton states were at  $k_{\parallel} \approx 0$ . As stated before, in principle, the decay of the FWM signal is due to optical dephasing,  $T_2$ , if the decay is exponential. Thus by measuring the decay of the diffracted FWM signal we can obtain a measure of the optical dephasing time  $T_2$ , this was discussed more fully in chapters 4 and 5. The relationship between the intensity of FWM and the dephasing time for a homogeneous system is given by equation (4.26). From the dephasing time the homogeneous linewidth ( $\Gamma_h$ ) can be determined using equation (4.27).

White light reflectivity was used to map the polariton detuning as a function of sample position and align the laser spectrum onto the LPB. The optics for the white light reflectivity were completely changed. The white light reflected from the sample was analysed by a 1m spectrometer (HR1000 Yobin-Yvonne) and a computer controlled CCD camera (LN<sub>2</sub> Princeton instruments). This greatly simplified the mapping of the polariton modes, as to obtain a spectrum we were no longer required to scan the wavelength across the PMT. As an example, spectra taken at different positions for the 1QW sample are shown in figure 6.3(a). When the minimum reflectivity positions are plotted against position the now familiar map of the polariton is obtained, see figure 6.3(b). Part (b) of this figure also shows the three positions where data was taken on the 1QW sample. The CCD camera also aided spectral alignment of the laser on the LPB, as the reflectivity spectrum of the LPB in the laser line could clearly be seen and an example of this is shown in the inset of figure 6.4 for the 2QW

---

<sup>1</sup>It should be noted that the assumption of a diffraction limited spot size is relative to the illuminated diameter on the lens, not the lens diameter itself.

sample.

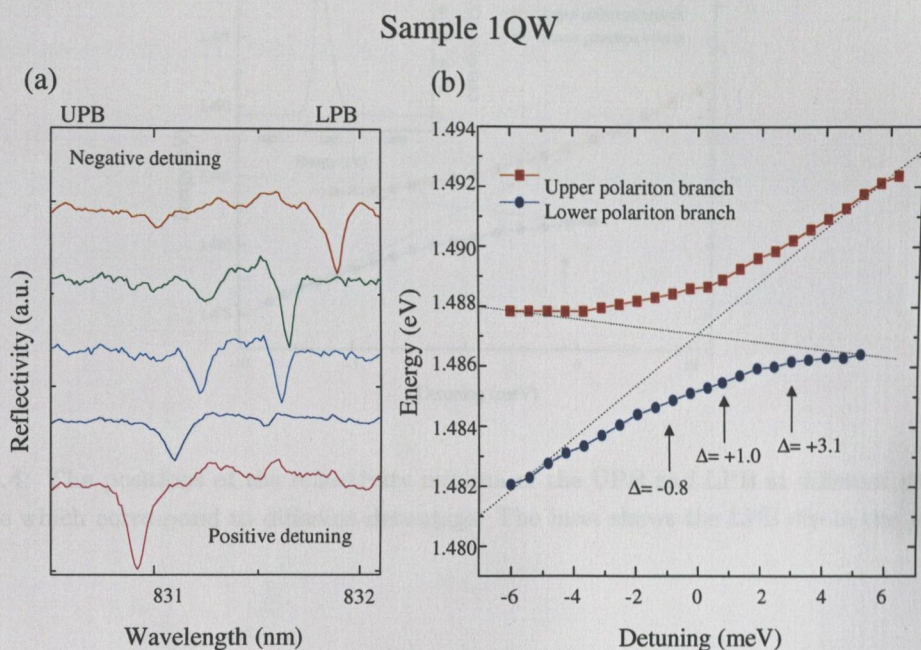


Figure 6.3: (a) The displaced reflectivity spectrum of the UPB and LPB branches at different positions across the 2QW sample. (b) The positions of the reflectivity minima of the UPB and LPB branches at different positions on the sample, the arrows point to the three detunings (in meV) where data was taken.

## 6.4 Experimental results

We present first the data taken on the 2QW sample at a detuning of  $+4.9\text{meV}$ , see figure 6.4. The FWM results are shown in figure 6.5. At low intensities it is clear that there is no change in the FWM signal while as the intensity is increased there is an abrupt decrease in the decay; for clarity not all ~~the~~ FWM data is presented.

### 6.4.1 Results on the 2QW sample

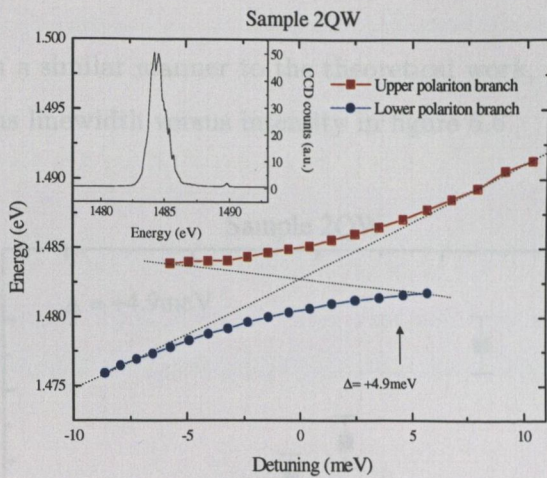


Figure 6.4: The positions of the reflectivity minima of the UPB and LPB at different positions on the sample which correspond to different detunings. The inset shows the LPB dip in the laser line.

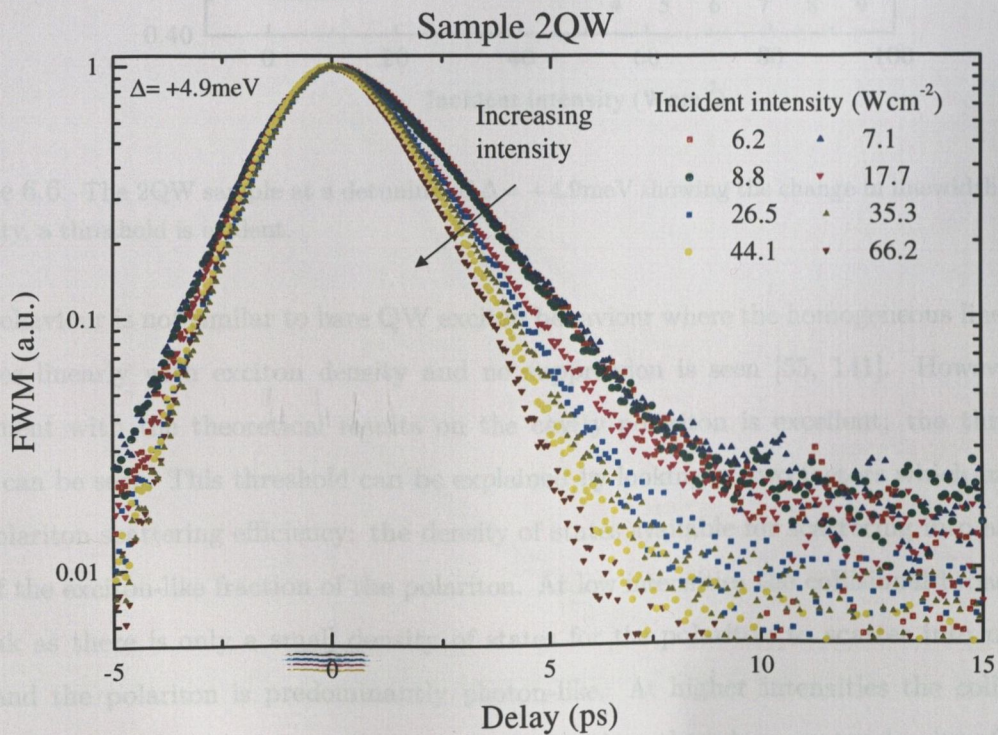


Figure 6.5: 2QW sample at  $\Delta = +4.9 \text{ meV}$ . FWM signal with increasing intensity.

### 6.4.1 Results on the 2QW sample

To present the data in a similar manner to the theoretical work, see figure 6.2, we show the change in homogeneous linewidth versus intensity in figure 6.6.

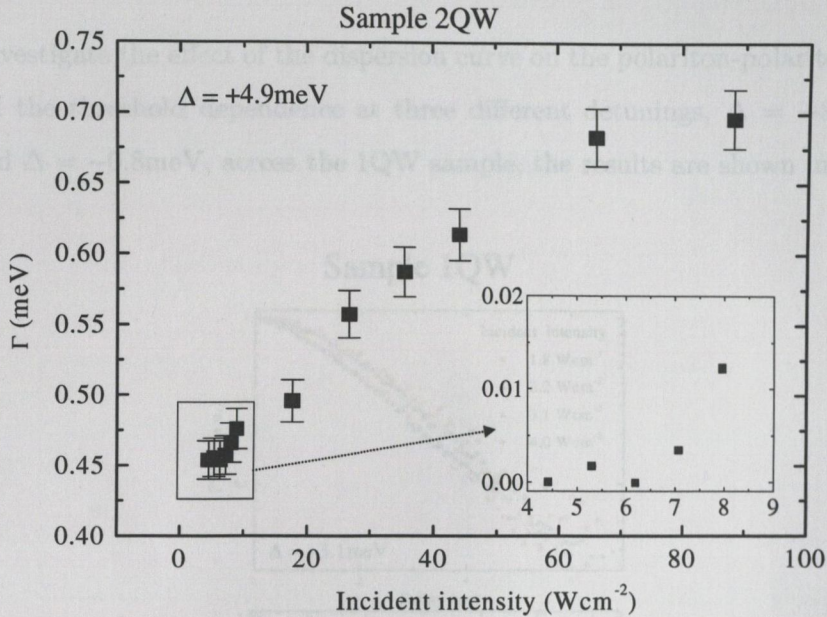


Figure 6.6: The 2QW sample at a detuning of  $\Delta = +4.9\text{meV}$  showing the change in linewidth versus intensity, a threshold is evident.

The behaviour is not similar to bare QW exciton behaviour where the homogeneous linewidth changes linearly with exciton density and no suppression is seen [55, 141]. However the agreement with the theoretical results on the cavity polariton is excellent; the threshold effect can be seen. This threshold can be explained by looking at two factors which increase the polariton scattering efficiency: the density of states available for scattering into and the size of the exciton-like fraction of the polariton. At low intensities the collisional broadening is weak as there is only a small density of states for the polariton to scatter into near  $k_{\parallel} \approx 0$  and the polariton is predominantly photon-like. At higher intensities the collisional broadening increases allowing scattering to larger  $k_{\parallel}$  where there is a greater density of states and the states are more exciton-like, see figure 6.1. These factors dramatically increase the scattering efficiency leading to the threshold like behaviour. Above threshold, see figure 6.6,

linearity is maintained until there is a flattening of the last two data points. This flattening is due to the FWM decay falling into the resolution of the pulse width.

### 6.4.2 Threshold dependence on detuning

To further investigate the effect of the dispersion curve on the polariton-polariton scattering, we examined the threshold dependence at three different detunings,  $\Delta = +3.1\text{meV}$ ,  $\Delta = +1.0\text{meV}$  and  $\Delta = -0.8\text{meV}$ , across the 1QW sample, the results are shown in figure 6.7.

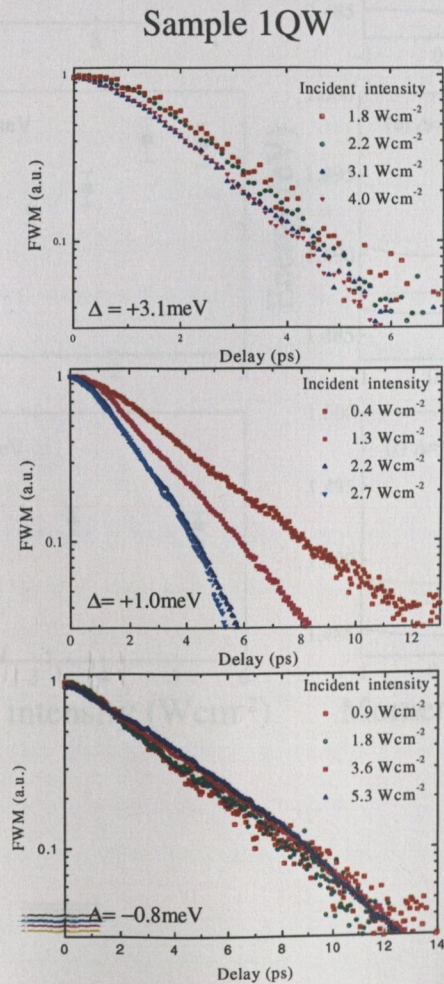


Figure 6.7: Intensity dependent FWM at three different detunings on the 1QW sample.

## Sample 1QW

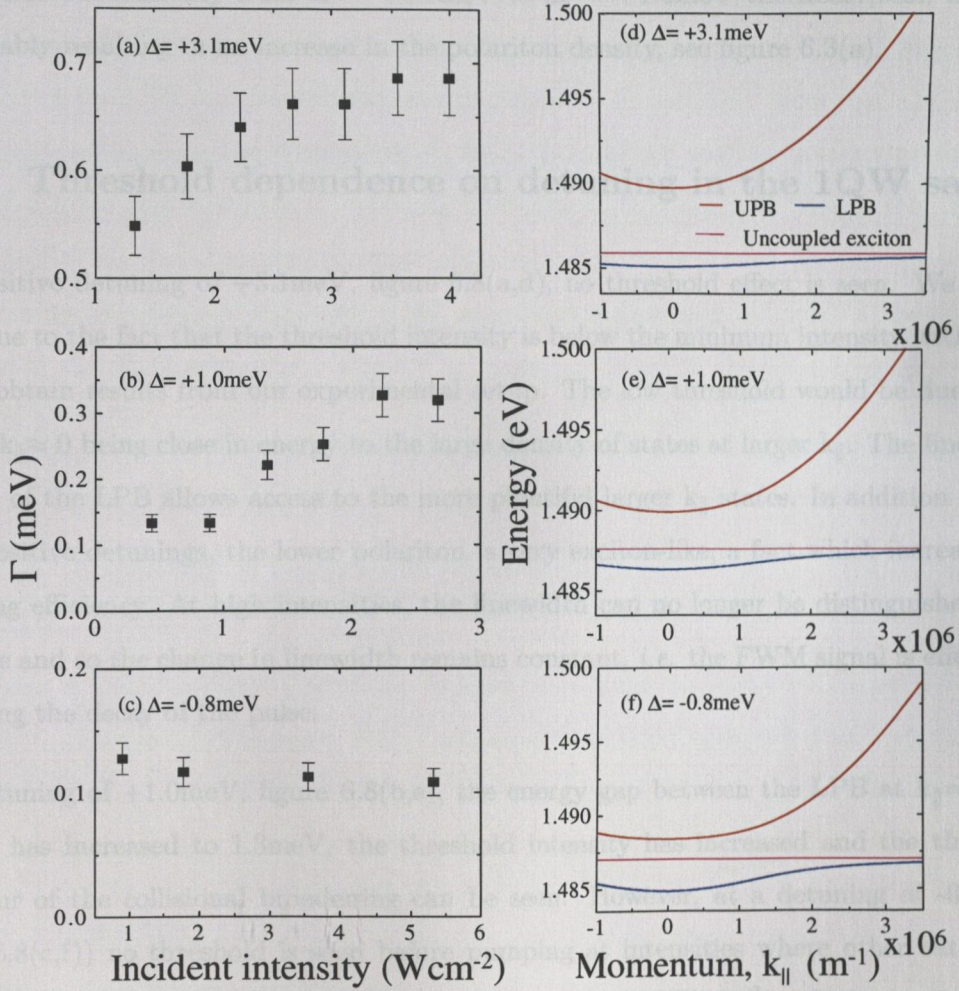


Figure 6.8: Homogeneous linewidth change versus incident intensity at three different detunings with respective dispersion curves.

As can be seen from figure 6.8(a) there is an immediate change in the linewidth at large positive detunings, while at negative detunings, see figure 6.8(c), no change in linewidth is evident with increasing intensity. The threshold polariton density increases as the detuning moves towards the negative. It should be noted that although the incident intensity does not increase substantially from  $\Delta = +3.1\text{meV}$  to  $\Delta = +1.0\text{meV}$  the absorption increases considerably resulting in an increase in the polariton density, see figure 6.3(a).

### 6.4.3 Threshold dependence on detuning in the 1QW sample

At a positive detuning of  $+3.1\text{meV}$ , figure 6.8(a,d), no threshold effect is seen. We believe this is due to the fact that the threshold intensity is below the minimum intensity with which we can obtain results from our experimental setup. The low threshold would be due to the LPB at  $k_{\parallel} \approx 0$  being close in energy to the large density of states at larger  $k_{\parallel}$ . The linewidth,  $0.4\text{meV}$ , of the LPB allows access to the more plentiful larger  $k_{\parallel}$  states. In addition to this, at far positive detunings, the lower polariton is very exciton-like, a fact which increases the scattering efficiency. At high intensities, the linewidth can no longer be distinguished from the pulse and so the change in linewidth remains constant, *i.e.* the FWM signal is effectively measuring the decay of the pulse.

At a detuning of  $+1.0\text{meV}$ , figure 6.8(b,e), the energy gap between the LPB at  $k_{\parallel} = 0$  and large  $k_{\parallel}$  has increased to  $1.3\text{meV}$ , the threshold intensity has increased and the threshold behaviour of the collisional broadening can be seen. However, at a detuning of  $-0.8\text{meV}$ , (figure 6.8(c,f)) no threshold is seen before pumping at intensities where other saturation effects become important; the highest pump intensity is  $5.3\text{Wcm}^{-2}$  and gives a polariton density of  $1.1 \times 10^{11}\text{cm}^{-2}$  which happens to be the same as our saturation intensity measured in chapter 2 of  $1.1 \times 10^{11}\text{cm}^{-2}$ . The increased threshold intensity is due to the steeper dispersion curve of the LPB and the increased cavity-like behaviour of the lower polariton at negative detunings which decreases the scattering efficiency.

#### 6.4.4 Comparing the two samples

Comparing the two samples it is important to note that although the polariton linewidths are similar in both cases, the splitting of the 1QW sample, at 3.5meV, is smaller than the 2QW sample, at 4.6meV. The larger splitting of the 2QW sample is the result of the larger oscillator strength, the exciton-photon coupling is larger and thus for a fixed detuning the decoupling of the LPB and the exciton branch is greater in the 2QW than the 1QW sample. In fact as a comparison, the decoupling of the LPB from the exciton is larger (0.9meV) in the 2QW sample at a detuning of +4.9meV than the 1QW sample (0.7meV) at a detuning of +3.1meV. This would suggest a larger threshold density is needed for the 2QW sample at a detuning of +4.9meV than the 1QW sample at a detuning +3.1meV. The measured threshold in the 2QW sample at +4.9meV is larger, as shown in the table in section 6.5.

The polariton threshold density of the 1QW sample was too small to be measured with our experimental setup. The decoupling of the 2QW sample of 0.9meV is, however, less than that of the 1QW (1.3meV) sample at a detuning of +1.0meV, and correspondingly the threshold density is less (see table in section 6.5).

To compare the results directly with the literature we must convert the incident intensities into polariton densities. There are many problems associated with this which we comment on briefly.

#### 6.4.5 Polariton density

In order to compare our results with the theory we now need to convert our values for incident intensity into polariton densities; the number of polaritons being generated inside the sample per unit area. Polariton densities are extremely difficult to measure experimentally as two of the values needed, spot size and absorption, are not as straightforward to measure experimentally as they may seem. Furthermore, the error in the spot size diameter gives a square in the error of the polariton density and to ascertain the absorption both the reflectivity and transmission need to be accurately obtained.



We have assumed a diffraction limited spot size of  $\simeq 40\mu\text{m}$  and no transmission *i.e.* the absorption is taken to be  $1-R$ , where  $R$  is the reflectivity. Both of these assumptions overestimate the polariton density. The diffraction limit is calculated assuming a Gaussian beam profile. The spot size is probably very close to the diffraction limit as an achromatic lens was used. Also, any defocusing, which would arise for example due to the reflection being from the surface of the sample and not the QW, only increases the spot size by a few microns. The focus would need to be several millimeters out to increase the spot size substantially. The assumption of zero transmission of the LPB at a positive detuning of  $4.9\text{meV}$  is justified; when looking at the transmission from the transfer matrix theory, (see chapter 2) the transmission is less than 5% of the absorption. The reflectivity as taken from the laser line, (see figure 6.4 (inset)) is the largest source of error with an uppermost error limit of 40%.

Calculating the polariton density with a  $40\mu\text{m}$  spot size, assuming no transmission and using our measured reflectivity, the broadening threshold is smaller than the polariton saturation reported in the literature [88, 94]. Our measured saturation polariton density is  $1.8 \times 10^{11}\text{cm}^{-2}$  for the 2QW sample. This is in reasonable agreement with the literature. Using these polariton densities would bring the data recorded at higher intensities into question, specifically the last two see figure 6.6. However it should be noted that the saturation densities are reported for non-resonant excitation conditions, where the strong coupling is destroyed at lower polariton densities than with resonant excitation. This is due to efficient free carrier scattering [88] at these temperatures [54]. For example, Litvinenko [143] quotes a saturation density of  $2.5 \times 10^{11}\text{cm}^{-2}$  for non-resonant excitation and a value of  $1 \times 10^{12}\text{cm}^{-2}$  for resonant excitation for bare QWs. Our measured saturation densities also included free carrier saturation due to the broad spectral pulse width, and showed some electron-hole pair effects in the pump-probe, see section 3.3.2.

The above considerations suggest it is likely that all the data points are valid with the uppermost point corresponding to a polariton density of  $2 \times 10^{11}\text{cm}^{-2}$ .

## 6.5 Comparison with literature, and conclusions

Our experimental results [117], indicating a threshold behaviour with a strong suppression of collisional broadening and an increase in threshold towards negative detuning, are found to be in good agreement with Ciuti's theory [144, 145]. Below is presented a table comparing Ciuti's theory and our experimental results.

	Theory*	1QW	Theory	1QW	Theory*	2QW
Splitting (meV)	3.0	3.5	3.0	3.5	5.0	4.9
Detuning (meV)	3.0	3.1	1.0	1.0	5.0	4.9
Threshold density $\times 10^{10}(\text{cm}^{-2})$	$\simeq 0.7$	$< 0.5$	2.0	2.0	1.3	1.5

\* These values have been extrapolated from Ciuti's data [145]

The results are also in moderate agreement with Baars [116]. Due to a different splitting and data taken at different detuning we cannot directly compare our results. Suffice as to know that his threshold densities are also in the regions of  $\simeq 1 \times 10^{10} \text{cm}^{-2}$ . Baars's excellent work also shows a strong suppression of collisional broadening with a threshold behaviour. However, the suppression was smeared out compared to the several orders of magnitude predicted by Ciuti, and witnessed by ourselves [117]. Baars suggested reason for this is the finite magnitude of the density independent part of the homogeneous linewidth, which indeed may have been a factor due to the large indium content (14%) of his samples. Our samples' linewidths are less than half of his linewidth. Ciuti states that in the range of  $\Gamma_0 = 0.01 - 0.1 \text{meV}$  the collisional broadening  $\Gamma - \Gamma_0$  is insensitive to  $\Gamma_0$ , however Baars' measured linewidth is  $1 \text{meV}$  compared to our value of  $0.3 \text{meV}$ . We have not compared the linewidth measured from the FWM data as this was not stated by Baars. Baars also showed an increase in threshold towards negative detunings and went on to analyse the scattering rates above threshold and found these were directly linked to the excitonic portion of the polariton.

In conclusion, we have seen a strong inhibition of polariton-polariton scattering below a threshold intensity at positive detunings in two strongly coupled microcavity samples. We

have seen a threshold, which was not apparent in bare QW excitons and is a feature of the modified dispersion curve and the photon fraction of the lower polariton.

The threshold intensity was investigated with detuning. At negative detunings no threshold behaviour was observed up to intensities where the strong coupling collapses. Towards positive detunings the intensity at which the threshold occurs decreased. At far positive detunings we did not see a threshold dependence with intensity and we believe this is due to the threshold occurring below the minimum intensity needed to obtain a FWM signal with our experimental setup.

The results are shown to be in good agreement with the theoretical work presented on polariton-polariton broadening and, accounting for sample deviations are also shown to be in reasonable agreement with other experimental work done on strong coupling microcavity samples.

## 7.1 Introduction

In the previous two chapters we studied the effect of temperature and excitation density on the linewidth of the LPB. We specifically looked at the effect of the dispersion curve of the LPB on two scattering processes, namely acoustic phonon scattering and polariton-polariton

# Chapter 7

To avoid any confusion regarding the terminology we state that a decrease in the FWM decay rate implies a decrease in the linewidth and an increase in the coherence time and vice versa.

## Excitation induced coherence

The idea of increasing the coherence of a system by adding more particles seems counter-intuitive. Normally, one would expect more scattering events to occur at higher densities.

In this chapter we discuss excitation induced coherence in the lower polariton. An intensity dependent increase in the coherence time is measured in the Lower Polariton Branch (LPB) using Four Wave Mixing (FWM). This effect is the reverse of what was seen in the previous chapter. Two important differences between the previous chapter's and this chapter's investigations should be noted, the angle between the pump and the probe beams used in the FWM was decreased, and the effect was only present at resonance and at negative detunings. An increase in coherence with intensity is unusual; we have performed several experiments to ensure that the longer coherence times with intensity were not due to experimental artifacts or the saturation of the polariton. For composite particles such as excitons and cavity polaritons the underlying particles are fermions and at high densities their fermionic nature dominates. However, our observations indicate that, for cavity polaritons at least, one can reach densities where a dramatic increase of the coherence time with intensity occurs, this being typical of composite bosons. The increased coherence of the LPB with increased occupation implies that a macroscopic phase exists within the system. This is one of the signatures of a Bose-Einstein Condensate (BEC).

increase in coherence with intensity is our experimental setup would be more characteristic of a BEC than a parametric amplifier where the emission is related to the coherence of the cw pump beam.

This chapter is set out as follows: we introduce BECs and their properties using the example

## 7.1 Introduction

In the previous two chapters we studied the effect of temperature and excitation density on the linewidth of the LPB. We specifically looked at the effect of the dispersion curve of the LPB on two scattering processes, namely acoustic phonon scattering and polariton-polariton scattering. In this chapter we turn to a different effect, that of excitation induced coherence. To avoid any confusion regarding the terminology we state that a decrease in the FWM decay rate implies a decrease in the linewidth and an increase in the coherence time and vice versa. To be consistent with the literature we use decay times as the characteristic parameter not linewidth, as used in the previous two chapters.

The idea of increasing the coherence of a system by adding more particles seems counter-intuitive. Normally, one would expect more scattering events to occur at higher densities resulting in a decrease in the coherence of the system. Nonetheless there are systems in which increased coherence with density is known to occur, for example in lasers where the addition of more photons causes a threshold as the light moves from incoherent spontaneous emission to coherent stimulated emission. As the photons in the laser systems have no rest mass, they are rarely considered a BEC. However, this increased coherence is a signature of the BEC formed by the photon within the laser. Liquid helium also shows an increased 'macroscopic' coherence under high densities when at low temperatures, and is another example of a BEC. BECs are not the only systems to show an increased coherence with excitation. A parametric amplifier, for example, will amplify a signal whilst imprinting it with the coherence of the pump beam. However in a pulsed system the imprinted coherence would last only for the duration of the pulse, unless the excited state maintains the coherence of the system. The FWM experiment generates a coherence in the system for approximately the duration of the pulse and the dephasing time indicates the decay of the coherence in the system, this was discussed in chapter 4. The FWM configuration which we use is specifically designed to measure the coherence time of the system. An increase in coherence with intensity in our experimental setup would be more characteristic of a BEC than a parametric amplifier where the emission is related to the coherence of the cw pump beam.

This chapter is set out as follows: we introduce BECs and their properties using the example

of excitonic and atomic systems. We present a brief summary of the research on BECs in these systems before discussing the novel field of BECs in polariton systems. We note a few changes made to the FWM experimental setup and then present our results. A simple rate equation model is shown to be qualitatively similar to our results, and finally conclusions are drawn.

## 7.2 Background

A large quantity of work presented recently examines the question as to whether cavity polaritons can form a BEC. Before reviewing this literature we examine the conditions required for the formation of a BEC and the progress made in generating a BEC in atomic and excitonic systems.

### 7.2.1 Bose-Einstein condensation

A Bose-Einstein condensate is a direct prediction of Bose-Einstein statistics, which was originally the idea of Bose [149]. The occupation number of bosonic particles is,

$$f(k) = \frac{1}{\exp\left(\frac{E(k)-\mu}{k_B T}\right) - 1} \tag{7.1}$$

In the case of excitons,  $E$  is the exciton energy at a given  $k$  ( $E = \frac{\hbar^2 k^2}{2m_{ex}}$ ),  $T$  is the temperature and  $k_B$  is Boltzmann's constant.  $\mu$  is the chemical potential, a quantity which is more familiar in chemistry, and measures the change in free enthalpy if you remove a particle from a system whilst keeping the temperature and pressure constant. This equation may seem familiar as we encountered it, with the chemical potential equal to zero, in section 5.2 when looking at phonons which are also bosons. The chemical potential is zero in the case of phonons because the number of phonons is defined by the temperature *i.e.* the number of particles is not an independent variable with respect to temperature. Bose-Einstein statistics are derived from the postulate that the probability of a particle scattering into a state  $k$  is proportional to the

number of particles in the state,  $P = 1 + f(k)$ . From equation (7.1) it can be inferred that as the number of particles increases, the distribution in energy narrows this is referred to as 'Bose narrowing'. On the other hand Fermi-Dirac statistics are derived from the opposing proposition, *i.e.* that the probability of scattering into a state decreases with the number of particles in the state,  $P = 1 - f(k)$ , as the number of particles increases the distribution widens.

The density of excitons,  $n$ , assuming they obey Bose-Einstein statistics is given by the integral of  $f(k)$  over all  $k$ :

$$n = \lim_{V \rightarrow \infty} \frac{N}{V} = \frac{g}{(2\pi)^3} \int_{-\infty}^{\infty} \frac{dk}{\exp\left(\frac{E(k)-\mu}{k_B T}\right) - 1} \quad (7.2)$$

$N$  is the number of excitons and  $V$  is the volume. Due to the linear relationship between  $N$  and  $V$ , the ratio of  $N$  to  $V$  remains finite even when both go to infinity. The spin degeneracy of the excitons is represented by  $g$ . Einstein [150] realised that this integral cannot account for all the particles in the system at all temperatures and chemical potentials. This is because the chemical potential has an upper limit of zero which is necessary for the integral to be defined at all energies. The intuitive explanation of this is that a system must lose free enthalpy when a particle is removed. When  $\mu = 0$  (as in the case of phonons) the integral becomes,

$$n = \frac{N}{V} = 2.612g \left( \frac{m_{\text{ex}} k_B T}{2\pi \hbar^2} \right)^{\frac{3}{2}} \quad (7.3)$$

To add more particles whilst keeping the temperature constant is only possible, as postulated by Einstein [150], if the added particles condense (there is a phase transition) into the ground state which is treated separately from the rest of the particles. Thus mathematically a Dirac delta function ( $\delta$ ) must be added at the lowest energy state, see figure 7.1(b). The same situation occurs if the temperature is lowered below a critical temperature whilst keeping the number of particles constant, see figure 7.1. Thus through Bose statistics and Einstein's insight the concept of a Bose-Einstein condensate was conceived. Although this was postulated

75 years ago, definitive proof of the first BEC was not observed until 1995 when an atomic condensate was created by the recent Nobel Prize winners, Cornell, Ketterle and Wiemann [151, 152] who pioneered a new technique to obtain the temperatures of a few billionths of a Kelvin needed to attain a BEC in an atomic system. Due to the small mass of excitons compared with atoms, and not considering other complications, an exciton BEC can occur at much higher temperatures. For example it has been predicted that an excitonic system with a particle density of  $10^{18}\text{cm}^{-3}$  can form a BEC at  $15\text{K}^1$  [153].

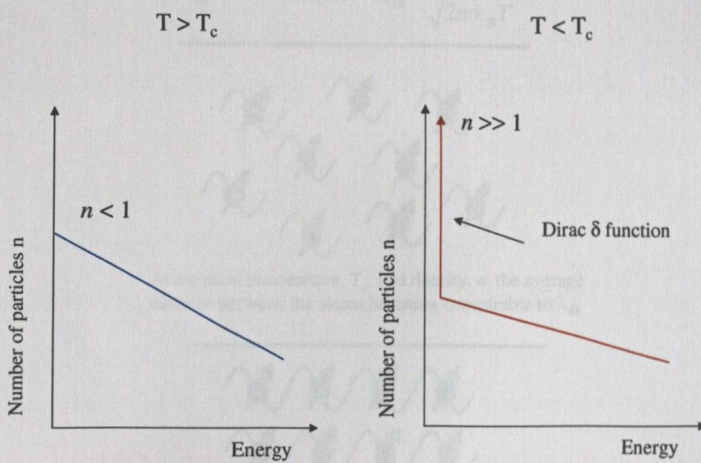


Figure 7.1: Schematic of the Bose-Einstein distribution of a system of particles at two different temperatures. (a) The general distribution above a critical temperature  $T_c$ . (b) The distribution below the critical temperature, a large number of particles can be seen to have condensed into the lowest energy state, creating a BEC. This is not predicted by equation (7.1) however a Dirac  $\delta$  function can be supplemented into the equation to account for this effect.

When Einstein postulated the condensate, the implications of such an unusual state were not fully realised and predicting the properties of a BEC is something that continues to be non-trivial [154]. A BEC is a group of particles which all condense into one quantum state, which then act as one particle with one wavefunction, in atomic physics this is sometimes called

<sup>1</sup>It is a common misconception that a BEC is created by cooling to low enough temperatures such that all particles must reside in the lowest energy state, so called 'brute cooling'. This is not true. A BEC can be created at relatively high temperatures when  $k_B T$  is large compared to the difference of energies of the quantum states of the system.



the ‘super atom’. In fact the condensate occurs when the distance between the particles is comparable to their de Broglie wavelength, see figure 7.2. The atoms then all condense into one wavefunction resulting in a macroscopic phase, one of the main properties of a BEC. As discussed above, the laser is the most common BEC system that readily shows macroscopic coherence with increased excitation.

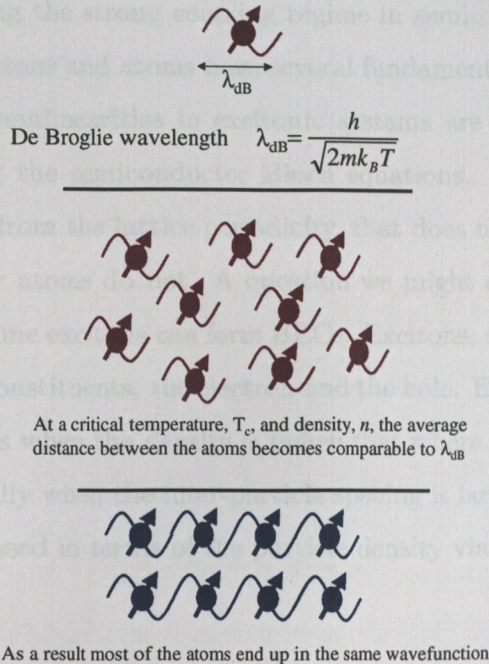


Figure 7.2: A schematic showing the formation of a BEC which occurs when the average distance between the particles, represented here as atoms, become comparable to their de Broglie wavelength. The fact that we can describe the large number of particles by one wavefunction, demonstrates the macroscopic phase of the system. This diagram is modified from [154].

## 7.2.2 Excitons as Bose particles

In the above section Bose Einstein condensation has been discussed for excitons and atoms assuming they have the same properties. However, atoms have been shown to form BECs, whereas excitons have not. Before further investigation of BECs in excitonic systems it is important to ascertain if there is a fundamental property of excitons which prohibits them

from behaving as bosons and forming BECs.

There are a number of similarities between excitons and atoms: the exciton is considered to be analogous with a hydrogen atom where an electron orbits a hole; the exciton has discrete absorption lines, below the conduction band, similar to an atom; the atomic analogy is used in the linear regime for the interpretation of data, [73, 155]. Indeed the atomic analogy is often used when explaining the strong coupling regime in semiconductor microcavities (see section 2.3). However excitons and atoms have several fundamental differences, for example, experimentally observed nonlinearities in excitonic systems are most often modelled with a continuum model using the semiconductor Bloch equations. This model is based on a band structure, resulting from the lattice periodicity, that does not exist in atomic systems. Also, excitons decay away atoms do not. A question we might ask is whether the analogy extends far enough to assume excitons can form BECs. Excitons, although bosonic composite particles, have fermionic constituents, the electron and the hole. Excitons have been shown to behave as bosonic particles when the density is below that where the sub-fermionic nature is apparent or more specifically when the inter-particle spacing is large compared to the exciton radius. This can be expressed in terms of the particle density via [156],

$$n \ll \frac{1}{8\pi a_{\text{ex}}^3}, \quad (7.4)$$

where  $a_{\text{ex}}$  is the excitonic radius. When this inequality is satisfied the density of excitons will be low enough such that the excitons do not 'see' each other's underlying fermionic structure and will be weakly interacting. At high densities the bosonic nature breaks down, the excitons 'see' each other's fermionic nature and phase space filling occurs as the excitons begin to obey Fermi-Dirac statistics. Thus there are two conflicting inequalities that must be satisfied for a BEC to be created. Equation (7.3) which gives a minimum critical density for a BEC to occur (provided the temperature remains constant) and equation (7.4) which refers to a maximum critical density for the excitons to remain bosonic. It should be noted, however, that even if this inequality is not satisfied in some systems the bosonic properties can dominate. For example in superfluid helium where the interparticle distance is small and the atoms are interacting a BEC can be formed. At high enough densities the bosonic nature

breaks down for all composite bosons.

Excitons have been shown to be bosonic through Bose-narrowing, initially this was demonstrated in Germanium [157] and more recently in GaAs quantum wells [158]. Although Bose narrowing of excitons has been observed and it has been theoretically predicted [159] that Bose-Einstein condensation can occur in exciton systems, BEC in exciton systems has not yet been proven experimentally. For a thorough summary of the experimental work to date, along with an involved theoretical description of the BEC see Moskaleiko and Snoke [153].

### 7.2.3 Cavity polaritons as Bose particles

In creating the mixed exciton-photon polariton state, a major change is the modified dispersion curve, this was discussed in detail in the last two chapters. The dispersion gradient increases by a factor of approximately  $10^{-4}$  relative to the bare QW exciton. In view of this, the de Broglie wavelength of the polariton is approximately 100 times larger than the size of the exciton's de Broglie wavelength, resulting in the fact that lower densities are needed to generate a BEC, see equation (7.3). The low mass also suppresses the scattering of acoustic phonons (see chapter 5) and thus prolongs the coherence lifetime of the polaritons. Another advantage when looking for a BEC in the polariton system is the reduction of the fermionic properties such as exciton-exciton interaction and phase space filling when compared to excitons at the same densities. This is due to the photon component of the polariton. Thus it is expected that below the Mott density, the density at which excitonic bond breaks down due to screening, the polariton should be able to undergo final state stimulation. Imamoğlu published two theoretical papers on the polariton condensate [160, 161]. However, the experimental path towards BEC in the polariton system has been long and difficult and there still much work to be done.

Early experiments, such as Non-Resonant Photo-Luminescence (NR-PL) experiments, attempted to show the bosonic nature of polaritons. In these experiments, the generated electron-hole pairs form a reservoir, from which they relax down the LPB to  $k_{\parallel}=0$  by phonon emission. When the polariton occupancy at  $k_{\parallel}=0$  becomes one (assuming the polaritons are

still bosonic) final state stimulation of the phonon relaxation process will occur and there will be a dramatic rise in the emission. While using this technique Pau *et al.* [162] believed they had observed final state stimulation. However, their paper was refuted and the experimental results were explained in terms of fermionic electron-hole correlations, implying the results were taken in the weak coupling regime [163, 164]. The density was too high to assume that the polariton was in the bosonic regime, in fact the strong coupling regime had broken down due to exciton saturation effects which rely on the excitons' fermionic nature. The paper was rescinded and experimental results showing a continuous transition from a microcavity polariton to a bare photon laser in agreement with the new theory was presented by Cao and Pau *et al.* [165].

A further setback in finding evidence of bosonic behaviour of the polariton occurred when, at extremely low intensities and in the strong coupling regime, nonlinear results in III-V materials using NR-PL [166] were explained [13] (and accepted [167]) within the framework of the fermionic theory as being due to exciton-exciton scattering. In fact, a paper by Tassone and Yamamoto [67] suggests that the polariton will break down before it is possible to obtain an occupation density of one in the LPB using NR-PL.

However this is not the case in II-VI semiconductor microcavities where stimulated emission via NR-PL has been more successful. In II-VI materials the larger exciton binding energy allows a higher density before the bosonic nature is affected. Using NR-PL a threshold with a narrowing of emission was seen from the LPB whilst in the strong coupling regime [23, 24].

In early 2000, two ingenious experiments by Huang *et al.* [19] and Savvidis *et al.* [20] experimentally showed the polariton to behave as a composite boson particle by showing final state stimulation. The experimental setup used by Huang is shown in figure 7.3(a). The LPB was excited resonantly with two pump pulses at large  $k_{\parallel}$  where the LPB is excitonic, this is above the bottleneck mentioned in section 2.7.2, and allows a quasi-thermal excitonic population to build up. A probe beam was then used to create a LPB population at  $k_{\parallel}=0$ . The emission at  $k_{\parallel}=0$  on the UPB was measured and found to be greater for large LPB probe powers as a result of stimulated exciton-exciton scattering by occupation of the LPB. Energy conservation was satisfied as the excitonic-polariton at large  $k_{\parallel}$  lost the equivalent

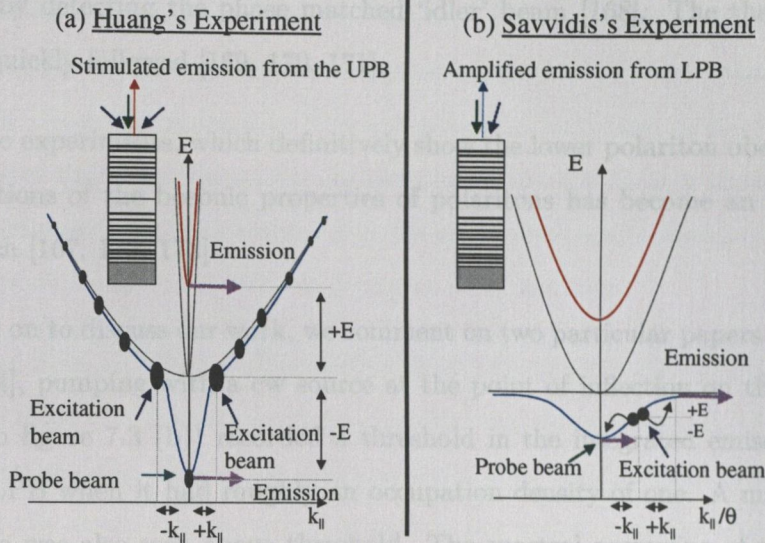


Figure 7.3: The dispersion curve of the UPB (red), LPB (blue), and the uncoupled exciton and photon modes (black), (not to scale). Grey lines show the conservation of energy and momentum. Schematic of: (a) Huang's experiment [19] showing the thermal distribution of excitons which are represented by black circles. The larger circles correspond to greater exciton population. By placing a probe at  $k_{||}=0$  on the LPB a stimulated emission is seen at  $k_{||}=0$  from the UPB. Inset shows the light direction into and out of the microcavity. (b) Savvidis' experiment [20], the dispersion curve is drawn on a larger scale. A probe excites  $k_{||}=0$  on the LPB which stimulates scattering from the polariton population at  $\theta=16^\circ$ ,  $k_{||}\neq 0$  to  $k_{||}=0$ . Savvidis went on to measure the emission (idler) at higher angles [168]. The inset shows the direction of the light onto the sample.

energy when scattering to the LPB at  $k_{||}=0$  that it gained when scattering to the UPB at  $k_{||}=0$ . Momentum conservation was satisfied by pumping at both +ve large  $k_{||}$  and -ve large  $k_{||}$ , see grey lines on figure 7.3(a).

Savvidis's experimental setup is shown in figure 7.3 (b). Once again the exciting pump pulse is resonant with the LPB, this time at an angle of approximately  $16^\circ$  roughly half-way in energy between the bottom of the LPB and the uncoupled exciton-like states. This is required in order to satisfy energy conservation. Similarly the momentum lost by the polariton scattering into the LPB at  $k_{||}=0$  is gained by the polariton scattered to large  $k_{||}$ . Probing at  $k_{||}=0$ , a probe amplification of nearly two orders of magnitude is seen when the pump is at the 'magic angle', *i.e.* the angle where energy and momentum conservation is satisfied, see grey line on

figure 7.3(b). Savvidis then went on to show that this process is analogous to parametric amplification by detecting the phase matched 'idler' beam [168]. The theoretical basis for these results quickly followed [169, 170, 171].

Since these two experiments, which definitively show the lower polariton obeying Bose statistics, investigations of the bosonic properties of polaritons has become an extremely active field of research [167, 172, 173].

Before moving on to discuss our work, we comment on two particular papers. Firstly, Stevenson *et al.* [174], pumping with a cw source at the point of inflection on the LPB, (see the pump beam in figure 7.3 (b)) recorded a threshold in the integrated emission intensity at  $k_{\parallel}=0$  on the LPB when it had roughly an occupation density of one. A marked narrowing of the emission was also seen above threshold. The spectral narrowing of the emission is a sign of the appearance of coherence in the system, analogous to a laser system narrowing its linewidth at threshold. An increase in the polariton's coherence would be indicative of the polaritons entering a single mode, which could be characterised by one wavelength, see figure 7.2. The coherence measured in this experiment is of the emitted optical field and not of the polaritons themselves, and as such cannot distinguish between a laser and a boson<sup>2</sup>. To know definitively that the system is a boson, a direct measure of the coherence of the polariton is needed.

The second paper, by Messin *et al.* [175], presented an experiment which, unlike the previous experiments, was performed in the degenerate configuration; the pump and probe and signal, generated from a cw Ti:Sapphire are all at  $k_{\parallel}=0$  on the LPB. A homodyne detection system was used to detect the light. A threshold effect is evident in the emission. The coherence was measured and found to be phase-sensitive and, as parametric amplification is phase sensitive [100] this suggests that the basis of the amplified emission is coherent polariton four-wave mixing [169]. If the system was truly boson-like the amplification would be phase-insensitive, analogous to a classical laser.

---

<sup>2</sup>A boson is similar to a laser but the coherence is contained in matter rather than light, sometimes it is referred to as a boson-laser. Population inversion is not attained as such, but final state stimulation can occur via stimulated scattering into a final state.

From these experimental papers two questions arise. Firstly, is the increased coherence of the emitted optical field a direct result of the increased coherence of the polaritons? Secondly, is there an increase in the coherence when pumping with a pulsed excitation which would be the result of a boson as opposed to coherent polariton four-wave mixing? Our experiment set out to answer these two questions. In essence we use FWM as a direct measure of the coherence of the polaritons with intensity in the degenerate configuration as used by Messin to see if the coherence of the polaritons increases with intensity.

The experiment is similar to that described in chapter 6 where the linewidth of the LPB was observed to increase above a threshold due to collisional broadening, *i.e.* the coherence time decreased. However, the reasons for this may have been that we were pumping at positive detunings and the angle was too large to satisfy the energy and momentum conservation needed. At positive detunings the LPB is more exciton-like and this could make it difficult to reach an occupation of one at densities where there is no phase space filling or collisional broadening. Most of the experiments discussed above on polaritons were done at resonance or at negative detunings on the LPB.

Messin pumped and detected near normal incidence to ensure momentum conservation was satisfied. The incident angle of between the pump and probe in chapter 5 was less than  $3^\circ$  to ensure the excited polariton states were at  $k_{\parallel} \approx 0$ . However if we further decrease the angle it may be that there is an increase in the coherence time rather than a shortening as in chapter 6.

### 7.3 Sample and experimental setup

For details of the samples please refer to chapter 3.

The FWM signal through  $\lambda$  is a measure of the coherence of the polaritons. The details of FWM was discussed in chapter 4. Here we repeat the FWM setup as a reminder, see figure 7.4. The FWM setup is similar to that used for chapter 6 in that a 1.1ps pulse is split into two pulses of equal power and the probe pulse was delayed with respect to the pump pulse. The two beams were then focused onto the sample, forming two spots of approximately  $40\mu\text{m}$  in

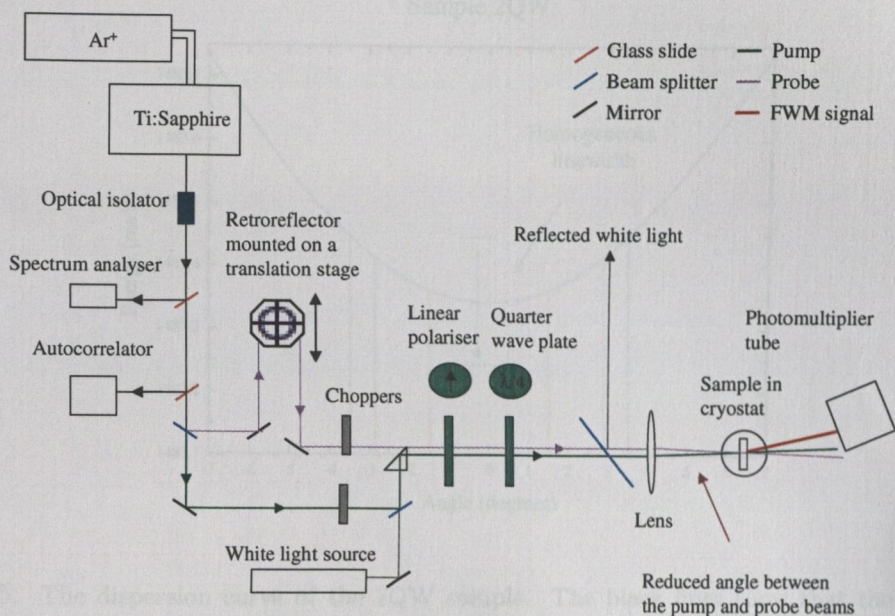


Figure 7.4: A schematic representation of the FWM setup. The pulsed light from the Ti:Sapphire was split into two beams, the pump and the probe. The probe was delayed with respect to the pump by a retroreflector. Both beams were focussed onto the sample, the diffracted signal was time integrated by a photomultiplier tube.

diameter. There was one important difference in this experimental setup compared to that of chapter 6; this being that the pump and probe beam were brought closer together to reduce the angle to satisfy momentum conservation. Nevertheless, it should be noted that both sets of data here, at an angle of  $1.5^\circ$ , and in the previous chapter, at an angle of  $3^\circ$ , were being pumped within the homogeneous linewidth at  $k_{\parallel}=0$ , see figure 7.5. Even at these narrow angles the diffracted signal is still well separated from the transmitted pulse beam in the geometry of our setup.

The FWM signal through  $\chi^{(3)}$  is a measure of the coherence of the polaritons. The decay of the coherence of a two-level system is governed by the decay of the population lifetime  $T_1$  and pure dephasing mechanisms  $T_2^*$  such as scattering. The net coherence lifetime  $T_2$  is thus given by



## 7.4 Experimental results

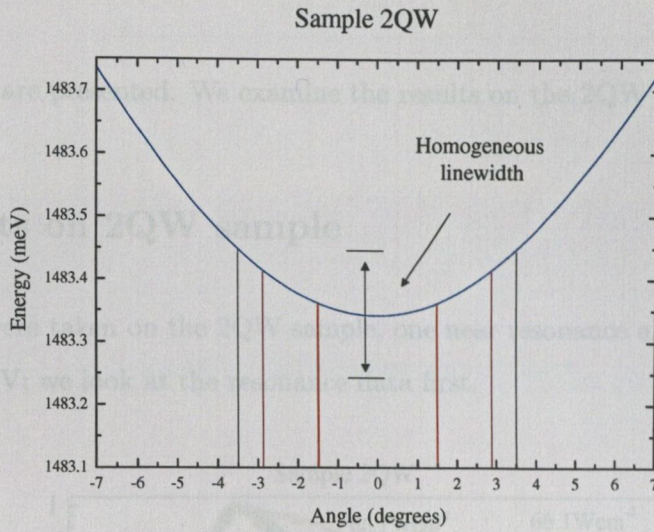


Figure 7.5: The dispersion curve of the 2QW sample. The black lines show that the maximum pump angle, to remain in the homogeneous linewidth of the lower polariton is  $3.5^\circ$ . The angle that the FWM data was taken at in chapter 6 is represented by the purple lines. Whilst the angle of the FWM taken in this chapter is represented by the red lines.

$$\frac{1}{T_2} = \frac{1}{2T_1} + \frac{1}{T_2^*}, \quad (7.5)$$

where the factor of two comes from the loss in intensity  $|\Psi|^2$  rather than the amplitude  $\Psi$  of the wavefunction. The shorter of the two decay mechanisms will dominate. Once again dephasing times,  $T_2$ , were derived from the decay of the FWM signal,

$$I_{\text{FWM}}(\tau_d) \propto \exp\left(-\frac{2\tau_d}{T_2}\right), \quad (7.6)$$

for a time integrated homogeneous system.

The reflectivity of the LPB was verified using the laser line, see figure 6.4 inset, to account for any drift in the position of the polariton, and the white light reflectivity was recorded as in chapter 6.

## 7.4 Experimental results

Three sets of data are presented. We examine the results on the 2QW sample first.

### 7.4.1 Results on 2QW sample

Two sets of data were taken on the 2QW sample, one near resonance and the second with a detuning of  $-1.7\text{meV}$ ; we look at the resonance data first.

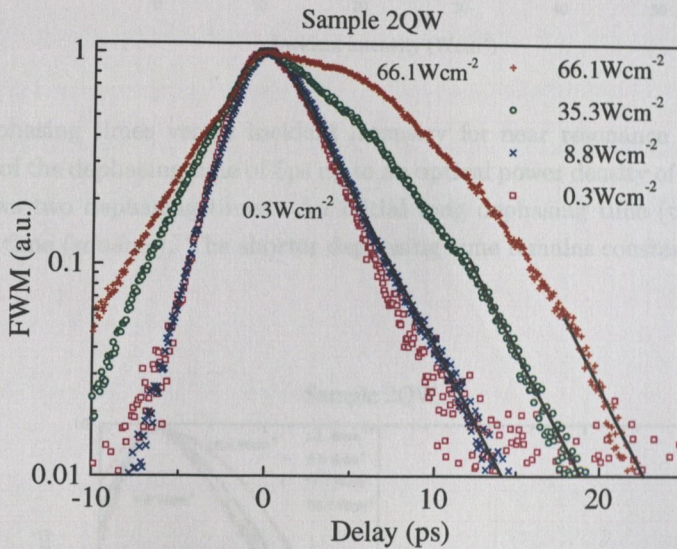


Figure 7.6: FWM data recorded for a range of incident intensities near resonance, showing an increase in FWM signal with intensity. A double slope is clearly evident at the higher intensities. The black lines on the data are a guide for the eye, illustrating that the second slope at higher intensities is approximately the same as the slope at low intensities.

It would normally be expected, as discussed in chapter 6, that the coherence of the polaritons would decrease with increasing intensity. This was observed as a decrease in the FWM signal. Figure 7.6 presents FWM data taken over a range of incident intensities. Dephasing times of 5ps are measured up to an incident intensity of  $8.8\text{Wcm}^{-2}$ . At higher photon densities the FWM signal no longer exhibits a single slope. The lower part of the FWM signal stays constant with excitation density, while the upper part becomes flatter with increasing excitation density. In order to obtain a quantitative analysis, we estimated dephasing times

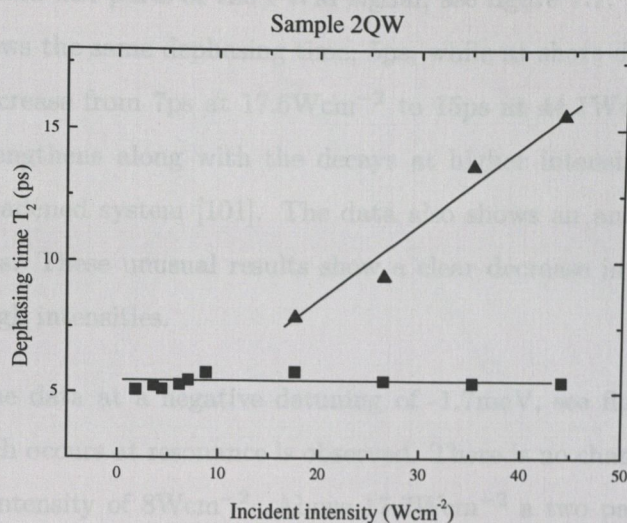


Figure 7.7: Dephasing times versus incident intensity for near resonance detuning. There is no significant change of the dephasing time of 5ps up to an optical power density of  $8.8\text{Wcm}^{-2}$ , whereupon the polariton shows two dephasing times. An initial long dephasing time (triangles) followed by a shorter dephasing time (squares). The shorter dephasing time remains constant, within experimental error, at 5ps.

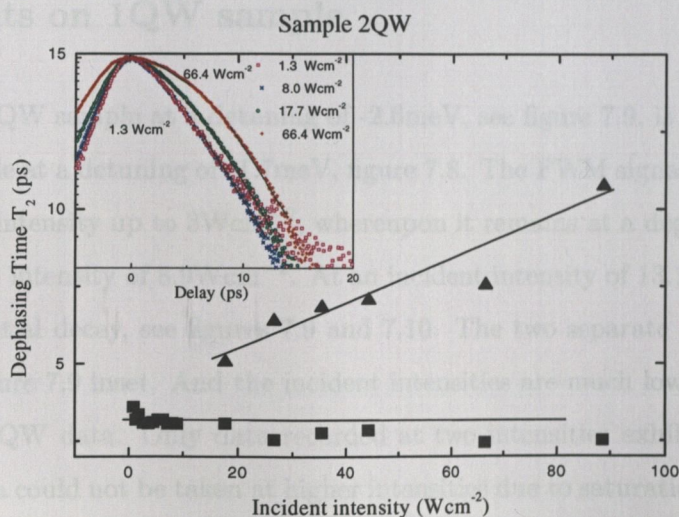


Figure 7.8: Dephasing times versus incident intensity at  $\Delta = -1.7\text{meV}$ . There is no significant change of the dephasing time at low intensities. At an incident intensity of  $17.7\text{Wcm}^{-2}$  the polariton shows two dephasing times. An initial long dephasing time (triangles) followed by a shorter dephasing time (squares). The inset shows the raw FWM data, the two separate decays at high intensity are not as easily distinguishable as in figure 7.6.

by fitting the first and last parts of the FWM signal, see figure 7.7. At long delay times all the FWM data shows the same dephasing time, 5ps, while at short delay times the deduced dephasing times increase from 7ps at  $17.6\text{Wcm}^{-2}$  to 15ps at  $44.1\text{Wcm}^{-2}$ . The rise-time of the FWM signal lengthens along with the decays at higher intensities, as expected for a homogeneously broadened system [101]. The data also shows an anomalous bump at high intensities near -5ps. These unusual results show a clear decrease in the dephasing rate at short delays and high intensities.

Next we look at the data at a negative detuning of  $-1.7\text{meV}$ , see figure 7.8. A behaviour similar to that which occurs at resonance is observed. There is no change in the FWM signal up to an incident intensity of  $8\text{Wcm}^{-2}$ . Above  $17.7\text{Wcm}^{-2}$  a two part decay of the FWM signal is observed, the first decay slowing with intensity whilst the second decay is the same as the decay at low intensities. The long decay is not as pronounced as at resonance and the bump seen previously in the rise of the FWM is absent. At extremely low densities there is a slight decrease in the dephasing time with intensity.

#### 7.4.2 Results on 1QW sample

The data on the 1QW sample at a detuning of  $-2.6\text{meV}$ , see figure 7.9, is similar to the data on the 2QW sample at a detuning of  $-1.7\text{meV}$ , figure 7.8. The FWM signal initially decreases very slightly with intensity up to  $3\text{Wcm}^{-2}$ , whereupon it remains at a dephasing rate of just under 5ps up to an intensity of  $8.9\text{Wcm}^{-2}$ . At an incident intensity of  $13.1\text{Wcm}^{-2}$  the FWM shows a biexponential decay, see figures 7.9 and 7.10. The two separate decays are hard to distinguish, see figure 7.9 inset. And the incident intensities are much lower than those used in collecting the 2QW data. Only data recorded at two intensities exhibit a biexponential behaviour and data could not be taken at higher intensities due to saturation of the polariton.

To summarise, we have seen an increase in the coherence time of the LPB at  $k_{\parallel}=0$  with increasing intensity. This effect only occurred above a threshold intensity. The decay time of the FWM signal above this threshold exhibits a biexponential decay. At short time delays the FWM signal increases with increasing intensity. At long time delays the FWM signal

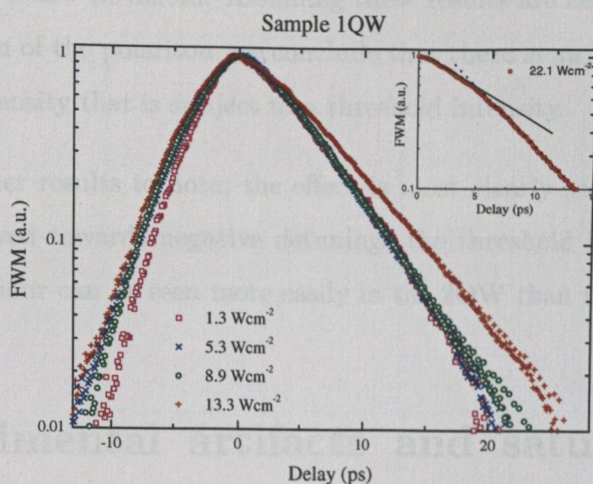


Figure 7.9: FWM data on the 1QW sample at a detuning of  $-2.6\text{meV}$  with intensity. Initially the FWM signal decreases slightly with intensity and then remains constant. At an incident intensity of  $13.3\text{Wcm}^{-2}$  the FWM shows a biexponential decay. The first decay increases with incident intensity, the second signal decays at the same rate as the FWM signal at low intensities. The two step decay is shown in the inset. The data is similar to that taken at a detuning of  $-1.7\text{meV}$  on the 2QW sample see figure 7.8, however, only two points show the biexponential decay. Higher intensity results are not obtainable due to the saturation of the polariton.

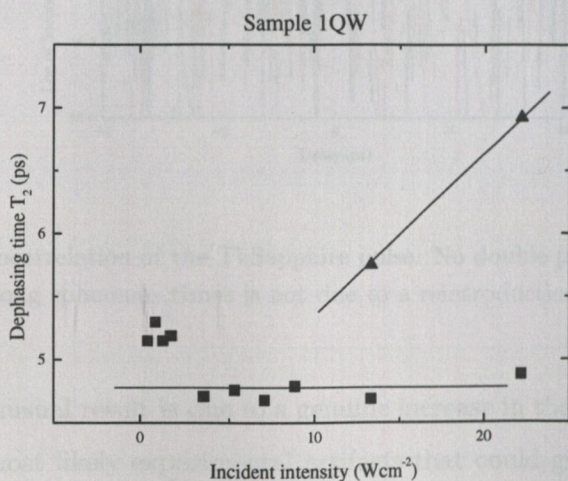


Figure 7.10: Dephasing times on the 1QW sample at a detuning of  $-2.6\text{meV}$ . Initially the dephasing times decrease with intensity, however at an incident intensity of  $13.3\text{Wcm}^{-2}$  two distinct dephasing times appear. The dephasing time at short delay times slows with intensity whilst the dephasing time at long delay times remains constant with the low intensity dephasing time. Only two points are taken showing the biexponential decay. Higher intensity results are not obtainable due to the saturation of the polariton.

remains the same as below threshold. Assuming these results are not due to an experimental artifact or saturation of the polariton, we conclude that there is an increase in the coherence of the LPB with intensity that is subject to a threshold intensity.

There are a few other results to note; the effect is most clearly seen at resonance. As the 2QW sample is moved towards negative detunings the threshold intensity increases. The biexponential behaviour can be seen more easily in the 2QW than the 1QW sample.

## 7.5 Experimental artifacts and saturation of the strong coupling regime

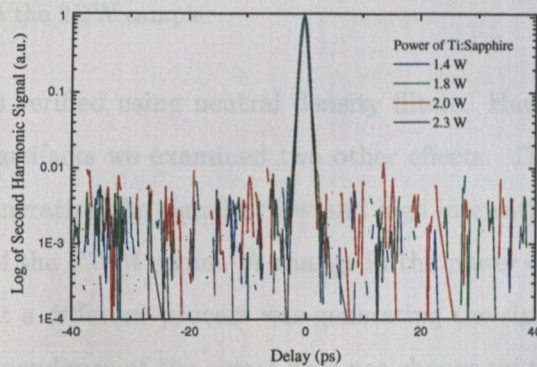


Figure 7.11: The autocorrelation of the Ti:Sapphire pulse. No double pulse of the laser is evident, thus the source of the long coherence times is not due to a reintroduction of coherence by a second pulse from the laser.

To ensure that this unusual result is due to a genuine increase in the coherence of the system we investigated the most likely experimental artifacts that could give rise to an increase in the FWM signal. The first is anomalous behaviour of the laser which could reintroduce coherence into the system. This was investigated by replacing the sample with the second harmonic lithium niobate ( $\text{LiNbO}_3$ ) crystal, with which an autocorrelation of the pulse width was obtained. No anomalous behaviour was evident, see figure 7.11.

Another possible source of the long FWM signals is that of detector saturation. The linear-

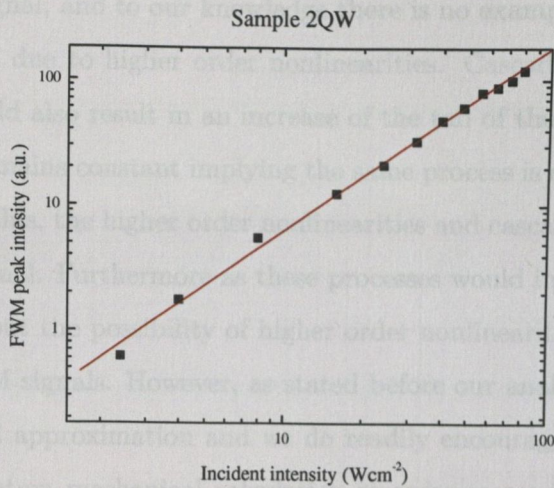


Figure 7.12: The integrated intensity of the FWM versus incident intensity, at resonance, showing a constant efficiency of the generated FWM signal to an incident intensity of  $80\text{Wcm}^{-2}$ . This implies that higher order nonlinear effects are not the cause of the long FWM decay times. The FWM signal was taken at resonance on the 2QW sample.

ity of the detectors was verified using neutral density filters. Having ruled out these most probable experimental artifacts we examined two other effects. The first was to check that the same process was generating the signal at low and high intensities. To do this we checked the power dependence of the FWM signal. A change in the power dependence at high intensities would suggest that a different process was generating the signal. As can be seen from figure 7.12 the power dependence of the signal does not change up to an incident intensity of  $80\text{Wcm}^{-2}$ .

This indicates that the same process generates the FWM signal up to this intensity and the signal is not being produced by some higher order nonlinear effect.<sup>3</sup> Higher order nonlinearities such as  $\chi^{(5)}$  and various cascade processes have been shown to have a dramatic effect on the FWM signal [176]. With our experimental setup however the  $\chi^{(5)}$  and cascade process are angularly separated from the  $\chi^{(3)}$  signal. This results in them being spatially resolved from our signal. Higher order nonlinearities such as the  $\chi^{(5)}$  processes initially increase, not

<sup>3</sup>Ideally the signal might be expected to increase with the cube of the intensity as it is a  $\chi^{(3)}$  process. However, our measured signal dependence was approximately half this; the gradient of figure 7.12 is approximately 1.5. This is not discussed any further here, although unexplained it does not reduce the strong argument that there has been no change in the process generating the signal.

decrease, the FWM signal, and to our knowledge there is no example of a longer followed by a shorter FWM signal due to higher order nonlinearities. Cascade processes would have a rise-time and this would also result in an increase of the tail of the FWM signal. Therefore, the FWM efficiency remains constant implying the same process is creating the FWM signal; and, notwithstanding this, the higher order nonlinearities and cascade processes are spatially separated from our signal. Furthermore as these processes would initially shorten the FWM signal, we have ruled out the possibility of higher order nonlinearities or cascades being the cause of the long FWM signals. However, as stated before our analysis of the FWM is by a simple two-level model approximation and we do readily encourage theorists to investigate a full many body quantum mechanical calculation in order to see if it is possible to obtain longer coherence times followed by shorter coherence times due to correlation effects in these systems.

The last effect we investigate, which we felt was the most probable cause of the long FWM signal, was the saturation of the LPB and its subsequent blue shift which would result in less intensity actually being absorbed. This may seem nonintuitive at first and is due to an effect called cavity pulling. Cavity pulling is the decreased absorption as the cavity is detuned towards the exciton resonance [177]. This effect already seems unlikely as, if less intensity was absorbed, there would be a decrease in the efficiency of the FWM which as just stated we did not see. However to further check this we compared the saturation densities of the femtosecond reflectivity to see if at these polariton densities there is any shift or saturation of the LPB exciton line. The maximum polariton density used in the FWM was less than half of the saturation density measured in the femtosecond reflectivity. The maximum FWM intensity of  $66.13 \text{ W cm}^{-2}$  corresponds to a polariton density of  $7.8 \times 10^{10} \text{ cm}^{-2}$  which is well below the saturation density,  $N_s$  of  $17.2 \times 10^{10} \text{ cm}^{-2}$  measured from the reflectivity, see figures 7.13 and 7.14. It should also be noted that there was some spectral overlap of the femtosecond pulse in the reflectivity data with the conduction band which would reduce the saturation density as compared with resonant pumping due to it introducing electron-hole pairs. The saturation data was measured using [57],

Figure 7.14: Femtosecond reflectivity of the 20W signal at resonance. From the absorption dip minimum with polariton density = saturation density,  $N_s$  of  $17.2 \times 10^{10} \text{ cm}^{-2}$  is obtained.



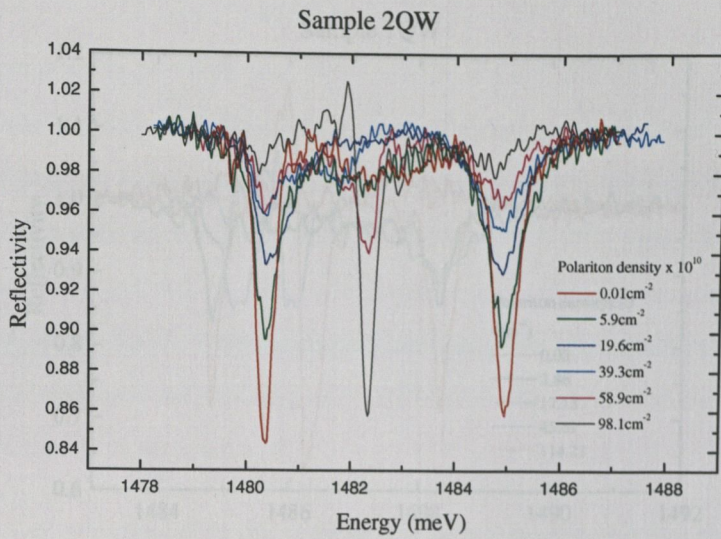


Figure 7.13: Femtosecond reflectivity of the 2QW sample at resonance. The reflectivity data taken at different intensities. No blue shift of the exciton line is evident before the collapse. The maximum FWM density would correspond to a density between the green and blue reflectivity data; well before the collapse of the strong coupling regime.

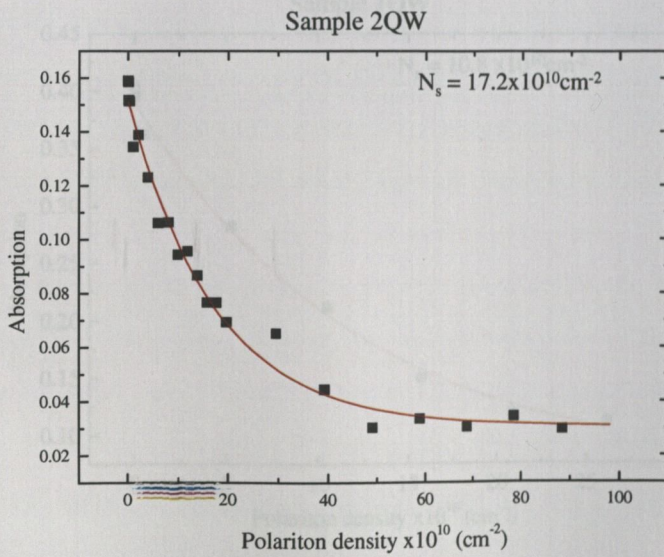


Figure 7.14: Femtosecond reflectivity of the 2QW sample at resonance. From the absorption dip minimum with polariton density a saturation density,  $N_s$  of  $17.2 \times 10^{10} \text{ cm}^{-2}$  is obtained.

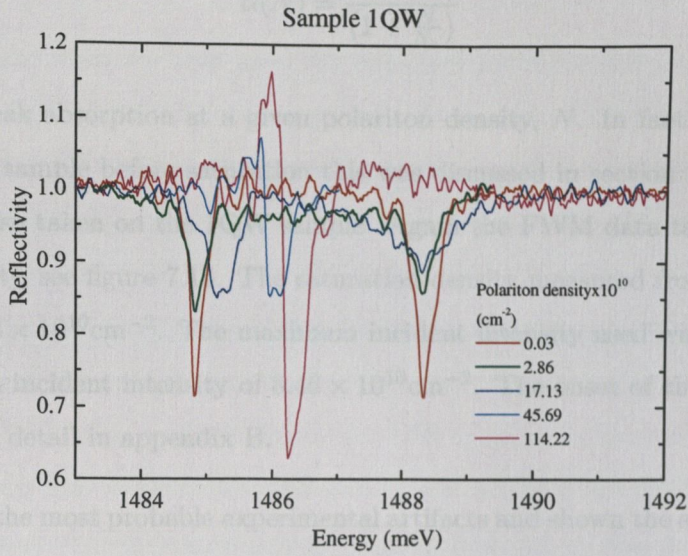


Figure 7.15: Femtosecond reflectivity of the 1QW sample at resonance. Reflectivity data was taken at a range of densities. A blue shift of the LPB is apparent prior to the collapse of the polariton.

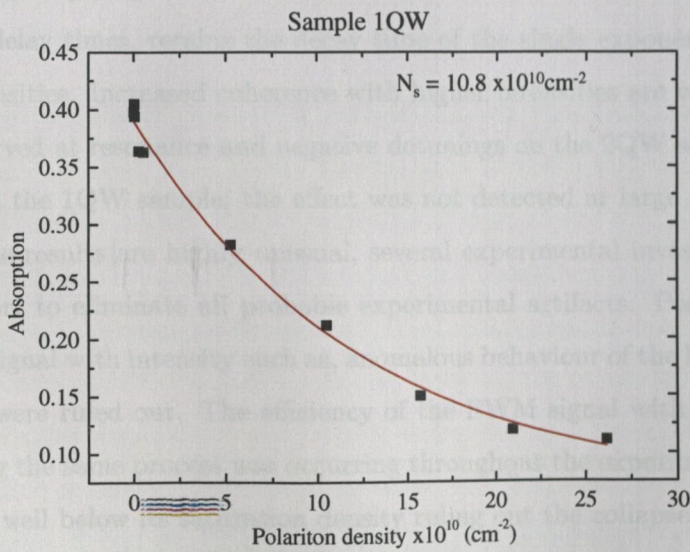


Figure 7.16: Femtosecond reflectivity of the 1QW sample at resonance. From the absorption dip minimum with polariton density, a saturation density  $N_s$  of  $10.8 \times 10^{10} \text{ cm}^{-2}$  is obtained.

## 7.6 Analysis of results

$$\alpha(N) = \frac{\alpha_0}{\left(1 + \frac{N}{N_s}\right)}, \quad (7.7)$$

where  $\alpha$  is the peak absorption at a given polariton density,  $N$ . In fact, there was no blue shift in the 2QW sample before saturation this was discussed in section 3.3.3. Femtosecond reflectivity was also taken on the 1QW sample. Again the FWM data taken was below the saturation intensity, see figure 7.15. The saturation density measured from the femtosecond reflectivity is  $10.8 \times 10^{10} \text{cm}^{-2}$ . The maximum incident intensity used was  $22.1 \text{Wcm}^{-2}$ , this corresponds to an incident intensity of  $8.46 \times 10^{10} \text{cm}^{-2}$ . The onset of the blue shift will be discussed in more detail in appendix B.

Having ruled out the most probable experimental artifacts and shown the samples to be in the strong coupling regime while taking the FWM data we deduce that the results are genuine.

In summary, we have measured a FWM signal that does not change significantly with increasing incident intensity until a critical density when the decay transforms from a single exponential to a biexponential. The first decay time, at short delay times, increases with increasing intensity implying an increase in the coherence of the system. Whilst the second decay, at larger delay times, retains the decay time of the single exponential decay encountered at low intensities. Increased coherence with higher intensities are very unusual. These effects were observed at resonance and negative detunings on the 2QW sample and at negative detunings on the 1QW sample; the effect was not detected at large angles and positive detunings. As the results are highly unusual, several experimental investigations were performed in an effort to eliminate all probable experimental artifacts. Possible causes of the increased FWM signal with intensity such as, anomalous behaviour of the laser and saturation of the detectors were ruled out. The efficiency of the FWM signal with intensity remained constant implying the same process was occurring throughout the experiment. The polariton was shown to be well below its saturation density ruling out the collapse of the polariton as a possible cause for these results.

## 7.6 Analysis of results

When analysing the data we have used the two-level approximation, which is often used at low excitation intensities [31], see chapter 4. As already mentioned, the decay of the coherence of a two-level system is governed by the decay of the population,  $T_1$ , and pure dephasing mechanisms,  $T_2^*$ , such as scattering. The net coherence lifetime,  $T_2$ , is given by equation (7.5). The shorter of  $T_1$  and  $T_2^*$  will dominate. The dephasing time due to the population decay time is about 20ps in high finesse microcavity samples, corresponding to a cavity decay time of 10ps see chapter 3. At low intensities we measure dephasing times of 5ps, implying a  $T_2^*$  of 6-7ps which is typical for QW excitons in these materials [139, 178]. Thus the dephasing time is primarily governed by scattering (pure dephasing) rather than radiative recombination (population decay). Experimentally, it was observed that as the intensity increases the measured dephasing time increases. This change cannot be due to an increase in  $T_1$  as the shorter of the two dephasing times will dominate, instead only an increase in  $T_2^*$  will have an appreciable effect on the dephasing rate. Therefore the effect of increasing intensity is to either inhibit scattering or to compensate out-scattering with in-scattering. If  $T_2$  becomes very large then the dephasing rate will depend on  $T_1$  and the dephasing time will depend on the population decay time of 20ps.

Consider a coherent population of excitons created at  $k_{||}=0$ . Elastic exciton-exciton collisions will scatter the exciton away from  $k_{||}=0$ . The gradient of the energy momentum dispersion is so flat that the  $k_{||}=0$  excitons occupy only a small part of the available k-space, so that back scattering (to  $k_{||}=0$ ) from  $k_{||}\neq 0$  will be small and these excitons will be dephased with respect to the original population, see figure 7.17(a). This type of scattering decreases the coherence as measured in FWM experiments and increases the linewidth in cw experiments. The modified polariton dispersion curve, which is steeper by a factor of  $10^4$ , is the result of a reduced k-space to scatter into resulting in an inhibition of the scattering process as examined in chapters 5 and 6. There will still be some scattering away from  $k_{||}=0$  (e.g. guided modes). There are now two possibilities: (1) Non-bosonic behaviour as observed in chapter 6 where the increase in density leads to more collisions which decrease the dephasing time with intensity, see figure 7.17(b). (2) Bosonic behaviour, as the density increases the

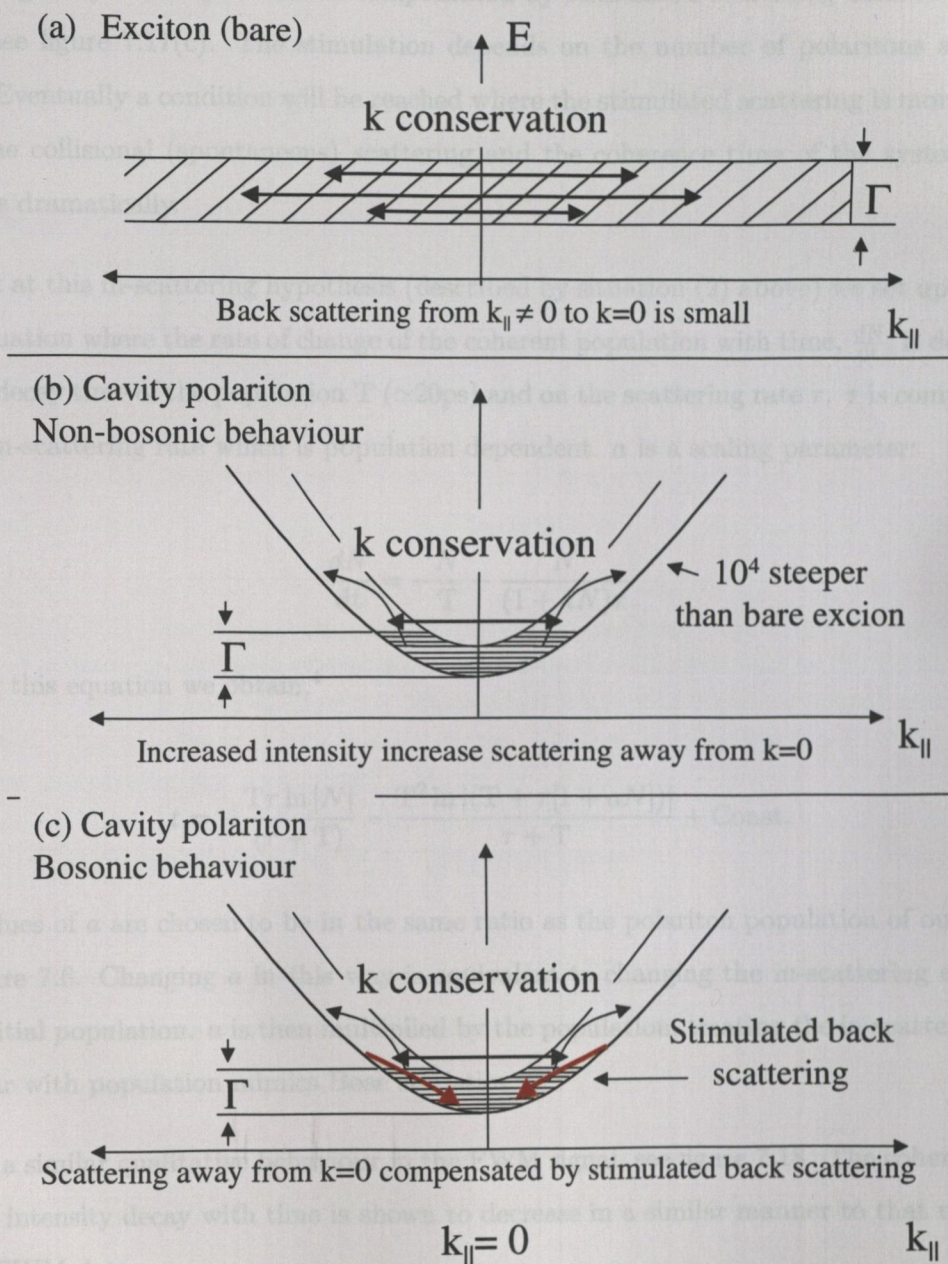


Figure 7.17: (a) Schematic of scattering of excitons created at  $k_{\parallel}=0$ . Scattering to  $k_{\parallel} \neq 0$  is efficient due to the large density of states (flat dispersion curve). Very few excitons will scatter back to  $k_{\parallel}=0$  and those that do will be dephased from the original population. (b) Schematic of scattering of non-bosonic polaritons created at  $k_{\parallel}=0$ . Scattering will be suppressed in part due to the small density of states (steep dispersion curve). However, above a critical intensity scattering away from  $k_{\parallel}=0$  will occur, as shown in chapter 6. These polaritons scattered to  $k_{\parallel} \neq 0$  will be dephased from the  $k_{\parallel}=0$  polaritons. (c) Schematic of scattering of bosonic polaritons created at  $k_{\parallel}=0$ . The scattering away from  $k_{\parallel}=0$  discussed for situation (b) will be compensated by stimulated back (to  $k_{\parallel}=0$ ) scattering.

scattering away from  $k_{\parallel}=0$  can be compensated by stimulated scattering back to the  $k_{\parallel}=0$  state, see figure 7.17(c). The stimulation depends on the number of polaritons already at  $k_{\parallel}=0$ . Eventually a condition will be reached where the stimulated scattering is more efficient than the collisional (spontaneous) scattering and the coherence time of the system should increase dramatically.

To look at this in-scattering hypothesis (described by situation (2) above) we set up a simple rate equation where the rate of change of the coherent population with time,  $\frac{dN}{dt}$ , is dependent on the decay time of the population  $T$  ( $\approx 20$ ps) and on the scattering rate  $\tau$ .  $\tau$  is compensated by an in-scattering rate which is population dependent.  $a$  is a scaling parameter:

$$\frac{dN}{dt} = -\frac{N}{T} - \frac{N}{(1+aN)\tau} \tag{7.8}$$

Solving this equation we obtain,<sup>4</sup>

$$t = -\frac{T\tau \ln |N|}{(\tau + T)} - \frac{T^2 \ln |(T + \tau[1 + aN])|}{\tau + T} + \text{Const.} \tag{7.9}$$

The values of  $a$  are chosen to be in the same ratio as the polariton population of our FWM, see figure 7.6. Changing  $a$  in this way is equivalent to changing the in-scattering efficiency with initial population.  $a$  is then multiplied by the population, treating the in-scattering rate as linear with population mimics Bose statistics.

We see a similar qualitative behaviour in the FWM signal, see figure 7.18. The coherent population intensity decay with time is shown to decrease in a similar manner to that measured in the FWM data.

Although this result is by no means proof of the theory it does suggest that our hypothesis for the long coherence times is plausible.

<sup>4</sup>This equation cannot be written as a population dependent on time ( $N(t)$ ) instead it is written as time dependent on population ( $t(N)$ ).

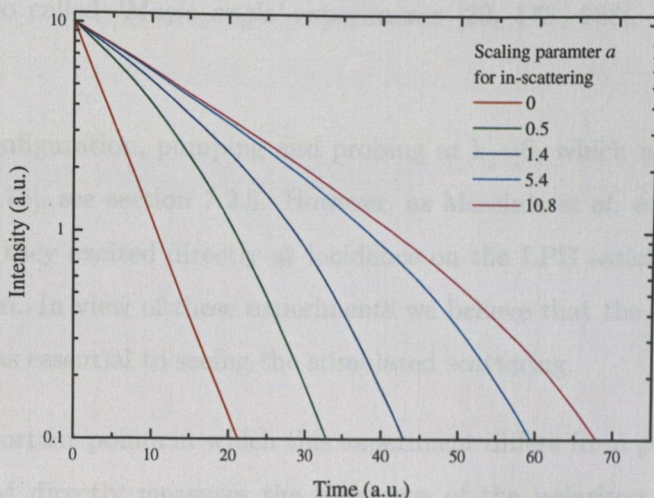


Figure 7.18: The relation between coherent population and time as described by equation (7.9) for several different in-scattering efficiencies,  $a$ .  $a$  is scaled in the same ratio as the initial polariton population in the data shown in figure 7.6. We assume the in-scattering varies linearly with coherent population. This is a signature of a bosonic system. The results show that qualitatively a density dependent in-scattering rate is plausible.

## 7.7 Comparison with literature

The stimulated scattering due to occupation on the LPB is not a new result in the field. Stimulated emission by occupation has already been demonstrated in polariton systems as mentioned above [20, 23, 24, 166, 174, 175].

The contrasting results between this chapter and chapter 6 are the consequence of two experimental changes. Firstly, the detuning of the polariton; the detuning was positive in the previous chapter and the detuning was resonant or negative in this chapter. Secondly, the angle between the pump and probe beam in the FWM experiment was reduced for the data taken in this chapter. These two experimental changes are investigated in appendix B. In most, though not all, of the other work mentioned, the detuning of the LPB was either resonant or negative when stated, suggesting that the stimulation by occupation is more easily seen at these detunings. The reduction of angle would be instrumental in satisfying energy and momentum conservation.

The strict angular dependence needed for energy and momentum conservation has been demonstrated in so called 'Magic angle' experiments [20, 173, 168], this was discussed in section 7.2.3.

The degenerate configuration, pumping and probing at  $k_{\parallel}=0$ , which we used was the same as Messin *et al.* [175], see section 7.2.3. However, as Messin's *et al.* experiment was in the frequency domain they excited directly at incidence on the LPB satisfying momentum and energy conservation. In view of these experiments we believe that the narrow angle used in this experiment was essential to seeing the stimulated scattering.

There are two important points in which this experiment differs from previous experimental work. First, FWM directly measures the coherence of the polariton system and not the coherence of the emitted photon. Secondly, the increased coherence of our system is unlike in cw experiments as the coherence of our system does not exhibit the coherence of the pump beam.

To compare this work with previous work performed on bare QWs we only state that increased coherence with intensity is an extremely unusual result and has not been observed in bare QW systems.

## 7.8 Conclusions

We conclude that we have seen an increase in the coherence time of the lower polaritons with excitation density. We believe this increase to be genuine as experimental and saturation effects have been ruled out. We have modelled our results using a simple rate equation model which used an in-scattering rate of the coherent population which was dependent on density.

Our results have been shown to be similar to the published literature and have shown the bosonic nature of the lower polaritons. There was initially stimulated emission shown by pumping at large  $k$  [19, 20]. Then stimulated emission was shown at  $k_{\parallel}=0$  in the frequency-domain [175]. We have shown an increased coherence at  $k_{\parallel}=0$  in the time-domain. However there is an important difference which has been demonstrated; that is, the polaritons maintain



their long coherence time without an external pump field. This contrasts with the coherence observed in previous 'parametric amplification' experiments which can be described in the polariton four wave mixing model [169]. The long coherence times, we believe, could plausibly be due to a BEC. Further experimental and theoretical work is needed however for the moment it does, seem a plausible explanation, see chapter 8.

## Chapter 8

## Conclusions

This thesis investigated the dynamic properties of cavity polaritons. The main aims of this thesis were to demonstrate the differences between a quantum well exciton and a polariton and to investigate the bosonic properties of polaritons.

The basic concepts of strong coupling were discussed. The strong coupling studied is in a III-V semiconductor microcavity between a quantum well exciton and a confined optical mode in a distributed Bragg reflector mirror. This regime and its new modes, polaritons, were compared with weak coupling in planar microcavities, strong coupling of atoms, and bare quantum well excitons. The important character differences between atomic and exciton strong coupling systems such as the dispersion curve were examined. Two models which lead different interpretations of polaritons were reviewed namely, the Jaynes-Cummings atomic model (a quantum model) and the linear dispersion model (a classical model). The fact that most of the results can be modelled using a classical model brings about the question: 'Is the system an exciton in a cavity filter or are there genuinely new quantum states?' The excellent agreement between the two models in the linear regime highlights the need for nonlinear experiments to answer this fundamental question.

## Chapter 8

## Conclusions

This thesis investigated the dynamic properties of cavity polaritons. The main aims of this thesis were to demonstrate the differences between a quantum well exciton and a polariton and to investigate the bosonic properties of polaritons.

The basic concepts of strong coupling were discussed. The strong coupling studied is in a III-V semiconductor microcavity between a quantum well exciton and a confined optical mode in a distributed Bragg reflector mirror. This regime and its new modes, polaritons, were compared with weak coupling in planar microcavities, strong coupling of atoms, and bare quantum well excitons. The important character differences between atomic and exciton strong coupling systems such as the dispersion curve were examined. Two models which lend different interpretations of polaritons were reviewed namely, the Jaynes-Cummings atomic model (a quantum model) and the linear dispersion model (a classical model). The fact that most of the results can be modelled using a classical model brings about the question. 'Is the system an exciton in a cavity filter or are there genuinely new quantum states?' The excellent agreement between the two models in the linear regime highlights the need for nonlinear experiments to answer this fundamental question.

We have shown that four wave mixing is a suitable nonlinear spectroscopic tool to measure the coherence of our system which can be characterised by linewidth.

Acoustic phonon scattering was the first study performed. It was shown that the lower polariton branch significantly differed from the bare quantum well exciton behaviour. Unlike bare quantum wells, whose linewidths increase linearly with temperature, a suppression of acoustic phonon interaction was observed in the lower polariton branch until a critical temperature. The critical temperature was shown to be strongly detuning dependent. The results were explained in terms of the modified dispersion curve. This clearly shows that the dynamic behaviour of the polariton can significantly differ from the bare quantum well exciton. Even above the critical temperature bare quantum well exciton behaviour was not recovered and the acoustic phonon scattering efficiency was reduced. This suppression, and scattering efficiency was investigated with detuning and the results were explained with a simple phenomenological model.

Collisional broadening was then studied using a similar experimental set up. Once again a stark difference was seen in the dynamic interaction of the lower polariton compared to the bare quantum well exciton. Collisional broadening was reduced in the lower polariton branch compared with the exciton system until a threshold intensity. The strong reduction in collisional broadening below threshold, by a predicted four orders of magnitude, resulted in no collisional broadening being detected within experimental error. The threshold behaviour was explained in terms of the modified dispersion curve. Both the threshold behaviour and its effect with detuning were in excellent agreement with theoretical predictions.

These two experiments showed that the dynamic behaviour of the lower polariton dramatically differs from the bare quantum well exciton. Although this does not prove that the cavity is not just a filtering effect, it demonstrates that the dynamic properties of polaritons are strongly modified by the cavity.

During the period of these experimental investigations, several exciting reports of stim-

ulated scattering of the polariton by other research groups in the field were made. These results showing bosonic behaviour have opened up new aspects of research. By several small modifications of the four wave mixing setup we explored the possibility of increased coherence with excitation, a bosonic effect. This increased coherence in a pulsed dynamic four wave mixing experiment in our configuration would imply a macroscopic phase. The increased coherence with excitation was demonstrated in both samples. This is an extremely interesting result and leads to the question whether a BEC could be formed in these systems, though more experimental work is needed to answer this important question. Bose Einstein condensates have been of interest for a long time in excitonic systems but due to the composite nature of the exciton and the high densities needed for Bose Einstein condensation, Bose Einstein condensation remains an experimental challenge. However, a mixed state of a photon and an exciton such as the cavity polariton would logically seem a more likely BEC candidate. Further work needs to be done on this but it is an exciting prospect. Perhaps experiments in II-VI will be more successful due to their stronger interaction.

After the initial flagging of the research in this area when it was found that fast recombination times were not realisable due to the relaxation bottleneck, worldwide research moved towards more fundamental issues. Spin off projects from this research have resulted in prospective commercial devices, such as the polariton-polariton lasers.

### **8.0.1 Future work**

A major interest in future work would be the confirmation or otherwise of the BEC theory. We have partially investigated this by trying to ascertain, if the coherence is increased by adding an incoherent polariton population. This would only occur if the system had a macroscopic coherence. We added a polariton population with a continuous source but a large amount of power is needed to generate a substantial number of carriers for the duration of the picosecond pulse. The results were plagued

by large thermal effects. To prevent thermal effects a source needs to be synchronised with the Ti:Sapphire (82MHz) in order to obtain a larger enough population during the picosecond pulse. The source would also need to be tunable and with at least 1mW average power. The most obvious solution is two synchronised Ti:Sapphire. However a laboratory with two synchronised Ti:Sapphire was not readily available to us.

## Appendix A

Another experiment alluded to in chapter 6 would be to investigate the polarisation dependence of the polariton-polariton broadening as by changing the polarisation the scattering to dark states can be selectively inhibited or allowed.

## Biexcitons

When two excitons are in close proximity their wavefunctions can combine either symmetrically or anti-symmetrically. The anti-symmetric wavefunction is at a higher energy and consequently does not form a bound particle; conversely the symmetric combination forms a bound state. Like the exciton, the properties of the biexciton depends on the parameters of the crystal and its binding energy increases when confined in a quantum well.

The selection rules for biexcitons originate from the angular momentum discussed in section 6.2. There are two optically active exciton cases. In the first case the first excited exciton, created by circularly polarised light  $\sigma^+$ , consists of  $J_z = -\frac{1}{2}$  electron and  $J_z = +\frac{1}{2}$  hole and the second excited state, excited by the opposite circularly polarised light  $\sigma^-$ , consists of  $J_z = +\frac{1}{2}$  electron and  $J_z = -\frac{1}{2}$  hole. These excitons are independent particles which can combine to form a biexciton. However two  $\sigma^+$  generated excitons are not distinguishable and thus cannot combine, similarly two  $\sigma^-$  generated excitons cannot combine.

The energy levels are shown in the figure A.1. The ground state is denoted by  $|0\rangle$  and the exciton state excited by  $\sigma^+$  light is represented by  $|1+\rangle$ . Analogously the

# Appendix A

## Biexcitons

When two excitons are in close proximity their wavefunctions can combine either symmetrically or anti-symmetrically. The anti-symmetric wavefunction is at a higher energy and consequently does not form a bound particle; conversely the symmetric combination forms a bound state. Like the exciton, the properties of the biexciton depends on the parameters of the crystal and its binding energy increases when confined in a quantum well.

The selection rules for biexcitons originate from the angular momentum discussed in section 6.2. There are two optically active exciton cases. In the basis used here the first excited exciton, created by circularly polarised light  $\sigma^+$ , consists of  $J_z = -\frac{1}{2}$  electron and  $J_z = +\frac{3}{2}$  hole and the second excited state, excited by the opposite circularly polarised light  $\sigma^-$ , consists of  $J_z = +\frac{1}{2}$  electron and  $J_z = -\frac{3}{2}$  hole. These excitons are independent particles which can combine to form a biexciton. However two  $\sigma^+$  generated excitons are not distinguishable and thus cannot combine, similarly two  $\sigma^-$  generated excitons cannot combine.

The energy levels are shown in the figure A.1. The ground state is denoted by  $|0\rangle$  and the exciton state excited by  $\sigma^+$  light is represented by  $|+1\rangle$ . Correspondingly the

exciton state excited by  $\sigma^-$  light is represented by  $| - 1 \rangle$ , both exciton states have the same energy,  $E_x$ . The two-exciton continuum has an energy  $2E_x$ . The biexciton had an energy of  $2E_x - \Delta_{bx}$ , where  $\Delta_{bx}$  is the biexciton binding energy.

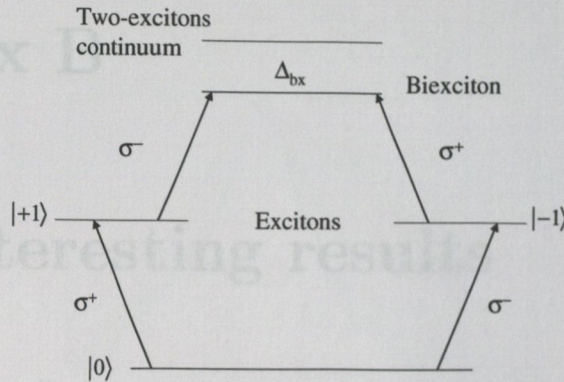
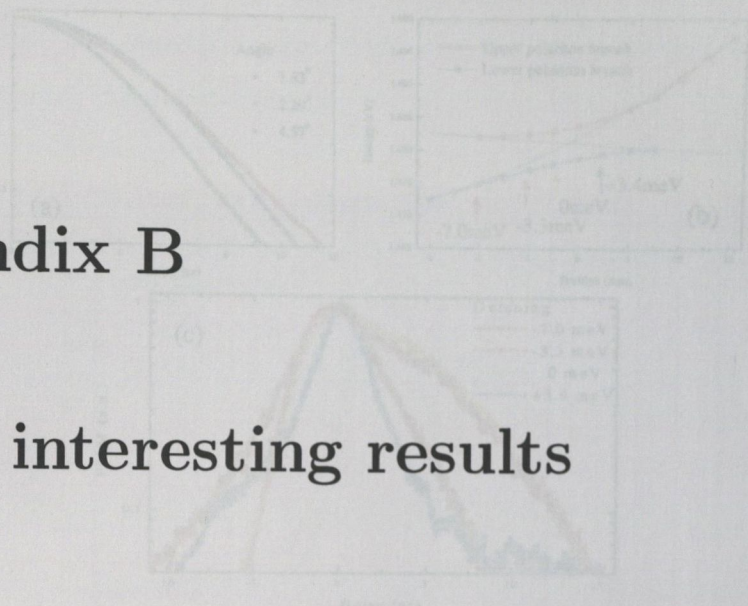


Figure A.1: Schematic diagram of the energy levels of biexcitons, showing the ground state,  $|0\rangle$ , the two optically active states,  $|+1\rangle$  and  $|-1\rangle$  and the biexciton state. The biexciton state is less than the two-exciton continuum by its binding energy  $\Delta_{bx}$ . The selection rules are shown; a biexciton cannot be created from the same exciton state.

The selection rules are summarised in figure A.1. An electromagnetic field with a given circular polarisation can induce a transition from the ground state to an exciton state and induce a transition from a exciton state, already created by light of the counter circular polarisation, to the biexciton. However, it cannot create a biexciton without an exciton being created from the opposite polarisation.

First transition	Second transition	Biexciton allowed?
$\sigma_+$	$\sigma_+$	No
$\sigma_+$	$\sigma_-$	Yes
$\sigma_-$	$\sigma_-$	No
$\sigma_-$	$\sigma_+$	Yes

Thus to prevent the formation of biexcitons, co-circularly polarised light should be used.



## Appendix B

### Other interesting results

In this appendix we investigate the effects of angle and detuning on the FWM results in the 2QW sample. Angle and detuning were both important parameters in the investigation into excitation induced coherence discussed in chapter 7.

The angular dependence was investigated by varying the angle between the two beams which we distinguish by naming them 'pump' and 'probe'. To vary the angle the probe beam was moved across the focussing lens. The pump beam was not moved and thus remained at the same position on the sample. Due to the low numerical aperture of the lens it was not possible to investigate very large angles, greater than  $5^\circ$ . However, as can be seen from figure 7.5, there is a large gradient in the LPB dispersion. Thus, pumping at large angles would prohibit absorption unless the energy was modified to take into account the curvature of the LPB dispersion; with no absorption no FWM signal can be generated. The results taken span from an angle of  $1.8^\circ$  to  $4.6^\circ$ , see figure B.1(a). The FWM signal is not strongly affected by the angle up to an angle of  $2.3^\circ$ . This suggests that the LPB is homogeneously broadened and that we are not pumping individual lines within the LPB, if this was occurring we would expect a change in the FWM signal. The FWM does decay more rapidly at an angle of  $4.7^\circ$ , this could be due to less light being absorbed by the LPB resulting in a drop in the in-scattering rate.



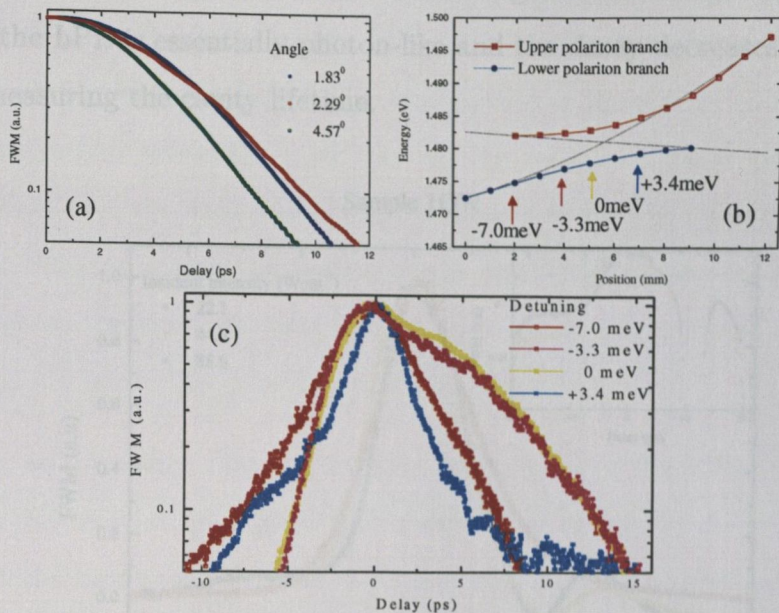


Figure B.1: (a) The affect of angle on the FWM signal. The affect of angle appears weak up to an angle of  $2.3^\circ$ , this is due to the angular linewidth of the LPB, see figure 7.5; although the angle increases the pump beam is still within the linewidth of the LPB. However at an angle of  $4.7^\circ$  the pump beam is no longer in the angular linewidth of the LPB and the FWM decays more rapidly. This quicker dephasing rate is probably due to less absorption and therefore less in-scattering. (b) The polariton-position map. The different positions across the sample where the FWM was taken is marked with arrows and the corresponding detuning. (c) FWM data showing the change in decay with detuning. The decay is fast for positive detunings due to collisional broadening. Towards resonance the FWM signal increases we believe this is due to an in-scattering process. At far negative detunings as the LPB is effectively a photon the FWM signal is measuring the pulse width of the photon.

The effect of detuning on the dephasing rate was ascertained by taking FWM decays at several positions across the sample; these positions correspond to different detunings, see section 3.2. Figure B.1(b) shows the positions and detunings where data was taken. The FWM results for an incident intensity of  $60\text{Wcm}^{-2}$  are presented in figure B.1(c). At a positive detuning of  $+3.4\text{meV}$ , and the above intensities, the polariton has a fast dephasing time due to collisional broadening of the polaritons. As the detuning is moved towards the negative the exciton fraction of the LPB decreases and consequently there is reduced collisional broadening. At resonance the FWM dephasing rate has increased, showing the now familiar increased coherence. This is shown to occur also

at small negative detunings of  $-3.3\text{meV}$ . At far negative detunings there is very little absorption, the LPB is essentially photon-like and the decay decreases as the FWM is effectively measuring the cavity lifetime.

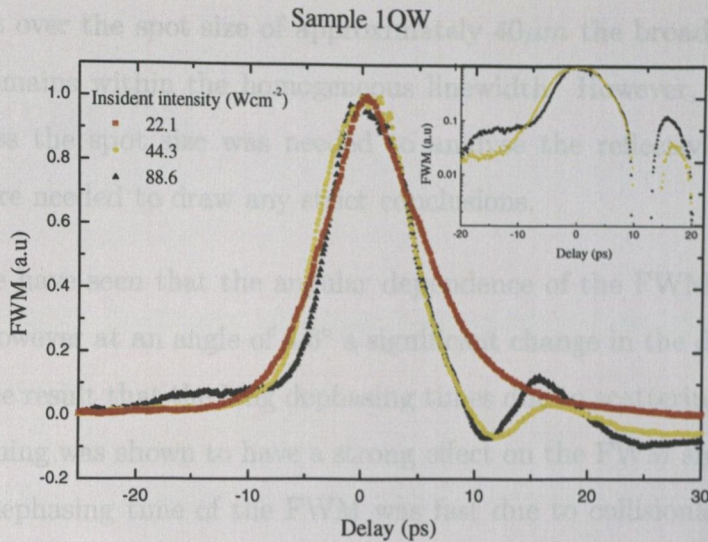


Figure B.2: FWM data on the 1QW sample at a detuning of  $-2.7\text{meV}$  for a range of intensities. The lowest intensity  $22.1\text{Wcm}^{-2}$ , depicted here was the highest intensity used in the long coherence experiment. At about twice this intensity,  $44.3\text{Wcm}^{-2}$ , the polariton has collapsed as the polariton density of  $17 \times 10^{10}\text{cm}^{-2}$  is nearly twice the saturation density as measured at resonance. In this case the FWM decay shows a fast decay followed by a bump at approximately  $14\text{ps}$ . We believe this could be a beating between the blue shifted exciton line and the unshifted exciton line.

Another interesting phenomenon apparent in the FWM signal is the collapse of the polariton. We have investigated this on the 1QW sample at a detuning of  $-2.7\text{meV}$ . From the femtosecond reflectivity we note that the LPB blue shifts before it collapses into the weak coupling regime, see figure 7.15. At the lowest FWM intensity, shown on figure B.2, there is no unusual behaviour in the FWM signal. However at an incident intensity of  $44.3\text{Wcm}^{-2}$  a second signal at approximately  $15\text{ps}$  can be seen. This incident intensity corresponds to a polariton density of approximately  $17 \times 10^{10}\text{cm}^{-2}$ . If we look at the femtosecond reflectivity at this polariton density we see that the blue shift of the polariton is  $0.3\text{meV}$ . A time difference of  $15\text{ps}$  corresponds to an energy difference of approximately  $0.02\text{meV}$ . At resonance the absorption of the polariton is

much higher than at far negative detunings. Thus it may be that the second peak is the result of a beating between the LPB at low intensities and the LPB which is blue shifted at higher intensities. The two polariton lines may coexist due to the intensity distribution across the laser spot on the sample. This is not substantiated by the fact that over the spot size of approximately  $40\mu\text{m}$  the broadening due to the cavity wedge remains within the homogeneous linewidth. However, a distribution of intensities across the spot size was needed to analyse the reflectivity data; further investigations are needed to draw any strict conclusions.

To conclude, we have seen that the angular dependence of the FWM is negligible for small angles. However at an angle of  $4.6^\circ$  a significant change in the dephasing time is evident, with the result that the long dephasing times due to scattering are not readily observed. Detuning was shown to have a strong effect on the FWM signal. At positive detunings the dephasing time of the FWM was fast due to collisional broadening, as the detuning was moved towards resonance the dephasing times increased. We believe this was due to the in-scattering effect discussed above. At far negative detunings the FWM signal decreases and we believe this is because the LPB is essentially photon-like and the FWM is effectively measuring the pulse width.

[4] C. Weisbuch, H. Benisty, and R. Houdre. Overview of fundamentals and applications of electrons, excitons and photons in confined structures. *J. Lumines.* 55(4):271, January 2000.

[5] L. A. Orozco, A. T. Rosenberger, and H. J. Kimble. Intrinsic dynamic instability in optical bistability with two-level atoms. *Phys. Rev. Lett.* 53(27):25-27, December 1984.

## Bibliography

- [1] A. Y. Cho and J. R. Arthur. Molecular beam epitaxy. *Prog. in Sol. Stat. Chem.*, 10(3):157, 1975.
- [2] D. A. B. Miller. Optoelectronic applications of quantum wells. *Opt. Phot. News*, 1(2):7, February 1990.
- [3] E. M. Purcell. Spontaneous emission probabilities at radio frequencies. *Phys. Rev.*, 69:681, 1946.
- [4] C. Weisbuch, H. Benisty, and R. Houdré. Overview of fundamentals and applications of electrons excitons and photons in confined structures. *J. Lumin.*, 85(4):271, January 2000.
- [5] L. A. Orozco, A. T. Rosenberger, and H. J. Kimble. Intrinsic dynamic instability in optical bistability with two-level atoms. *Phys. Rev. Lett.*, 53(27):2547, December 1984.

- [6] P. R. Berman. *Cavity quantum electrodynamics*. Advances in Atomic, Molecular and Optical processes. Academic Press, 24-28 Oval Road, London, NW1 7DX, England, 1994.
- [7] J. J. Hopfield. Aspects of polaritons. *J. Phys. Soc. Japan*, 22(77-88):771, 1966.
- [8] H. Sumi. On the exciton luminescence at low temperatures: Importance of the polariton viewpoint. *J. Phys. Soc. Japan*, 21(2):1936, August 1976.
- [9] C. Weisbuch and R. Ulbrich. Spatial and spectral features of polariton fluorescence. *J. Lumin*, 18/19(1):27, January 1979.
- [10] C. Weisbuch, M. Nishioka, A. Ishikawa, and Y. Arakawa. Observation of the coupled exciton-photon mode splitting in a semiconductor quantum microcavity. *Phys. Rev. Lett.*, 69(23):3314, December 1992.
- [11] H. Yokoyama and K. Ujikara, editors. *Microcavities and semiconductors: The strong coupling regime*. CRC press, 1995.
- [12] M. S. Skolnick, T. A. Fisher, and D. M. Whittaker. Strong coupling phenomena in quantum microcavity structures. *Semicond. Sci. Technol.*, 13(7):645, July 1998.
- [13] G. Khitrova, H. M. Gibbs, F. Jahnke, M. Kira, and S. W. Koch. Nonlinear optics of normal-mode-coupling semiconductor microcavities. *Reviews of Modern Physics*, 71(5):1591, October 1999.

- [14] M. Bertolotti, editor. *Physics and devices with semiconductor microcavities*, volume 560. AIP, USA, 2001.
- [15] J. Bloch, R. Planel, V. Thierry-Mieg, M. M. Gérard, D. Barrier, J. Y. Marzin, and E. Costard. Strong-coupling regime in pillar semiconductor microcavities. *Superlattices Microstruct.*, 22(3):749, 1997.
- [16] M. A. Kaliteevski, S. Brand, and R. A. Abram. Exciton polaritons in a cylindrical microcavity with an embedded quantum wire. *Phys. Rev. B*, 61(20):13791, May 2000.
- [17] D. G. Lidzey, D. D. C. Bradley, A. Virgili, A. Armitage, M. S. Skolnick, and S. Walker. Room temperature polartion emission from strongly coupled organic semiconductor microcavities. *Phys. Rev. Lett.*, 82(16):3316, April 1999.
- [18] F. Tassone, C. Piermarocchi, V. Savona, and A. Quattropani. Bottleneck effects in the relaxation and photoluminescence of microcavity polaritons. *Phys. Rev. B*, 56(12):7554, September 1997.
- [19] R. Huang, F. Tassone, and Y. Yamamoto. Experimental evidence of stimulated scattering of excitons in to microcavity polaritons. *Phys. Rev. B*, 61(12):7854, March 2000.
- [20] P. G. Savvidis, J. J. Baumberg, R. M. Stevenson, M. S. Skolnick, D. M. Whitaker, and J. S. Roberts. Angle-resonant stimulated polariton amplifier. *Phys. Rev. Lett.*, 84(7):1547, February 2000.

- [21] H. Ulmer-Tuffigo, J. Bleuse, and F. Kany. Magnetic tuning of exciton-photon resonance in II-VI microcavities. *Superlattices Microstruct.*, 22(3):749, 1997.
- [22] F. Quochi, G. R. Hayes, R. André, G. Bongiovanni, A. Mura, J. L. Staehli, and Le Si Dang. Coherent exciton-photon dynamics in high-quality II-VI semiconductor microcavities. *J. Cryst. Growth*, 184:754, February 1998.
- [23] Le Si Dang, D. Heger, R. André, F. Bœuf, and R. Romestain. Stimulation of polariton photoluminescence in semiconductor microcavity. *Phys. Rev. Lett.*, 81(18):3920, November 1998.
- [24] F. Boeuf, R. André, R. Romestain, Le Si Dang, E. Péronne, J. F. Lampin, D. Hulin, and A. Alexandrou. Evidence of polariton stimulation in semiconductor microcavities. *Phys. Rev. B*, 62(4):2279, July 2000.
- [25] J. Rarity and C. Weisbuch, editors. *Dynamical Studies of Cavity Polaritons in Semiconductor Microcavities*, volume 324 of *NATO ASI series E, Applied Sciences*. Kluwar Academic Publishers, September 1996.
- [26] J. M. Gérard, B. Sermage, B. Gayral, B. Legrand, E. Costard, and V. Thierry-Mieg. Enhanced spontaneous emission by quantum boxes in a monolithic optical microcavity. *Phys. Rev. Lett.*, 81(5):1110, August 1998.
- [27] E. Burstein and C. Weisbuch, editors. *Spontaneous emission control in semiconductor microcavities*, NATO ASI series E, Applied Sciences. Plenum, New York, September 1995.

- [28] P. T. Worthing, J. A. E. Wasey, and W. L. Barnes. Rate and efficiency of spontaneous emission in metal-clad microcavities. *J. Appl. Phys.*, 89(1):615, September 2001.
- [29] H. Yokoyama and K. Ujihara, editors. *Dielectric Spontaneous emission in planar dielectric microcavities*, CRC press laser and optical science and technology series. CRC press, Boca Raton, Florida, USA, September 1995.
- [30] B. Gayral, M.-M Gérard, B. Sermage, A. Lemaitre, and C. Dupuis. Time-resolved probing of the Purcell effect for InAs quantum boxes in GsAs microdisks. *Appl. Phys. Lett.*, 78(19):2828, May 2001.
- [31] H. Benisty, J. M. Gérard, R. Houdré, J. Rarity, and C. Weisbuch. *Confined photon systems fundamentals and applications*. Lecture notes in physics: Vol 531. Springer-Verlag, Berlin, 1998.
- [32] H. Benisty, H. De Neve, and C. Weisbuch. Impact of planar microcavity effect on light extraction: Basic concepts and analytical trends. *IEEE*, 34(9):1612, September 1998.
- [33] L. Allen and J. H. Eberly. *Optical resonance and two-level atoms*, volume 28 of *Interscience monographs and texts in physics and astronomy*. Wiley, New York, USA, 1975.
- [34] B. Sermage, S. Long, I. Abram, J. Y. Marzin, J. Block, R. Planel, and V. Thierry-Mieg. Time-resolved spontaneous emission of excitons in a micro-



- [41] cavity: Behaviour of the individual exciton-photon mixed states. *Phys. Rev. B*, 53(24):16516, June 1996.
- [35] J. J. Sanchez-Mondragon, N. B. Narozhny, and J. H. Eberly. Theory of spontaneous emission line shape in an ideal cavity. *Phys. Rev. Lett.*, 51(7):550, August 1983.
- [36] S. Haroche and D. Kleppner. Cavity quantum electrodynamics. *Phys. Today*, 42(1):24, January 1989.
- [37] P. R. Berman, editor. *Structure and Dynamics in Cavity Quantum Electrodynamics*, volume 2 of *Advances in Atomic, Molecular, and Optical Physics*. Academic press, San Diego, CA, USA, 1983.
- [38] Yifu Zhu, Daniel J. Gauthier, S. E. Morin, Qilin Wu, H. J. Carmichael, and T. W. Mossberg. Vacuum Rabi splitting as a feature of linear-dispersion theory: Analysis and experimental observations. *Phys. Rev. Lett.*, 64(21):2499, May 1990.
- [39] M. Born and E. Wolf. *Principles of Optics: electromagnetic theory of propagation interference and diffraction of light*. Cambridge University Press, University press, Cambridge, England, 1997.
- [40] V. Savona, L. C. Andreani, P. Schwendimann, and A. Quattropani. Quantum well excitons in semiconductor microcavities: Unified treatment of weak and strong coupling regimes. *Sol. Stat. Comm.*, 93(9):733, March 1995.

- [41] F. L. Pedrotti and L. S. Pedrotti. *Introduction to optics*. Prentice-Hall international, London, UK, 1993.
- [42] G. Haas, editor. *Theory and calculations of optical thin films*, volume 1. Academic Press, 1965.
- [43] H. Benisty, J-M. Gérard, R. Houdré, J. Rarity, and C. Weisbuch, editors. *Linear optical properties of semiconductor microcavities with embedded quantum wells*, volume 531 of *Lecture notes in physics*. Springer-Verlag Berlin Heidelberg, August 1998.
- [44] L. W. Tu, E. F. Schubert, R. F. Kopf, G. J. Zydzik, M. Hong, S. N. G. Chu, and J. P. Mannaerts. Vertical cavity surface emitting lasers with semitransparent metallic mirrors and high quantum efficiencies. *Appl. Phys. Lett.*, 57(20):2045, November 1990.
- [45] A. Yariv. *Quantum Electronics*, volume 3 of 12. John Wiley and Sons, New York, 1989.
- [46] E. P. O'Reilly and G. P. Witchlow. Theory of hole subband dispersion in strained and unstrained quantum wells. *Phys. Rev. B*, 34(8):6030, October 1985.
- [47] G. Bastard. *Wave mechanics applied to semiconductor heterostructures*. Les éditions de physique, 919444 Les Ulis Cedex, France, 1994.

- [48] J. Hegarty and M. D. Sturge. Studies of exciton localization in quantum-well structures by nonlinear-optical techniques. *J. Opt. Soc. Am. B*, 2(7):1143, July 1985.
- [49] H. B. Bebb, E. H. Williams R. K. Williardson, and A. C. Beer. *Semiconductors and semimetals*, volume 8. Academic, New York, USA, 1972.
- [50] S. E. Esipov and Y. B. Levinson. The temperature and energy distribution of photo-excited hot electrons. *Adv. Phys.*, 36(3):331, May-June 1987.
- [51] J. Lee, E. S. Koteles, and M. O. Vassal. Luminescence linewidth of excitons in GaAs quantum wells below 150K. *Phys. Rev. B*, 33(8):5512, April 1985.
- [52] L. Schultheis, A. Honold, J. Kuhl, K. Köhler, and C. W. Tu. Optical dephasing of homogeneously broadened two-dimensional exciton transitions in GaAs quantum wells. *Phys. Rev. B*, 34(12):9027, December 1986.
- [53] N. Peyghambarian, H. M. Gibbs, J. L. Jewell, A. Antonetti, A. Migus, D. Hulin, and A. Mysyrowicz. Blue shift of the exciton resonance due to exciton-exciton interactions in a multiple-quantum-well structure. *Phys. Rev. Lett.*, 53(25):2433, December 1984.
- [54] S. Schmitt-Rink, D. S. Chemla, and D. A. B. Miller. Theory of transient excitonic optical nonlinearities in semiconductor quantum-well structures. *Phys. Rev. B*, 32(10):6601, November 1985.

- [55] A. Honold, L. Schultheis, J. Kuhl, and C. Tu. Collisional broadening of two-dimensional excitons in a GaAs single quantum well. *Phys. Rev. B*, 40(9):6442, September 1989.
- [56] B. Deveaud, F. Clerot, N. Roy, K. Satzke, B. Sermage, and D. Katzer. Enhanced radiative recombination of free excitons in GaAs quantum wells. *Phys. Rev. Lett.*, 67(17):2355, October 1991.
- [57] S. Schmitt-Rink, D. S. Chemla, and D. A. B. Miller. Linear and nonlinear optical properties of semiconductor quantum wells. *Phys. Adv.*, 38(2):89, March/April 1989.
- [58] D.R. Wake, H. W. Yoon, J. P. Wolfe, and H. Morkoc. Response of excitonic spectra to photoexcited carrier in GaAs quantum wells. *Phys. Rev. B*, 46(20):13452, November 1992.
- [59] S. Schmitt-Rink, D. S. Chemla, and D. A. B. Miller. Linear and nonlinear optical properties of semiconductor quantum wells. *Phys. Rev. Lett.*, 63(3):240, July 1989.
- [60] D. S. Chemla and D. A. Miller. Room-temperature excitonic nonlinear-optical effects in semiconductor quantum-well structures. *J. Opt. Soc. Am. B*, 2(7):1155, December 1985.
- [61] F. Tassone and Y. Yamamoto. Exciton-exciton scattering dynamics in a semiconductor microcavity and stimulated scattering into polaritons. *Phys. Rev. B*, 59(16):10830, April 1999.

- [61] R. Zimmermann, R. Kilimann, K. Kraeft, W. D. Kremp, and G. Roepke. Dynamical screening and self-energy of excitons in electron-hole plasma. *Phys. Stat. Sol. (b)*, 90:175, 1978.
- [62] J. J. Hopfield. Theory of the contributions of excitons to the complex dielectric constant of crystals. *Phys. Rev.*, 112:1555, 1958.
- [63] E. Burstein and C. Weisbuch, editors. *Optical transitions, excitons, and polaritons in bulk and low-dimensional semiconductor structures*, volume 320 of *NATO ASI series E, Applied Sciences*. Kluwar Academic Publishers, July 93 1995.
- [64] R. Houdré, C. Weisbuch, R. P. Stanley, U. Oesterle, and P. Pellandini and M. Illegems. Measurement of cavity-polariton dispersion curve from angle-resolved photoluminescence experiments. *Phys. Rev. Lett.*, 73(15):2043, October 1994.
- [65] R. P. Stanley, R. Houdré, C. Weisbuch, U. Oesterle, and M. Illegems. Cavity-polariton photoluminescence in semiconductor microcavities. *Phys. Rev. B*, 53(16):10995, April 1996.
- [66] S. Pau, G. Björk, H. Cao, R. Huang, Y. Yamamoto, and R. P. Stanley. LO phonon enhanced microcavity polariton emission. *Phys. Rev. B*, 55(4):1942, January 1997.
- 
- [67] F. Tassone and Y. Yamamoto. Exciton-exciton scattering dynamics in a semiconductor microcavity and stimulated scattering into polaritons. *Phys. Rev. B*, 59(16):10830, April 1999.

- [68] A. I. Tartakovskii, M. Emam-Ismail, R. M. Stevenson, M. S. Skolnick, V.N. Astratov, D. M. Whittaker, J. J. Baumberg, and J. S. Roberts. Relaxation bottleneck and its suppression in semiconductor microcavities. *Phys. Rev. B*, 62(4):R2283, July 2000.
- [69] V. Savona and C. Weisbuch. Theory of time-resolved light emission from polaritons in a semiconductor microcavity under resonant excitation. *Phys. Rev. B*, 54(15):10835, October 1996.
- [70] T. B. Norris, J-K. Rhee, C. Y. Sung, Y. Arakawa, M. Nishioka, and C. Weisbuch. Time-resolved vacuum Rabi oscillations in a semiconductor quantum microcavity. *Phys. Rev. B*, 50(19):14663, November 1994.
- [71] G. Bongiovanni, A. Mura, F. Quochi, S. Gürter, J. L. Staehli, F. Tassone, R. P. Stanley, U. Oesterle, and R. Houdré. Coherent exciton-photon dynamics in semiconductor microcavities: The influence of inhomogeneous broadening. *Phys. Rev. B*, 55(11):7084, March 1997.
- [72] R. Houdré, R. P. Stanley, and M. Ilegems. Vacuum-field Rabi splitting in the presence of inhomogeneous broadening: Resolution of a homogeneous linewidth in an inhomogeneously broadened system. *Phys. Rev. A*, 53(4):2711, April 1996.
- [73] J. Rarity and C. Weisbuch, editors. *Critical issues on the strong coupling régime in semiconductor microcavities*, volume 324 of *NATO ASI series E, Applied Sciences*. Kluwer Academic Publishers, September 1996.

- [74] R. J. Thompson, G. Rempe, and H. J. Kimble. Observation of normal-mode splitting for an atom in an optical cavity. *Phys. Rev. Lett.*, 68(8):1132, February 1992.
- [75] A. V. Kavokin. Motional narrowing of inhomogeneously broadened excitons in a semiconductor microcavity: semiclassical treatment. *Phys. Rev. B*, 57(7):3757, February 1998.
- [76] C. Ell, J. Prineas, T. R. Nelson Jr., S. Park, H. M. Gibbs, G. Khitrova, S. W. Koch, and R. Houdré. Influence of structural disorder and light coupling on the excitonic response of semiconductor microcavities. *Phys. Rev. Lett.*, 80(21):4795, May 1998.
- [77] D. M. Whittaker, P. Kinsler, T. A. Fisher, M. S. Skolnick, A. Armitage, A. M. Afshar, M. D. Sturge, and J. S. Roberts. Motional narrowing in semiconductor microcavities. *Phys. Rev. Lett.*, 77(23):4792, December 1996.
- [78] V. Savona, C. Piermarocchi, A. Quattropani, F. Tassone, and P. Schwendimann. Microscopic theory of motional narrowing of microcavity polaritons in a disordered potential. *Phys. Rev. Lett.*, 78(23):4470, June 1997.
- [79] D. M. Whittaker. What determines inhomogeneous linewidths in semiconductor microcavities? *Phys. Rev. Lett.*, 80(21):4791, May 1998.
- [80] M. Razeghi. *The metal-organic chemical vapour deposition challenge*. Adam Hilger, Bristol, England, 1989.

- [81] E. H. C. Parker. *The technology and physics of molecular beam epitaxy*. Plenum, New York USA, 1985.
- [82] J. P. Van de Ziel and M. Ilegems. Multilayer GaAs-Al/sub 0.3/Ga/sub 0.7/As dielectric quarter wave stacks grown by molecular beam epitaxy. *Applied Optics*, 14(11):2627, November 1975.
- [83] T. P. Aherne. *Optical characterisation of ZnCdSe/ZnSe and InGaAs/GaAs Microcavity Light Emitters*. Phd thesis, Trinity College Dublin, Physics Department, Trinity College Dublin, Dublin 2, Ireland, April 1998.
- [84] R. P. Stanley, R. Houdré, and U. Oesterle. Spectral information and reflectivities of the s1312, s1313 and s1314 samples. Technical Report 1, EPFL, EPFL Institut de Micro et Opto-electronique CH-1015 Lausanne, Switzerland, 2002.
- [85] G. R. Hayes, S. Haacke, M. Kauer, R. P. Stanley, R. Houdré, U. Oesterle, and B. Deveaud. Resonant Rayleigh scattering versus incoherent luminescence in semiconductor microcavities. *Phys. Rev. B*, 58(16):10175, October 1998.
- [86] R. F. Schnabel, R. Zimmermann, D. Bimberg, H. Nickel, R. Lösch, and W. Schlapp. Influence of exciton localization on recombination line shapes:  $\text{In}_x\text{Ga}_{1-x}\text{As}/\text{GaAs}$ . *Phys. Rev. B*, 46(15):9873, October 1992.
- [87] A. G. Gorshunov, V. N. Grigorév, V. I. Griven, K. L. Litvinenko, and V. G. Lyssenko. Dependence of the four-wave mixing signal on the spectrum of excited states in GaAs/AlGaAs multiple quantum wells. *JETP*, 83(4):809, October 1996.



- [88] F. Jahnke, M. Kira, S.W. Koch, G. Khitrova, E. K. Lindmark, T. R. Nelson Jr., D. V. Wick, J. D. Berger, O. Lyngnes, H. M. Gibbs, and K. Tai. Excitonic nonlinearities of semiconductor microcavities in the nonperturbative regime. *Phys. Rev. Lett.*, 77(26):5257, December 1996.
- [89] F. Jahnke, M. Kira, and S. W. Koch. Theory of nonlinear exciton saturation in semiconductor microcavities. *Phys. Stat. Sol. (b)*, 206(1):19, March 1998.
- [90] O. Lyngnes, J. D. Berger, J. P. Prineas, S. Park, G. Khitrova, H. M. Gibbs, F. Jahnke, M. Kira, and S. W. Koch. Nonlinear emission dynamics from semiconductor microcavities in the nonperturbative regime. *Solid State Commun.*, 104(5):297, November 1997.
- [91] J. Rarity and C. Weisbuch, editors. *Dynamical studies of cavity polaritons in semiconductor microcavities: Pump probe measurements and time-resolved photoluminescence*, volume 324 of *NATO ASI series E, Applied Sciences*. Kluwer Academic Publishers, September 1995.
- [92] Shudong Jiang, Susumu Machida, Yoshihiro Takiguchi, and Yashihisa Yamamoto. Direct time-domain observation of transition from strong to weak coupling in a semiconductor microcavity. *Appl. Phys. Lett.*, 73(21):3031, November 1998.
- [93] R. Huang, H. Cao, and Y. Yamamoto. Measurement of the intensity and phase of microcavity exciton-polariton emission in the linear and nonlinear regime. *Phys.*

- [93] *Rev. B*, 56(15):9217, October 1997.
- [94] R. Houdré, J. L. Gibernon, P. Pellandini, R. P. Stanley, U. Oesterle, C. Weisbuch, J. O'Gorman, B. Roycroft, and M. Ilegems. Saturation of the strong-coupling regime in a semiconductor microcavity: Free-carrier bleaching of cavity polaritons. *Phys. Rev. B*, 52(11):7810, September 1995.
- [95] S. Park, V. Zapasskii, D. V. Wick, T. R. Nelson, C. Ell, H. M. Gibbs, G. Khitrova, A. Schülzgen, M. Kira, F. Jahnke, and S. W. Koch. Spontaneous emission lifetime of carriers in a semiconductor microcavity measured by photoluminescence without distortion by reabsorption. *Opt. Exp.*, 4(13):512, June 1999.
- [96] D.-S. Kim, J. Shah, T. C. Damen, W. Schäfer, F. Jahnke, S. Schmitt-Rink, and K. Köhler. Unusually slow temporal evolution of femtosecond four-wave-mixing signal in intrinsic GaAs quantum wells: Direct evidence for the dominance of interaction effects. *Phys. Rev. Lett.*, 69(18):2725, November 1992.
- [97] S. T. Cundiff and D. G. Steel. Coherent transient spectroscopy of excitons in GaAs-AlGaAs quantum wells. *J. Quant. Elec.*, 28(10):9197, October 1992.
- [98] J. Kuhl, A. Honold, L. Schultheis, and C. Tu. Optical dephasing and orientational relaxation of Wannier-excitons and free carrier in GaAs/AlGaAs. *Festkörperprobleme*, 29:157, January 1989.

- [99] T. Yajima and Y. Taira. Spatial optical parametric coupling of picosecond light pulses and transverse relaxation effect in resonant media. *J. Phys. Soc. Japan*, 47(5):1620, November 1979.
- [100] P. N. Butcher and D. Cotter. *The elements of non-linear optics*, volume 9 of *Cambridge studies in modern optics*. Cambridge, The Pitt Building, Trumpington Street, Cambridge CB2 1RP, UK, 1998.
- [101] Jagdeep Shah. *Ultrafast spectroscopy of Semiconductors and Semiconductor Nanostructures*, volume 115 of *Solid-State Sciences*. Springer, New York, USA, 1996.
- [102] S. M. Murry. *Quantum Mechanics*. Addison-Wesley, The Addison-Wesley Pub. Co., Wokingham, UK, 1993.
- [103] S. Schmitt-Rink, S. Mukamel, K. Leo, J. Shah, and D. S. Chemla. Stochastic theory of time-resolved four-wave mixing in interacting media. *Phys. Rev. A*, 44(3):2124, August 1991.
- [104] H. Wang, K. B. Ferrio, D. G. Steel, P. R. Berman, Y. Z. Hu, R. Binder, and S. W. Koch. Transient four-wave-mixing line shapes: Effects of excitation-induced dephasing. *Phys. Rev. A*, 49(3):1551, March 1994.
- [105] K. Leo, E. O. Göbel, T. C. Damen, J. Shah, S. Schmitt-Rink, W. Schäfer, J. F. Müller, K. Köhler, and P. Ganser. Subpicosecond four-wave mixing in GaAs/Al<sub>x</sub>Ga<sub>1-x</sub>As quantum wells. *Phys. Rev. Lett.*, 67(17):2355, October 1991.

- [106] J. Hegarty, M. D. Sturge, A. C. Gossard, and W. Wiegmann. Resonant degenerate four-wave mixing in GaAs multi-quantum well structures. *Appl. Phys. Lett.*, 40(2):132, January 1982.
- [107] T. Takagahara. Excitonic relaxation processes in quantum well structures. *J. Cryst. Growth*, 44(4-6):347, December 1989.
- [108] D. Oberhauser, K. H. Pantke, J. M. Hvam, G. Weimann, and C. Klingshirn. Exciton scattering in quantum wells at low temperatures. *Phys. Rev. B*, 47(11):6827, March 1993.
- [109] K. Leo, M. Wegener, J. Shah, D. S. Chemla, E. O. Göbel, T. C. Damen, S. Schmitt-Rink, and W. Schäfer. Effects of coherent polarization interactions on time-resolved degenerate four-wave mixing. *Phys. Rev. Lett.*, 65(11):1340, September 1990.
- [110] S. T. Cundiff, H. Wang, and D. G. Steel. Polarization-dependent picosecond excitonic nonlinearities and the complexities of disorder. *Phys. Rev. B*, 46(11):7248, September 1992.
- [111] R. Zimmermann. Polarization dependence of four-wave-mixing signal in quantum wells. *Phys. Rev. B*, 47(20):13485, May 1993.
- [112] D. Birkedal, V. G. Lyssenko, K.-H. Pantke, J. Erland, and J. M. Hvam. Nanoroughness localisation of excitons in GaAs multiple quantum wells studied by transient four-wave mixing. *Phys. Rev. B*, 51(12):7977, March 1995.

- [113] H. Wang, J. Shah, T. C. Damen, W. Y. Jan, and J. E. Cunningham. Coherent oscillation in semiconductor microcavities. *Phys. Rev. B*, 51(20):14713, May 1995.
- [114] M. Shirane and C. Ramkumar. Degenerate four-wave mixing measurements on an exciton-photon coupled system in a semiconductor microcavity. *Phys. Rev. B*, 58(12):7978, September 1998.
- [115] A. L. Bradley, L. A. Dunbar, J. P. Doran, J. Hegarty, R. P. Stanley, R. Houdré, U. Oesterle, and M. Illegems. Suppression of acoustic phonon scattering in strong coupling microcavities. *EQEC oral presentation*, July 1998.
- [116] T. Baars, M. Bayer, A. Forchel, F. Schäfer, and J. P. Reithmaier. Polariton-polariton scattering in semiconductor microcavities: Experimental observation of threshold-like density dependence. *Phys. Rev. B*, 61(4):2409, January 2000.
- [117] L. A. Dunbar, M. Lynch, A. L. Bradley, J. F. Donegan, J. Hegarty, R. P. Stanley, U. Oesterle, R. Houdré, and M. Illegems. Collisional broadening of semiconductor microcavity polaritons - accepted. *Phys. Stat. Sol (b)*, September 2001.
- [118] V. Savona and C. Piermarocchi. Microcavity polaritons: Homogeneous and inhomogeneous broadening in the strong coupling regime. *Phys. Stat. Sol. (a)*, 164(1):45, December 1997.
- [119] A. R. Pratt, T. Takamori, and T. Kamijoh. Temperature dependence of the cavity-polariton mode splitting in a semiconductor microcavity. *Phys. Rev. B*, 58(15):9656, October 1998.

- [120] J. S. Blakemore. *Solid State Physics*. Cambridge University Press, The Pitt Building, Trumpington Street, Cambridge, CB2 1RP, UK, 1993.
- [121] C. Patel, T. J. Parker, H. Jamshidi, and W. F. Sherman. Phonon frequencies in GaAs. *Phys. Stat. Sol. (b)*, 122:461, 1984.
- [122] C. Piermarocchi, F. Tassone, V. Savona, and A. Quattropani. Nonequilibrium dynamics of free quantum-well excitons in time-resolved photoluminescence. *Phys. Rev. B*, 53(23):15834, June 1996.
- [123] K. W. Böer. *Survey of Semiconductor Physics*. Van Nostrand Reinhold, 115 Fifth Avenue, New York, 10003, 1990.
- [124] S. Pau, G. Björk, J. Jacobson, H. Cao, and Y. Yamamoto. Stimulated emission of a microcavity dressed exciton and suppression of phonon scattering. *Phys. Rev. B*, 17(11):50, November 1995.
- [125] P. Bhattacharya. *Properties of lattice-matched and strained Indium Gallium Arsenide*. Emis data reviews series No. 8. Inspec, The institution of Electrical Engineers, London, UK, 1993.
- [126] T. Takagahara. Localization and energy transfer of quasi-two-dimensional excitons in GaAs-AlAs quantum-well heterostructures. *Phys. Rev. B*, 31(10):6552, May 1985.
- [127] M. S. Skolnick, A. Armitage, M. S. Skolnick, and J. S. Roberts. Suppressed polariton scattering in semiconductor microcavities. *Phys. Rev. Lett.*, 81(3):661, July 1998.

- [127] H. Stolz, D. Schwarze, W. van der Osten, and G. Weimann. Transient optical alignment and relaxation of excitons in GaAs/AlGaAs. *Superlattices Microstruct.*, 6(3):271, 1989.
- [128] V. Savona, C. Piermarocchi, A. Quattropani, P. Schwendimann, and F. Tassone. Optical properties of microcavity polaritons. *Phase Transitions*, 1998.
- [129] Y. Chen, G. P. Kothiyal, J. Singh, and P. K. Bhattacharya. Absorption and photoluminescence studies of the temperature dependence of exciton lifetime in lattice-matched and strained quantum well systems. *Superlattices Microstruct.*, 3(6):657, 1987.
- [130] J. L. Shen, C. Y. Chang, W. C. Chou, M. W. Wu, and Y. F. Chen. Temperature dependence of the reflectivity in absorbing Bragg reflectors. *Opt. Exp.*, 9(6):287, September 2001.
- [131] S. Pau, G. Björk, J. Jacobson, and Y. Yamamoto. Phonon-polariton interaction in a microcavity. *Nuovo Cimento*, 51(11):7090, March 1995.
- [132] G. Cassabois, A. L. C. Triques, F. Bogani, C. Delalande, Ph. Roussignol, and C. Piermarocchi. Polariton-acoustic-phonon interaction in a semiconductor microcavity. *Phys. Rev. B*, 61(3):1696, January 2000.
- [133] J. J. Baumberg, A. Armitage, M. S. Skolnick, and J. S. Roberts. Suppressed polariton scattering in semiconductor microcavities. *Phys. Rev. Lett.*, 81(3):661, July 1998.

- [134] R. T. Williams and W. M. Yen, editors. *Dephasing of Strongly Coupled Exciton-Photon systems*, volume 98-25 of *Excon '98*. The Electrochemical Society Inc., December 1998.
- [135] G. Cassabois, A. L. C. Triques, D. Larousserie, C. Delalande, Ph. Roussignol, P. Senellart-Mardon, J. Bloch, V. Thierry-Mieg, and R. Planel. Stationary coherence in semiconductor microcavities. *Phys. Rev. B*, 59(16):10429, April 1999.
- [136] X. Marie, P. Renucci, S. Dubourg, T. Amand, P. Le Jeune, J. Barrau, J. Bloch, and R. Planel. Coherent control of exciton polaritons in a semiconductor microcavity. *Phys. Rev. B*, 59(4):2494, January 1999.
- [137] P. Renucci, X. Marie, T. Amand, M. Paillard, and J. Barrau. Microcavity polariton scattering probed by coherent control experiments. *Superlattices Microstruct.*, 26(2):61, May 1999.
- [138] P. Renucci, M. Paillard, X. Marie, T. Amand, J. Barrau, and C. Ciuti. Temporal coherent control in semiconductor quantum structures. *Phys. Stat. Sol. (a)*, 178(1):373, August 2000.
- [139] L. Schultheis, J. Kuhl, and A. Honold. Ultrafast phase relaxation of excitons via exciton-exciton and exciton-electron collisions. *Phys. Rev. Lett.*, 57(13):1635, September 1986.



- [140] M. T. Peortella J. Y. Bigot, R. W. Schroenlein, J. E. Cunningham, and C. V. Shank. Two-dimensional carrier-carrier screening in a quantum well. *Phys. Rev. Lett.*, 67(5):636, July 1991.
- [141] R. Eccleston, B. F. Feuerbacher, J. Kuhl, W. W. Rühle, and K. Ploog. Density-dependent exciton radiative lifetimes in GaAs quantum wells. *Phys. Rev. B*, 45(19):11403, May 1992.
- [142] G. W. Fehrenbach, W. Schäfer, J. Treusch, and R. G. Ulbrich. Transient optical spectra of a dense exciton gas in a direct-gap semiconductor. *Phys. Rev. Lett.*, 49(17):1281, October 1982.
- [143] K. Litvinenko, D. Birkedal, V. G. Lyssenko, and J. M. Hvam. Exciton dynamics in GaAs/Al<sub>x</sub>Ga<sub>1-x</sub>As quantum wells. *Phys. Rev. B*, 59(15):10255, April 1999.
- [144] C. Ciuti, V. Savona, C. Piermarocchi, and A. Quattropani. Role of exchange of carriers in elastic exciton-exciton scattering in quantum wells. *Phys. Rev. B*, 58(12):7926, September 1998.
- [145] C. Ciuti, V. Savona, C. Piermarocchi, and A. Quattropani. Threshold behavior in the collision broadening of microcavity polaritons. *Phys. Rev. B*, 58(12):7926, September 1998.
- [146] Y. Feng and H. N. Spector. Scattering of excitons by free carriers in semiconductor quantum well structures. *J. Phys. Chem. Solids*, 48(7):593, 1987.

- [147] G. Manzke, K. Henneberger, and V. May. Many-exciton theory of multiple quantum-well structures. *Phys. Stat. Sol. (b)*, 139:233, 1987.
- [148] T. Koh, Y. Feng, and H. N. Spector. Elastic scattering of excitons by excitons in semiconducting quantum-well structures: finite confining-potential model. *Phys. Rev. B*, 55(15):9271, April 1997.
- [149] S. N. Bose. Plancks gesetz und lichtquantenhypothese. *Z. Phys.*, 26:178, 1924.
- [150] A. Einstein. Quantentheorie des einatomigen idealen gases. *Sitzber Preuss. Akad. Wiss.*, 22:261, 1924.
- [151] M-O. Mewes, M. R. Andrews, N. J. Van Druten, D. M. Kurn, D. S. Durfee, and W. Ketterle. Bose-Einstein condensation in a tightly confining dc magnetic trap. *Phys. Rev. Lett.*, 77(3):416, July 1995.
- [152] D. S. Jin, J. R. Ensher, M. R. Matthews, C. E. Wieman, and E. A. Cornell. Collective excitations of a Bose-Einstein condensate in a dilute gas. *Phys. Rev. Lett.*, 77(3):420, July 1996.
- [153] S. A. Moskalenko and D. W. Snoke. *Bose-Einstein condensation of excitons and biexciton and coherent nonlinear optics with excitons*. Cambridge University Press, The Edinburgh Building, Cambridge CB2 2RU, UK, 2000.
- [154] K. Burnett, M. Edwards, and C. Clark Eds. Bose Einstein condensation, very cold indeed: The nanoKelvin physics of Bose-Einstein condensation. *J. Res. Ntl. Inst. Stand. Technol.*, 101(4):419, July-August 1996.

- [155] Y. Yamamoto, F. Tassone, and H. Cao. *Semiconductor cavity quantum electrodynamics*. 169 Springer tracts in modern physics. Springer, Springer-Verlag Berlin Germany, 2000.
- [156] A. L. Fetter and J. D. Walecka. *Quantum theory of many-particle systems*, volume 8. McGraw-Hill, New York, USA, 1971.
- [157] V. B. Timofeev, V. D. Kulakavskii, and I. V. Kukushkin. Spin aligned exciton gas in uniaxially compressed Ge. *Physica B and C*, 117-8:327, March 1980.
- [158] J. C. Kim and J. P. Wolfe. Bose-Einstein statistics of an excitonic gas in two dimensions: Excitons and biexcitons in GaAs quantum wells. *Phys. Rev. B*, 57(16):9861, April 1998.
- [159] D. W. Snoke and J. P. Wolfe. Population dynamics of a Bose gas near saturation. *Phys. Rev. B*, 39(7):4030, March 1989.
- [160] A. Imamoğlu, R. J. Ram, S. Pau, and Y. Yamamoto. Nonequilibrium condensates and lasers without inversion: exciton-polariton lasers. *Phys. Rev. A*, 53(6):4250, June 1996.
- [161] A. Imamoğlu, R. J. Ram, S. Pau, and Y. Yamamoto. Quantum dynamics of exciton lasers. *Phys. Rev. Lett.*, 214(3-4):193, May 1996.
- [162] S. Pau, H. Cao, J. Jacobson, G. Björk, Y. Yamamoto, and A. Imamoğlu. Observation of a laserlike transition in a microcavity exciton polariton system. *Phys. Rev. A*, 54(3):1789, September 1996.

- [163] M. Kira, F. Jahnke, S. W. Koch, J. D. Berger, D. V. Wick, T. R. Nelson, Jr., G. Khitrova, and H. M. Gibbs. Quantum theory of nonlinear semiconductor microcavity luminescence explaining boson experiments. *Phys. Rev. Lett.*, 79(25):5170, December 1997.
- [164] G. Khitrova, D. V. Wick, J. D. Berger, C. Ell, J. P. Prineas, T. R. Nelson Jr., O. Lyngnes, H. M. Gibbs, M. Kira, F. Jahnke, S. W. Koch, W. Rühle, and S. Hallstein. Excitonic effects, luminescence and lasing in semiconductor microcavities. *Phys. Stat. Sol. (b)*, 206(1):3, March 1998.
- [165] H. Cao, S. Pau, J. M. Jacobson, G. Björk, and Y. Yamamoto. Transition from a microcavity exciton polariton to a photon laser. *Phys. Rev. A*, 55(6):4632, June 1997.
- [166] P. Senellart and J. Bloch. Nonlinear emission of microcavity polaritons in the low density regime. *Phys. Rev. Lett.*, 82(6):1233, February 1999.
- [167] P. Senellart, J. Bloch, B. Sermage, and J. Y. Marzin. Microcavity polariton depopulation as evidence for stimulated scattering. *Phys. Rev. B*, 62(24):16263, December 2000.
- [168] P. G. Savvidis, J. J. Baumberg, R. M. Stevenson, D. M. Whittaker, and J. S. Roberts. Asymmetric angular emission in semiconductor microcavities. *Phys. Rev. B*, 62(20):13278, November 2000.

- [169] C. Ciuti, P. Schwendimann, B. Deveaud, and A. Quattropani. Theory of angle-resonant polariton amplifier. *Phys. Rev. B*, 62(8):4825, August 2000.
- [170] C. Ciuti, P. Schwendimann, and A. Quattropani. Parametric luminescence of microcavity-polaritons. *Phys. Rev. B*, 63(1):41303, January 2000.
- [171] P. G. Savvidis, C. Ciuti, J. J. Baumberg, D. M. Whittaker, and J. S. Roberts. Off-branch polaritons and multiple scattering in semiconductor microcavities. *Phys. Rev. B*, 64(1):75311, July 2001.
- [172] R. Houdré, C. Weisbuch, R. P. Stanley, U. Oesterle, and M. Ilegems. Nonlinear emission of semiconductor microcavities in the strong coupling regime. *Phys. Rev. Lett.*, 85(13):2793, September 2000.
- [173] J. J. Baumberg, P. G. Savvidis, R. M. Stevenson, A. I. Tartkovskii, M. S. Skolnick, D. M. Whittaker, and J. S. Roberts. Parametric oscillation in a vertical microcavity: A polariton condensate or micro-optical parametric oscillation. *Phys. Rev. B*, 62(24):16247, December 2000.
- [174] R. M. Stevenson, V. N. Astratov, M.S. Skolnick, D. M. Whittaker, M. Emam-Ismael, A. I. Tartakovskii, P. G. Savvidis, J. J. Baumberg, and J. S. Roberts. Continuous wave observation of massive polariton redistribution by stimulated scattering in semiconductor microcavities. *Phys. Rev. Lett.*, 85(17):3680, October 2000.

- [175] G. Messin, J. Ph. Karr, A. Bass, G. Khitrova, R. Houdré, R. P. Stanley, U. Oesterle, and E. Giacobino. Parametric polariton amplification in a semiconductor microcavity. *Phys. Rev. Lett.*, 87(12):127403, September 2001.
- [176] D. S. Chemla, A. Maruani, and F. Bonnouvrier. Interference between four-wave and six-wave mixing in resonant coherent scattering from biexcitons in CuCl. *Phys. Rev. A*, 26(5):3026, November 1982.
- [177] J. Rarity and C. Weisbuch, editors. *Cavity-Polaritons in semiconductor microcavities*, volume 324 of *NATO ASI series E, Applied Sciences*. Kluwar Academic Publishers, September 1996.
- [178] A. Honold, L. C. Shulteis, J. Kuhl, and C. W. Tu. Reflected degenerate four-wave mixing on GaAs single quantum wells. *Appl. Phys. Lett.*, 52(25):2105, June 1988.